Single-trial correlates of decision-making in dorsal premotor and primary motor cortices

Diogo Manuel Barros Magalhães da Rocha Peixoto

Dissertation presented to obtain
the Ph.D degree in Biology - Neuroscience

Instituto de Tecnologia Química e Biológica António Xavier | Universidade Nova de Lisboa

Oeiras,
July, 2016

INSTITUTO
DE TECNOLOGIA
QUÍMICA E BIOLÓGICA
ANTÓNIO XAVIER /UNL

Knowledge Creation

Single-trial correlates of decision-making in dorsal premotor and primary motor cortices

Diogo Manuel Barros Magalhães da Rocha Peixoto

Dissertation presented to obtain
the Ph.D degree in Biology - Neuroscience

Instituto de Tecnologia Química e Biológica António Xavier | Universidade Nova de Lisboa

Research work coordinated by:

FUNDAÇÃO CALOUSTE GULBENKIAN
Instituto Gulbenkian de Ciência

Oeiras, July, 2016

INSTITUTO
DE TECNOLOGIA
QUÍMICA E BIOLÓGICA
ANTÓNIO XAVIER /UNL

Knowledge Creation

Single-trial correlates of decision-making in dorsal premotor and primary motor cortices

Diogo Manuel Barros Magalhães da Rocha Peixoto

Champalimaud Neuroscience Programme

Instituto de Tecnologia Química e Biológica

Stanford University

A thesis submitted for the degree of

Doctor of Philosophy (PhD)

August 2016

Abstract

Everyday, as we move through the world we seamlessly make hundreds of perceptual decisions often without fully appreciating the underlying fast and precise computations going on in our brains. A fundamental question in the decision-making field is to understand how and where in the brain information is combined to form decisions that lead to appropriate responses.

While fascinating, perceptual decision-making is a especially challenging process to study due to its covert nature: so much can be going on at neural level and yet we only directly observe the behavioral response when all deliberation is over. Moreover, even when the behavioral response is the same the neural patterns that lead to it could be dramatically different from trial to trial. These unique features of decision formation create a strong need for precise single-trial estimates of the neural state. Though much has been learned about the mechanisms of integration of visual evidence and motor preparation (Shadlen and Newsome, 2001; Roitman and Shadlen, 2002; Mante et al., 2013), these studies have relied on average estimates of neural state eliminating crucial trial-to-trial variability.

Here, we trained monkeys on a modified motion discrimination task, in which the operant response was a an arm reach, making it more suitable for studying decision-making in the somatomotor system. Crucially, while the subjects performed the task we recorded the simultaneous activity of hundreds of neurons using multi-electrode arrays. Simultaneous recordings of many neurons allow for more accurate estimation of neural states on single trials serving as a window into the dynamics and variability of the decision formation process.

We studied the responses of heterogeneous populations of neurons in dorsal premotor (PMd) and primary motor (M1) cortices and asked: 1) what signals are present in the two areas, 2) how they compare to the decision related signals reported in oculomotor areas 3) how to interpret the dynamics of single trial signals and validate their predictions.

We found that 1) besides classical motor planning and execution signals, low latency choice predictive signals are present in PMd and M1, 2) these signals have the same features seen in the oculumotor system and resemble a decision variable (DV) 3) fluctuations in this decision variable are meaningful and can be directly validated.

The first two observations were made using a combination of multi-electrode recordings, population single-trial analysis and decision-making models. The final observation required going one step further by bringing into play a real-time system to estimate a DV and use it to act on the task, effectively closing the loop in our experiment. To our knowledge, this framework has only been used to implement brain-machine interfaces but we demonstrate here for the first time it can be used to understand covert cognitive processes.

Acknowledgements

First and foremost I would like to thank my Stanford advisors Bill Newsome and Krishna Shenoy. I could not have been any luckier and I am deeply thankful for the opportunity to learn from and be friends with, such great scientists and human beings. From Bill, amongst uncountable things, I learned how to be my own harshest critic, to always triple check every result and line of code and to always strive for a cleaner and more accurate way of interpreting data. I also learned how to clearly convey a scientific concept and how, regardless of skill and experience, there is no such thing as over-practicing a presentation! From Krishna I learned that politeness and incisive scientific criticism are not at odds and also how important it is to frame your results within a bigger picture. I also witnessed first hand how one can stay true to his principles in the face of overwhelming adversity.

I am deeply thankful to my non-official committee members at Stanford, Kwabena Bohaen and Anthony Norcia, for being so generous with their time. They had no obligation to join my non-official committee but by voluntarily doing so they made it possible for me to have the full PhD experience at Stanford.

I also want to thank my CNP advisor Joe Paton for being incredibly helpful and supportive not only in the early stages of my project as I navigated through a completely new field but throughout my entire degree. My committee members Megan Carey and Adam Kampff made sure I stayed on track throughout the project and encouraged me over the years to aim higher and higher and I am very grateful for it.

I could have never have gotten started without Zach Mainen's and Rui Costa's help setting up the collaboration between Bill Newsome and Krishna Shenoy and defining the scope of my project. I am extremely thankful for their crucial effort and support in that very early stage.

Going back a few years further, I recognize I was very privileged to have had Jorge Pacheco as my first mentor during my Physics major senior year. It was through him that I first experienced what research is actually like and what it takes to make valuable contributions to Science. It was also him who sparked my interest in Neuroscience in the first place and who guided me throughout my transition between scientific fields.

Once I joined INDP I was lucky to be part of a very diverse class who just like me was searching for its identity and path in Neuroscience. We struggled through some of the same issues together and cherished each other's small victories along the way.

Later, I had the unique opportunity to have Roozbeh Kiani as my first hands-on mentor at Stanford University. From coding complex algorithms to isolating individual neurons I owe Roozbeh a tremendous amount of what I learned during my PhD. He always believed in the merits of my project, and will remain my reference of scientific excellence. In return, I was fortunate to have had the opportunity to pass along some of this knowledge to Bora Erden, a fantastic undergraduate student I was lucky to mentor.

I must thank Jessica Powell and Sania Fong for tirelessly sharing their expertise in behavioral training and helping me progress from a clueless graduate student to a proficient primate trainer. Sania, went far beyond the traditional role of a research technician and not only helped me discover more efficient ways to train monkeys on an extremely complex task but also helped collecting data herself cutting the duration of my projects by a few valuable months.

One of my project's core features was the use of chronically implanted Utah arrays through which we collected precious simultaneous neural data which allowed for novel single trial analyses. The chronic implantation was only possible thanks to Stephen Ryu's incredible surgical skills. He performed several of these delicate surgeries with absolute perfection and removed immense amounts of stress and uncertainty from the single most stressful moments of the entire project on which everything else relies. In the process he was generous enough to teach me basic surgery skills and practices and I am extremely thankful for his contributions.

The work would not have been possible without the help and support of many collaborators. Chandramouli Chandrasekaran was my partner in crime all along having collaborated closely with me and carried out a complementary project. He was often the first I sought to share new results or bounce ideas off and regularly the one highlighting the validity and importance of the findings. He was also there in the harder times to commiserate about the difficulties of our line of research.

Paul Nuyujukian, Jonathan Kao and Julian Brown were an essential driving force that helped make the real-time decoding project a reality. Their networking, coding and electrical engineering skills were absolutely crucial to get the setup running in a very short period, and that entire line of research would not have been possible without their contribution.

Just as important as all the scientific support I got, was the friendship, camaraderie and love I received throughout this journey. As a close friend and classmate sharing the Portuguese expat experience, David Raposo was often the one I shared my small successes and frustrations with. Despite being on the other US coast he was always available and able to relate to and empathise with my experiences.

Suraj Pradhan, was the first of many new friends at Stanford and one who introduced me to many new people and in the process expanded my cultural horizons more so than I could ever have imagined. He was also the instigator of many events that lead to great memories during my Stanford experience.

Justin Foster became a very close friend and one who was extremely important to help me maintain a healthy and rewarding work and life balance. I am thankful for all the adventures and activities we shared (from tennis to cooking and from swimming to weight lifting) and for everything I learned along the way. He was also a strong intellectual influence who often made me question my own biases and in the process hopefully become a better person.

My long time friends Antonio Quintino and Mario Cruz have always been incredibly supportive through the ups and downs of graduate shcool and remain as proof that true friendship withstands distance and separation.

To all my friends, I am deeply thankful for your friendship and I look forward to seeing you succeed in whatever paths you choose for your life. My life was vastly enriched through your influence.

And above all, I need to thank those closest to my heart: my brother, my parents and my girlfriend Tatyana. Tatyana made my life infinitely better since we met 2 years ago and has always been there for me with nothing but love encouragement to offer. I don't think I could have pulled through the final and very stressful stage of the PhD without her and I am incredible grateful to have her in my life.

My parents were extremely supportive and caring throughout my life and all the steps that lead to graduate school. Even when my passion for Science made me move thousands of miles away from home to complete my PhD, their support was unconditional . It is impossible to overestimate how much they contributed in small and big ways to make this journey possible.

My brother was always my inspiration since I can remember and to this day I admire his fearlessness and ability to take on any challenge to comes up. I am grateful for all the adventures we shared and look forward to many more in the future.

Finally, I want to thank all the organisations that made this work possible: IGC for hosting the doctoral programme during its first years, ITQB for partnering with the Champalimaud Foundation to confer the graduate degrees and FCT and HHMI for funding the research. Huge thanks to the Champalimaud Foundation for accepting me in programme and giving me such a fantastic scientific environment to grow as a researcher. Lastly, I would like to thank everyone at Stanford University who directly or indirectly supported my research. It's been a great honor to be a visiting graduate student at Stanford and I couldn't have had a better host institution.

Dedication

I would like to dedicate this work to my parents, my brother and my avó Maria Antónia.

Contents

List of figures

1

Introduction

It's just another work day and you are driving to the office in dense traffic. Without you even being fully aware, your brain is continuously doing multiple calculations regarding the position and speed of nearby cars, having very limited time to fully integrate that information. It might even be evaluating other stimuli that abstractly represent rules like a red light or yield sign. And it is doing all this almost seamlessly to ensure you make decisions that lead to the most appropriate action, such as breaking steering or staying on the throttle. Of course at times mistakes are made, but the brain's ability to combine external information often of different modalities (motion and sound for example) is remarkable and often unappreciated. Intriguingly, even though these abilities are often taken for granted they are still not fully understood in the context of neuroscience. What areas are responsible for this chain of processes? How do they adapt to different contexts and rules? What mechanisms do they use to integrate and select relevant evidence? What leads us to make mistakes? All these questions remain to a large extent unanswered and are at the core of what the perceptual decision-making field is pursuing.

Naturally, not all decisions we make are of this nature. We can make choices that require more abstract concepts such as buying a car or deciding between two items at the grocery store. These types of decisions often depend on an abstract valuation of the options and fall under the scope of the value-based decision-making field.

The interest in studying decision-making from a neuroscience perspective comes

not just from the possibility of understanding those specific process but because it provides a unique "window on cognition" (Shadlen and Gold, 2004). Decisions go far beyond the association between stimuli and responses and can be conceptualized as the weighed the deliberation of evidence towards multiple choices. This deliberation process can take into account very different sources of evidence (sensory or not) and combine it to reach a categorical decision. Understanding the computations underlying these processes will allow further understanding of cognition itself.

In this work we explore signatures of perceptual decision-making in the somatomotor system and at the level of individual trials.

1.1 Perceptual decision-making

Perceptual decision-making can be defined as the field of Neuroscience that studies the neural processes responsible for weighing available evidence in the world and deliberating on it with the purpose of reaching a commitment to a proposition or selecting an appropriate action. Classically, this sequence of neural events has been broken down into three consecutive stages (Graham, 1989):

1. Stimulus processing stage during which a representation of the relevant stimulus is created in primary and secondary sensory areas;

2. This representation is then used in the deliberation stage during which the stimulus is evaluated and a categorical decision is reached.

3. This information is then fed to the appropriate motor area responsible for implementing the corresponding behavior. This stage can be interpreted as the action execution stage

Despite being a conceptual simplification, this framework has been extremely informative in terms of guiding the design of experiments and interpretation of data. There are some hints that some of these stages might be more blended both in time and brain regions than initially suggested but the intuition still stands (Shadlen and Newsome, 2001; Cisek, 2006) . The previously mentioned "driving through traffic"

scenario is a great example of perceptual decision-making in real-life since all stages are present and clear. However, such a scenario would be too unconstrained to realistically be useful to start understanding the underlying neural processes. Instead, researchers have had to design tightly parametrised paradigms that allow as much control as possible over the stimulus being presented and the subject's behavior. Only then meaningful correlations between neural signals and behavior could start being established. Decision-making is too hard of a process to initially approach in an unconstrained manner.

Faced with these constraints researchers have converged on a basic formula for perceptual decision-making paradigms: a stimulus is presented to the subject for a certain period of time after which a categorical decision must be reached and reported by performing the contingent operant response. The same sequence is repeated for hundreds or thousands of trials during which certain parameters under the experimenters' control will be randomly or deterministically changed. In most variants there are only 2 categorical choices available to the subject hence their designation: 2 Alternative Forced Choice (2AFC) tasks. 2AFCs have been used to study perceptual decision-making across modalities from visual (Britten et al., 1992), to somatosensory (Romo et al., 1998) to auditory or audiovisual (Chandrasekaran et al., 2013).

Historically, this line of research started with the visual system of primates in Bill Newsome's laboratory (for a review, see Shadlen and Kiani, 2013). Bill Newsome, Tony Movshon and Ken Britten were at the time interested in describing the visual responses of area MT/V5. To this end they recorded extra-cellular activity from this area while rhesus macaques performed a challenging motion discrimination task. This paradigm, known as the random dots paradigm (Figure 1.1) has been a true workhorse in the field and is still actively used today. The task assigned to the monkey consists of discriminating the net direction of a noisy visual stimulus. The stimulus is formed by dots that flicker on a computer screen and that, with a given probability, move in a direction specified by the experimenter. This probability is termed stimulus coherence and quantifies the net direction of dots motion. The difficulty of a given trial can be tightly parametrised by the coherence of the stimulus. Because of the stochastic

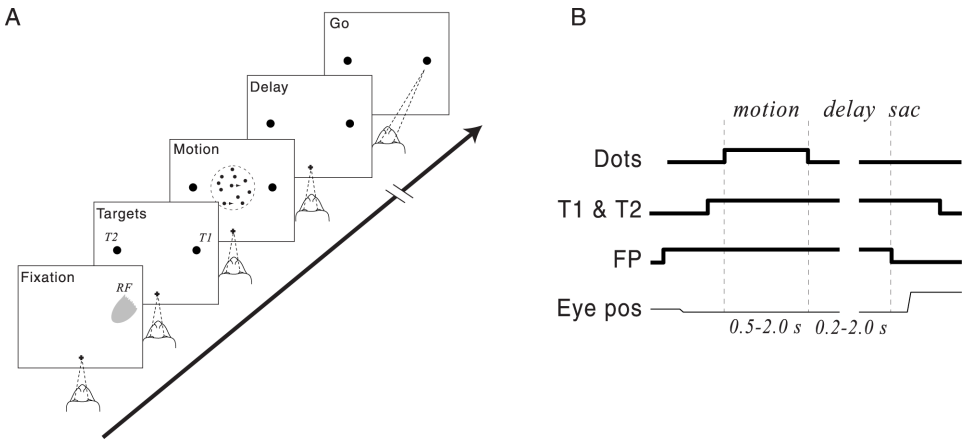

Figure 1.1: **Motion discrimination task. a)** Dots task structure. The monkey starts the trial by fixation on a fixation point on the screen. After a fixed delay two targets appear on opposite locations. The monkey is then asked to discriminate the net direction of motion of a visual stimulus consisting of flickering dots. The duration of the stimulus presentation was fixed and the difficulty of the trial adjusted by the coherence of the stimulus. Once the stimulus is removed from the screen the monkey is asked to withhold its response for a variable period of time. The go cue is signaled by the offset of the fixation point after which the monkey is free to report its choice by saccading to one of the two visual targets on the screen. The monkey was trained to saccade to the left for leftward motion and right for rightward motion. **b)** Dots task timing. After a fixed delay from the fixation point onset the two targets were shown and would remain on until the end of the trial. The stimulus was shown for 1 of 3 durations which was constant for each session. The fixation point was removed after a random delay period had elapsed. The duration was random to prevent the monkey from timing its response. Adapted from (Shadlen and Newsome, 2001)

nature of the stimulus though, for a given coherence some sequences of frames will have slightly higher or slightly lower motion information and the best strategy for the subject to decipher the true coherence (and thus direction) is to integrate as many samples as possible over time. This created the perfect setting for studying the visual responses to a time-varying stimulus and later on to study decisions that unfold over time. After viewing the stimulus, the monkey was asked to report its perceived direction by performing a saccadic eye movement to one of two visual targets on the screen (each corresponding to one direction of motion).

It was already known that neurons in area MT are tuned to the direction of motion of visual stimuli and that these neurons clustered in columns of other neurons with similar preferred direction (Albright et al., 1984). What these researchers found

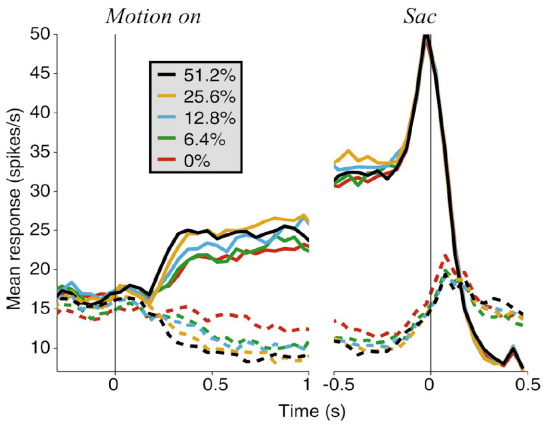

Figure 1.2: **Average neural response in LIP.** Firing rates as a function of time averaged for all 104 LIP neurons recorded. Activity was aligned to motion stimulus onset (left) and saccade initiation (right). Trials were sorted by choice and stimulus coherence (error trials not shown). Trials in which the monkey chose the target in (opposite to) the Response field (RF) are shown in solid (dashed) traces and. Adapted from (Shadlen and Newsome, 2001)

was that this brain area was in fact required to perform the dots task (Newsome and Paré, 1988) (through lesion experiments) and that one could bias the monkey's judgement by applying an external electrical current to a patch of tissue in MT (Salzman et al., 1990). This technique, known as electrical microstimulation took advantage of the columnar organisation of cells in MT and biased the monkey in a predictable way: stimulating a patch of cells that prefer leftward motion would lead to a strong leftward behavioral bias. Together these results suggested a causal role for MT in processing the visual stimulus, allowing the subjects to perform the task. Moreover, by recording individual neuron responses in MT while monkeys performed the task, these researchers found that these neurons responded in a way that covaried tightly with the stimulus direction and coherence and its ability to discriminate stimuli rivaled that of the subject (Britten et al., 1992).

Finally, these neurons also displayed trial to trial fluctuations, which weakly but significantly correlated with the ultimate choice of the monkey on those trials (Britten et al., 1996). Together, these results lead to the hypothesis that signals from pools of MT neurons with opposite preferred directions were being compared (subtracted) and informing the decision of the monkey (Britten et al., 1992). The researchers

hypothesized this resulting signal would be integrated over time by another brain area and used as a "decision variable" to determine which categorical choice would be made. Amongst candidate areas where this function could be implemented was Lateral Intraparietal Area (LIP). It receives strong visual inputs from MT (and MST) and projects to areas that directly control eye movements (Andersen et al., 1990) conferring it with the appropriate set of inputs and output to combine visual information about the stimulus and inform downstream areas about what movement to execute. Moreover, other studies had also demonstrated (Barash et al., 1991; Gnadt and Andersen, 1988) this area kept a steady representation of the location monkeys were asked to saccade to seconds before the action was initiated. Despite the promising combination of features no one knew what signals would be present in LIP during a cognitive task. The results of these experiments would transform the field of decision-making and have a strong impact in systems neuroscience as a whole. While monkeys performed the dots task, Bill Newsome and Michael Shadlen found cells in LIP that indeed seem to represent the integral of the difference in MT activity (Shadlen and Newsome, 2001). These cells responded to the dots presentation $\sim$ 200 msec after the stimulus onset (Figure 1.2). For stimuli supporting a saccade in the cell's response field (RF) firing rates were increased with a rate that covaried tightly with the motion magnitude. Symmetrically, for motion in the opposite direction firing rates were suppressed in a way that was also directly proportional to the motion magnitude. These observations suggest that indeed LIP is representing the accumulation of evidence captured by MT. During the delay period, the firing rates for each choice start to converge regardless of coherence, and for the choice to the RF they peak right around the initiation of the saccadic movement. This data suggests that late into the delay period and around the time of movement the integration of evidence has stopped and given way to a categorical choice that leads to the appropriate saccade.

More recently, additional experiments have suggested that motion information is indeed integrated by LIP. In these experiments pulses of motion were added to the regular stimulus on individual trials and LIP reflected the additional information (Huk and Shadlen, 2005) as did the subject's choice and reaction time. A microstimulation

experiment showed a causal but small effect of LIP stimulation in biasing the monkey's behavior towards the contralateral choice (Hanks et al., 2006). Other experiments performed without pre-selecting LIP neurons show that besides the canonical response profile (Figure 1.2) many other signals are present in LIP suggesting its involvement in other aspects of action selection.

Using a modified version of the task Kiani and Shadlen showed that not only choice and motion strength are reflected in LIP activity but also the uncertainty of the subject about its own decision (Kiani and Shadlen, 2009) and post-error adjustments in strategy (Purcell and Kiani, 2016), expanding even further the functions present in this area.

Complementing the findings from historical and current studies of perceptual decision-making in primate brain regions, newer studies have begun to employ rodents as an animal model and also the same rigorous psychophysical techniques and paradigms (Carandini and Churchland, 2013; Murakami and Mainen, 2015). For instance, researchers were able to train rats to proficiently perform complex olfactory (Uchida and Mainen, 2003), auditory (Brunton et al., 2013) and audiovisual discrimination tasks (Raposo et al., 2012). Combining proficient discrimination behavior with recordings from somewhat analogous brain structures to the primate brain, these researchers demonstrated that neurons in the posterior parietal cortex (Raposo et al., 2014), frontal orienting fields (Hanks et al., 2015), and secondary motor cortex (Murakami et al., 2014) amongst other areas, contain clear decision related activity that often conforms to predictions made by mathematical models of integration of evidence (Ratcliff, 1978; Mazurek et al., 2003). Besides faster iteration times and lower costs and risks associated with this type of research, rats also offer the exciting opportunity do take full advantage of genetic and optogenetic tools (Carandini and Churchland, 2013; Zalocusky et al., 2016). Optogenetics allows researchers to manipulate activity in specific circuits by shining light on targeted neurons, expressing light sensitive ion channels. By doing so, it is possible to dissect circuit function and establish a causal link between activity in these circuits and behavior. In recent studies (Hanks et al., 2015; Erlich et al., 2015) researchers combined a carefully designed behavioral

paradigm, electrophysiological recordings, and optogenetics to causally differentiate the roles of frontal orienting field neurons and parietal neurons in the integration of auditory evidence. While, opotogenetic tools are in development for primates (Diester et al., 2011) they are still not as robust and ubiquitous compared to those for rodents.

On the opposite end of the spectrum of model complexity, human studies have also made a significant contribution to the field of perceptual decision-making. Taking advantage of not invasive techniques (such as EEG or MEG) and similar behavioral paradigms to those used in animal models, researchers have shown the existence of signals that predict choice (Donner et al., 2009) and reaction time (Dmochowski and Norcia, 2015) and whose features are reminiscent of signals present on individual neurons of oculomotor structures of macaques. In some cases these signals are modulated by the quality of evidence on individual trials (Kubanek et al., 2013; O'Connell et al., 2012) suggesting similar processes of accumulation of evidence between humans and non-human primates. Importantly in several of these studies the areas thought to be the source of these signals are central and parietal areas of the brain which integrate the oculomotor and somatomotor system (Kubanek et al., 2013; O'Connell et al., 2012; Dmochowski and Norcia, 2015). These results further justify the study of individual neurons and populations of neurons in analogous brain areas of non-human primates by hinting at common mechanisms for cognition.

1.2 Primary Motor Cortex and Dorsal Premotor Cortex

Early on researchers hypothesized that areas that combine visual information and hold the decision of the subject in working memory might themselves "lend insight into the computation of the decision itself" (Shadlen and Newsome, 2001). Following this rationale the main targets for studying visually based decision making have been premotor structures that receive strong visual inputs and send signals to motor structures to execute movements. Since much of the work in the field has focused on the

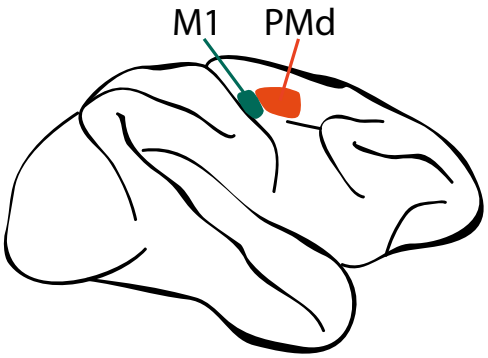

Figure 1.3: **Macaque Cortex.** Gross anatomy of the macaque cortex with M1 and PMd areas highlighted. Right side is anterior. Courtesy of Matthew Kaufman

oculomotor system, LIP and FEF have been the main targeted brain areas in previous studies. We wanted to expand and adapt this framework to the somatomotor system, a more complex modality used by primates to act on the world. The primate motor system is a complex network involving many cortical areas (parietal and frontal), as well as sub cortical areas and the cerebellum. In this project we focused on Dorsal Premotor (PMd) and Primary Motor (M1) cortices (Figure 1.3). The reasons for this particular choice are of anatomical, functional and also practical nature.

Anatomically, these areas receive short latency visual signals (as short as 80 msec in latency, see Song and McPeek (2010)) and also project directly to the spinal cord. In fact, together they account for 60% of the cortical spinal projections (Dum and Strick, 1991; He et al., 1995; Dum and Strick, 2002). The combination of inputs and outputs in these areas is at the base of their involvement in control of visually guided movements and potentially places them in a analogous position to LIP and FEF in the motor system.

Functionally, both PMd and M1 have been demonstrated to be responsible for movement execution and planning (Boussaoud and Wise, 1993; Weinrich and Wise, 1982; Weinrich et al., 1984; Tanji and Evarts, 1976). Besides extensive correlational data, microstimulation experiments have shown that muscle twitches can be evoked (Strick and Preston, 1978; Weinrich and Wise, 1982), movement plans can be disrupted (Churchland and Shenoy, 2007b) and simple or complex movements evoked Graziano et al. (2002) when external electrical current is applied to these brain re-

gions. These results confirm the causal role of these brain areas in both movement planning and execution. Together these functions have comprised the more canonical view of the functions carried out by PMd and M1. However, recent studies have expanded the repertoire of functions of circuits in PMd including a more cognitive role in decisions reported with arm movements. In one of these studies (Cisek and Kalaska, 2005) it was suggested that in a cued choice task, before the correct target was signaled, both choice plans were represented in some neurons in PMd, well before movement initiation. Later, the same group of researchers showed results supporting a more sophisticated mechanism that tracked the evidence supporting either categorical choice over time (Thura and Cisek, 2014).

Finally, another study showed strong evidence for the presence of neural correlates of complex cognitive operations such as vacillation or deliberation in PMd during a free or forced choice task (Kaufman et al., 2015). In comparison, M1 remains much more poorly characterised in the context of cognitive tasks perhaps due to the prevalent idea that it ought to *only* be involved in motor planning and execution given the overwhelming amount of evidence supporting that role. In that sense it wasn't as suitable as a candidate area for studying decision formation but the differences between M1 and PMd in a more cognitive setting had never been established in a way that was satisfactory to us.

In the end practical aspects also played a role in our choice of brain areas in which to study perceptual decision-making. Since performing multi-electrode recordings that could allow for single-trial analysis was a requirement, flat brain areas suitable for Utah array implantation were preferred. This method had been extensively and successfully used in PMd and M1 to implement Brain-Machine Interfaces (Santhanam et al., 2006; Gilja et al., 2012, 2015) and to study motor preparation (Churchland et al., 2006; Afshar et al., 2011; Kaufman et al., 2014) further supporting our choice.

1.3 Summary of thesis work

The subsequent chapters contain the main findings of my doctoral thesis project and their interpretation in the context of the existing literature. The methods used are described at the beginning of the corresponding chapter.

In Chapter 2 we describe the modified motion discrimination task and multi-electrode recordings we use to study decision formation. We demonstrate that subjects perform extremely well and that diverse neural responses are present in both PMd and M1. Crucially a fraction of the recorded neurons represents the evolving decision from very early on in the trial, which will serve as a window into the decision formation process.

In Chapter 3, we take full advantage of our simultaneous recordings and show evidence for strong and interpretable single-trial decision formation signals in both areas. These signals are surprisingly flexible and adapt to the cognitive demands imposed on the subject.

In Chapter 4, we start by drawing comparisons between our own results and data obtained in LIP by another research group. We go beyond describing choice predictive signals and provide a more complete picture of other variables represented in PMd and M1 during the motion discrimination task. Furthermore, we compare our decision-related activity in PMd and M1 across motor effectors and demonstrate some of these signals are supra-modal.

In Chapter 5, we go one step further and test a real-time setup we built, that attempts to decode nearly instantaneous decision states. We find an impressive match between predicted and observed likelihood of choice and validate small and fast fluctuations in the decision state. After learning our nearly instantaneous Decision Variable has a clear and predictable bearing on behavior we use this setup and framework as a tool to study changes of mind. Changes of mind are a complex cognitive phenomenon whose validation at the neural level has been extremely challenging to perform.

Finally in Chapter 6 we discuss the results reported in this thesis and elaborate on how they fit with the literature in the field.

2

Response properties of dorsal premotor and primary motor cortex

The perceptual decision-making field has, to a large extent, been shaped by seminal studies done in parietal and frontal areas of the oculomotor system (Shadlen and Newsome, 2001; Roitman and Shadlen, 2002; Mante et al., 2013). Individual neurons in these areas carry choice-related signals that match predictions made by mathematical models of integration of visual evidence (Ratcliff, 1978; Mazurek et al., 2003) and have been interpreted as correlates of decision-formation that express "decision variables". The main hallmarks of these choice predictive signals are:

- Short latency from the onset of the stimulus which the subject is going to evaluate in the process making a choice.
- Increasing magnitude over time as more evidence comes in through the visual system and the decision becomes categorical.
- Lawful dependence on stimulus difficulty: stronger rise (slope) for easier stimuli and weaker rise for harder stimuli.
- Stronger dependence on choice than stimulus: for two presentations of the same stimulus that lead to opposite choices, the activity levels should be quite dif-

ferent since the decision-signals are strongly choice predictive and only slightly stimulus predictive.

- Stronger magnitude for correct than incorrect choices within a stimulus difficulty level.

While a tremendous amount of knowledge has been acquired through past studies many questions and limitations remain. First, are the mechanisms general or are they specific for the oculomotor system? In most prior studies the decision-related areas being studied are part of the visual stream processing the stimulus itself. It could be that the properties reported in these decision areas are a consequence of the projections from visual areas processing the motion and strength of the stimulus such as area MT. Moreover, while having monkeys report a decision with an eye movement enables high experimental control and precise quantification of the subject's behavior it is not the only type of response primates would likely use in a naturalistic context. Limb movements such as arm movements are used to report decisions in different contexts such as running or climbing to avoid predators or grooming another member of the colony. While (especially) PMd and (perhaps) M1 seemed good candidate areas for studying decision formation in the somatomotor system, the literature in this field is still scarce despite the growing interest in this line of research in recent years (Coallier et al., 2015; Thura and Cisek, 2014; Kaufman et al., 2015; Hoshi, 2013; Pastor-Bernier and Cisek, 2011). PMd and M1 have been extensively studied in the context of motor preparation and execution (Georgopoulos et al., 1982; Churchland and Shenoy, 2007a; Churchland et al., 2010), but in comparison to oculomotor structures, little has been done using cognitive tasks. This difference comes from the fact that, until recently(Cisek and Kalaska, 2005), somatomotor areas such as PMd and M1 were thought to mostly carry motoric signals due to their proximity to the motor periphery. Despite being tempting to speculate about parallels between the cognitive signals extensively described in the oculomotor system and those hinted by some of these recent studies in the somatomotor system, there is little hard data to establish that comparison. Second, most studies in the oculomotor system (Shadlen and New-

some, 2001; Roitman and Shadlen, 2002; Kiani et al., 2008) have pre-selected neurons for strong delay period activity during delayed saccade or memory saccade tasks. This response feature has been assumed to be a good predictor of decision related activity in perceptual discrimination tasks. While this approach has yielded neurons with fairly homogeneous and task relevant responses, it also hides the natural diversity of neural responses in these areas. A recent study has tackled this limitation with surprising results (Meister et al., 2013).). By recording LIP neurons without pre-screening them for strong delay activity, researchers found the canonical ramping neurons are just a subset of much more diverse pool of neurons. Many other neurons represent other signals that, despite being task-related, can't easily be interpreted as a neural correlate of evidence accumulation. Moreover, even the correlation between delay activity in a memory guided saccade task and decision related activity during the dots task turned out to be weaker than initially expected, especially when considering a larger pool of neurons. In another study (Mante et al., 2013), researchers applied a similarly unbiased approach and combined it with an order of magnitude increase of the typical number of recorded units from one to two hundred to over a thousand. Having such a massive dataset allowed researchers to determine that all combinations of selectivity for task relevant signals (context, stimulus motion, stimulus color and choice) were present across cells in PFC, with no clear distinct clusters or categories. Obtaining a deeper understanding of what neural circuits are doing in the context of perceptual decision tasks requires an unbiased recording and analysis approach.

Our goals for the studies in this chapter were fourfold:

1. To successfully employ a variant of the classical motion discrimination task in which we replaced the eye movement response with an arm movement response. This change will allow us to tackle the lack of cognitive tasks used study decision formation in somatomotor areas PMd and M1.

2. To implement, in parallel, a chronic multi-electrode recording technique widely used to study motor preparation and execution in these same brain areas (Church-

land et al., 2006; Afshar et al., 2011; Kaufman et al., 2014) and to implement neural prostheses for the motor system in both human and non-human primates (Santhanam et al., 2006; Gilja et al., 2012, 2015). This technique provides great spatial coverage of these superficial areas and enables an unbiased characterization of neural responses. We further this unbiased approach by analyzing all recorded units without a pre-screening process.

3. To broadly describe the spectrum of individual neural responses during the fixed duration motion discrimination task by leveraging goals 1 and 2 and look for examples of neurons carrying decision-related signals as defined by their hallmarks.

4. To obtain an overall picture of the strength and distribution of choice predictive activity across units and time.

Author contributions: Diogo Peixoto, Roozbeh Kiani and William Newsome designed the behavioral task. Diogo Peixoto and Sania Fong trained the subjects until full proficiency was achieved. Diogo Peixoto and Stephen Ryu performed the surgery to implant the Utah arrays. Diogo Peixoto ran the experiments to collect the data, performed the analysis and generated the figures presented in this chapter.

2.1 Methods

2.1.1 Subjects

We recorded from populations of neurons in dorsal premotor and primary motor cortex of two macaque monkeys performing a direction discrimination task with arm reaches as the operant response. All training, surgery, and recording procedures conformed to the National Institutes of Health Guide for the Care and Use of Laboratory Animals and were approved by Stanford University Animal Care and Use Committee.

2.1.2 Direction Discrimination Task

The task employed is a variation of the classical dots discrimination task, in which uses an arm movement as the operant response. We used two variants of this task that differed based on the stimulus duration employed. The first version we implemented was a classical fixed duration task, in which every stimulus presentation lasted 1000 ms. We termed this version the fixed duration task. In contrast, we also employed a version in which the duration of the stimulus presentation varied from trial to trial. The stimulus duration ranged from 200-1000 (median 435 ms) and it was randomly chosen on each trial by sampling an exponential distribution. We termed this version, the variable duration task. Within the variable duration task we employed two sub-variants: one with delay period, similar in that regard to the fixed task and one without delay period. We will refer to the two specific tasks as variable duration with delay and variable duration with no delay from here on. For all variants, the trial starts with the onset of a fixation point (FP; 1.5 degree diameter) on a video touchscreen (ELO Touchsystems 1939L, Figure 2.1). To initiate the task, the monkey was required to maintain both eye and hand fixation within +/- 3 degrees of the FP as long as it remained on the screen. Eye position was continuously tracked with an electronic eye tracker at 1KHz (EyeLink 1000, SR Research, Canada) and hand position was tracked at 75Hz using the video touchscreen Importantly, throughout the entire trial, the monkey was required to always maintain direct hand contact with the screen otherwise the trial would be aborted.

After 300 ms of fixation, two targets (1.5 degree diameter) appeared on opposite sides of and at same distance from the FP. After a 500 ms delay the random dot stimulus was presented for either 1000 ms (fixed duration) or 200-1000 ms (variable duration), depending on the task variant, after which it was removed from the screen. On each trial a fraction of the dots moved coherently along the horizontal axis in the 0 and 180 degrees directions. The monkey was asked to report the net direction of motion by reaching to the target in the corresponding direction. The difficulty of the task was adjusted by changing the fraction of dots moving coherently in one direction

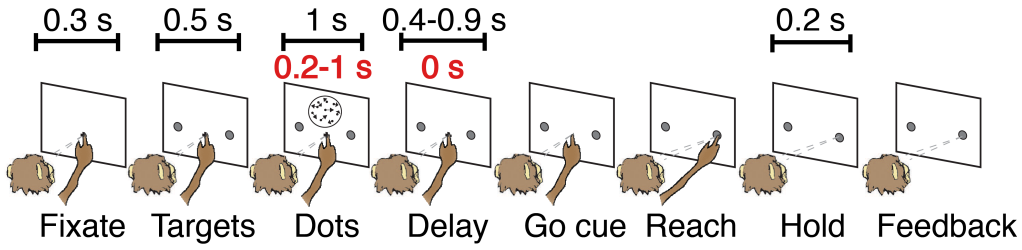

Figure 2.1: **Behavioral Task.** a) Direction discrimination task structure - Trials start with the onset of a fixation point (FP) on the touchscreen. Once both eye and hand fixation are acquired two targets appear on the screen. The motion stimulus was shown after a short delay (500 ms) and lasted 1000 ms (200-1000 ms) for the fixed (variable) duration version. The dots offset was followed by a 400-900 ms delay in the fixed duration and variable duration with delay versions whereas no delay was present for the variable duration with no delay task. At the end of the delay or dots (if there was no delay), the offset of the FP cued the monkey to go and report his decision by making a hand reach movement to the appropriate target. Correct trials (for which the monkey reached for the target corresponding to the stimulus net direction of motion) were rewarded with a drop of juice whereas incorrect trials lead to a small timeout (2-4 seconds).

(motion strength) (Britten et al., 1992). After the stimulus offset the monkey either entered a delay period during which it was required to withhold his response for 400-900 ms (for the fixed duration task and the variable duration task with delay) or was immediately presented the go cue (variable duration task with no delay). The go cue was then signaled by the offset of the FP at which point the monkey was free to gaze anywhere and report his decision with his arm by reaching one of the two targets. Although gaze was monitored, reward acquisition depended solely on reaching to the correct target. Finally, for a response to be considered valid, the monkey was required to hold its hand position within +/- 4 degrees of the center of the target for 200 ms. The monkey was then rewarded with a drop of juice for correct choices and given a timeout (2-4 seconds) for incorrect ones. Zero coherence trials were rewarded randomly with a probability of 0.5 since there was no correct response on these trials.

2.1.3 Random dots stimuli

The stimuli used in our psychophysical experiment were random dot kinematograms (RDK) generated using MATLAB and Psychophysics Toolbox. Stimuli were presented on a 19-inch LCD touch monitor (Elo Touchsystems) with 75 Hz frame rate and 800 x 600 pixels resolution positioned 30 cm away from the monkey. The details for generating the random dots stimuli have been described previously (Kiani et al., 2008). We used the same algorithm and parameters except: (1) the stimulus duration was fixed at 1 s for the fixed duration task and variable from 0.2s -1 s in the variable duration task; (2) the diameter of the stimulus aperture was 14 degrees, and (3) the speed of the dots was 8 degrees / second. The dot density was 16.7 dots deg-2 s-1, and the dot size 2 pixels. To create the impression of motion, the dots in the RDK were split into 3 consecutive sets with the same number of elements (1 set displayed for each individual frame) and displaced 3 frames (40 ms) later. The fraction of dots displaced coherently toward one of the two targets was determined by the coherence (motion strength), with the remaining dots being displaced randomly. For both monkeys, the motion strength could take one of 6 possible values: 0%,3.2%,6.4%,12.8%,25.6% and 51.2%. The direction and coherence of the motion were randomly assigned on each trial by sampling from a uniform distribution with replacement. For zero-coherence stimuli all dots were displaced randomly but, due to the stochasticity of that process, one obtains non-zero net motion toward the targets over a small number of frames.

2.1.4 Behavioral Performance

Training 2 monkeys to perform all versions of the dots discrimination task with excellent behavior required a very thorough operant conditioning protocol. The protocol had to be adapted to the individual monkeys since they had very different training histories: monkey H was a naive monkey whereas monkey F had been trained on a saccade version of the motion discrimination fixed duration task. Monkey H started by being rewarded just for touching the touchscreen and then gradually progressed to an instructed reach task and from there to a delayed reach task. Once he was pro-

ficient in using the touchscreen, the dots stimulus was introduced, cueing the correct target to reach to at the end of the trial. Only easy coherences were used at first, with lower and lower coherences being introduced gradually until the final set was used. The final component of training was eye fixation. Eye fixation was trained by introducing blocks of trials for which the front plate of the primate chair was closed, cueing the monkey to perform the task with eye movements. The fixation window size was gradually decreased, and then eye fixation was also required during the reach blocks. By aborting trials if eye or hand fixation was broken the subject learned both were required to perform the final task. Monkey F on the other hand was already proficient at discriminating motion so the main focus of training was achieving proficient use of the touchscreen with his hand. The same initial sequence of steps was used to train monkey F to perform delayed reaches. From that point on, the training was focused on combining the knowledge about the previous knowledge dots task with the reaching response. Coherences were also introduced sequentially from highest to lowest but at much faster pace compared to monkey H. Recording sessions only started when good psychophysical performance was achieved. Psychophysical performance was assessed in two ways: by describing the percentage of correct choices as a function of (unsigned) stimulus coherence and by describing the percentage of right choices as a function of signed stimulus coherence. The percentage of correct choices as a function of motion strength (stimulus coherence) was fit by a cumulative Weibull distribution function:

$$P_{correct}(c) = 1 - 0.5 \times e^{(-c/\beta)^{\alpha}} \tag{2.1}$$

where $P_{correct}(c)$ is probability correct, c is motion strength, α is the psychophysical threshold (the value of c that corresponds to 82% correct responses), and β is a parameter that controls the shape of the function, especially its steepness.

The percentage of rightward choices as a function of motion strength and direction, P_{right}, was fit by a logistic regression:

$$P_{right}(c) = \frac{1}{1 + e^{-\beta_1 \times (\beta_0 + c)}} \tag{2.2}$$

The motion strength corresponding to the indifference point, β_0, was used to assess the monkeys bias on each session.

In addition to psychophysical performance two behavioral metrics related to the arm reach itself were also quantified: reaction time (RT) and hand velocity. To obtain precise measurements of reaction times and maximum hand velocity we used the raw hand position data on each trial. We started by up-sampling the raw data by a factor of 13 to obtain artificial 1 ms resolution (since it had been acquired at 75Hz). Then we smoothed the up-sampled data by performing local linear regression to obtain smooth hand traces for each trial. The instantaneous velocity was calculated as the norm of the sum of vertical and horizontal speed components (the instantaneous derivative of the position). The peak hand velocity was calculated for each trial and reaction time was determined as the interval between the presentation of the go signal and the time point at which 20% of the peak velocity was reached.

2.1.5 Array locations and recordings

2 multielectrode arrays (Blackrock Microsystems, Utah) with 96 electrodes each (1mm long platinum-iridiidium electrodes, 0.4 mm spacing, impedance 400 KOhm) were implanted in primary motor and dorsal premotor cortex of each monkey (Figure 2.2). The arrays were placed anterior to the central sulcus, posterior to the arcuate sulcus and lateral but near the superior pre-central dimple (Churchland et al., 2010). Prior to the array implantation, single electrode recordings were performed (FHC, Maine) by lowering dura-piercing electrodes (tungsten, average impedance 6 MOhm) through burr holes, to determine the best location for the arrays. M-L position was determined by performing muscle palpation during recordings and searching for a strong upper arm representation; A-P position was determined by strong perimotor/delay activity in a delayed reach task for M1/PMd, respectively. The coordinates for the best sites were calculated with respect to the center of the chamber and verified during surgery

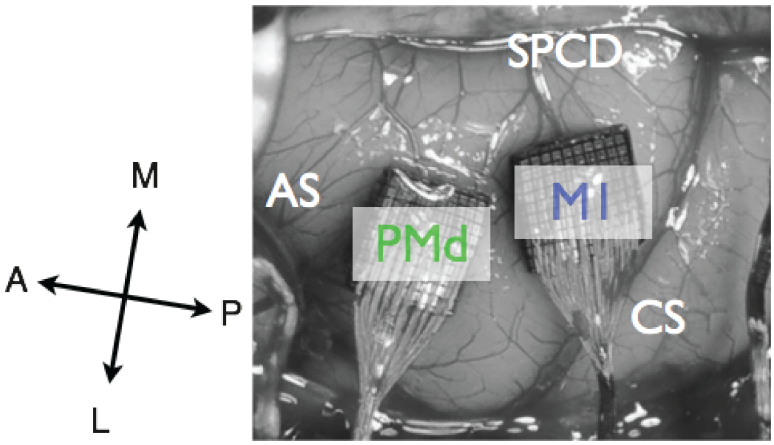

Figure 2.2: .
Chronic implantation of Utah arrays. Location of the two multielectrode arrays implanted in primary motor and dorsal premotor cortex with respect to anatomical references (Monkey H): A-anterior P-posterior M-medial L-lateral. Arcuate Sulcus (AS), Central Sulcus (CS), Superior Pre-central Dimple (SPCD)

using stereotaxic measurements. These coordinates were used to the best extent to determine the final location of the arrays, subject to anatomical constraints (curvature of the cortex, blood vessels etc). Continuous neural data were acquired and saved to disk from each channel (sampling rate 30 kHz) and thresholded at -4.5 RMS (Figure 2.3). Waveforms corresponding to threshold crossings were sorted offline (Plexon Inc., Dallas) using both semi-automatic clustering methods and manual sorting. For all analysis presented in this thesis we did not differentiate between single-units and multi-units. Our goal was maximize population predictive power and spatial coverage of the cortex and not just to select the very best isolated single-units. The number of units collected in each experimental session typically ranged from 100-180 per array.

2.1.6 Datasets

For each task version and monkey we analyzed all datasets from each brain area that met two behavioral inclusion criteria: 1) over 750 trials and 2) a behavioral bias ($|\beta_0|$) under 5%, as determined by a logistic regression fit.. These criteria were imposed to guarantee we have a sizeable number of trials per condition (6 coherence x 2 directions = 12 conditions) and that the behavior of the monkey is virtually

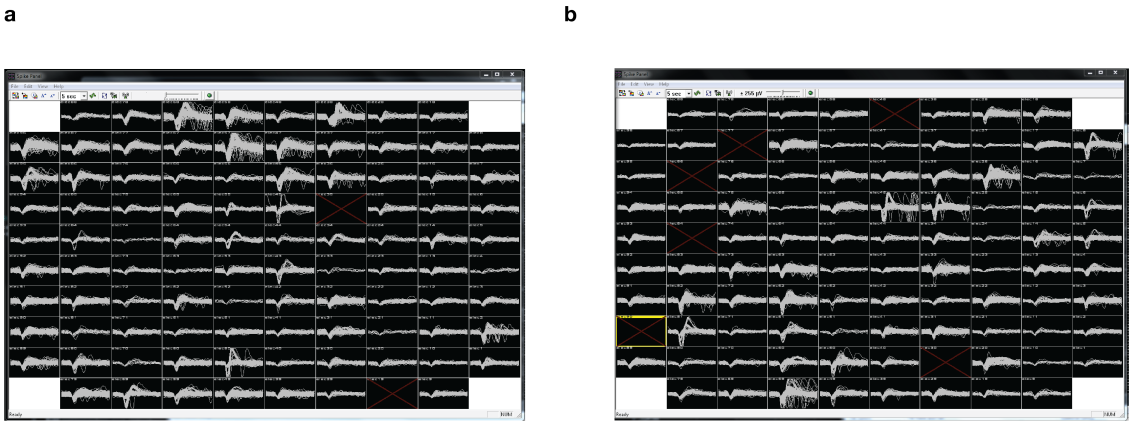

Figure 2.3: **Electrophysiological Recordings.** Snapshot of the waveforms captured through the 192 Channels corresponding 2 the Utah Arrays in **a)** PMd and **b)** M1. Data is shown for the same recording session in Monkey H.

unbiased, such that both neural and behavioral results are more easily interpretable. These criteria resulted in a selection of 9 (7) sessions of the fixed duration task and 6 (5) sessions of the variable duration task with no delay for monkey H (F), respectively. Data from both areas was collected simultaneously and the same recording sessions were used.

2.1.7 Peri-stimulus time histograms (PSTHs)

PSTHs were generated by aligning spike trains of each trial to relevant task events: target onset, stimulus onset, go cue, and movement initiation. These spike trains were then convolved with a gaussian kernel with a 50 msec acausal and a 50 ms causal component. The standard deviation of the gaussian used was 30 msec. The resulting spike density functions were then sorted by experimental condition. For the red/blue PSTHs we sorted trials based on the final choice of the monkey (left or right) and whether the reported decision was correct or wrong (correct wrong). For the black and grey PSTHs we focused on coherence and choice effects thus sorting the trials by choice (left or right) and the coherence of the stimulus: 3.2%, 12.8% and 51.2%. The other 3 coherences were not plotted to prevent crowding the figures. Only correct choices were selected for this figure, meaning the direction of the stimulus and the choice of the monkey are always congruent. Once the trials were selected for the

specified condition, their spike density functions were averaged.

2.1.8 Choice predictive activity

For each cell, choice modulation was calculated as the average difference in spike counts between correct right choices and correct left choices in a 50 msec window. These spike counts were calculated at 3 different timepoints in the trial (end of dots presentation, go cue and reach initiation) and then converted into firing rates. To assess the statistical significance of the difference between the two choices we implemented a Wilcoxon rank sum test that tests the hypothesis that median firing rates for the two choices are identical and rejects it at $p<0.001$.

2.2 Results

2.2.1 Behavioral results

We employed a classical direction discrimination task (Britten et al., 1992), in which monkeys are asked to report the net direction of motion in a random dot kinematogram presented on a LCD touchscreen Figure 2.1). In contrast to most studies that have used this paradigm (Britten et al., 1992, 1996; Shadlen and Newsome, 2001), the operant response was an arm reach to one of two targets corresponding to the perceived direction of motion instead of a saccadic eye movement. In the fixed duration task the stimulus was always presented for 1000 ms followed by random delay period (400-900 ms) after which the monkey was cued to report a decision. After extensive training on this task and as expected from previous studies using a similar paradigm, monkeys displayed excellent behavioral performance in this task, achieving close to 100% accuracy for high coherence stimulus (Figure 2.4). The monkeys' performance decreased smoothly with stimulus difficulty (lower coherence) and remained above chance for the lowest (non-zero) coherence stimulus (3.2%). For 0% trials the performance was at chance levels as expected. Psychophysical thresholds were 11.1% and 12.8% stimulus coherence for Monkey H and F, respectively (see Methods).

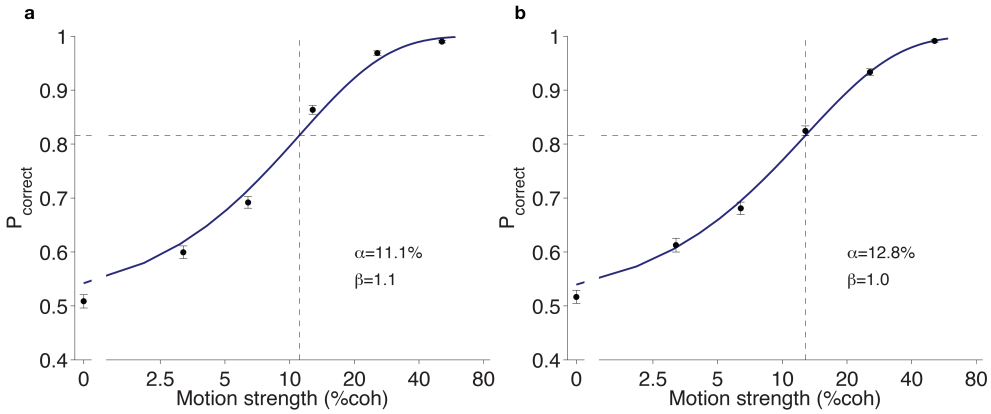

Figure 2.4: **Behavioral performance - Fixed duration task. a)** Psychophysical performance for Monkey H in the variable duration task. Percentage correct is plotted as a function of net motion coherence (calculated for both directions). Data points are fit with a Weibull curve. **b)** Same as **a)** for Monkey F.

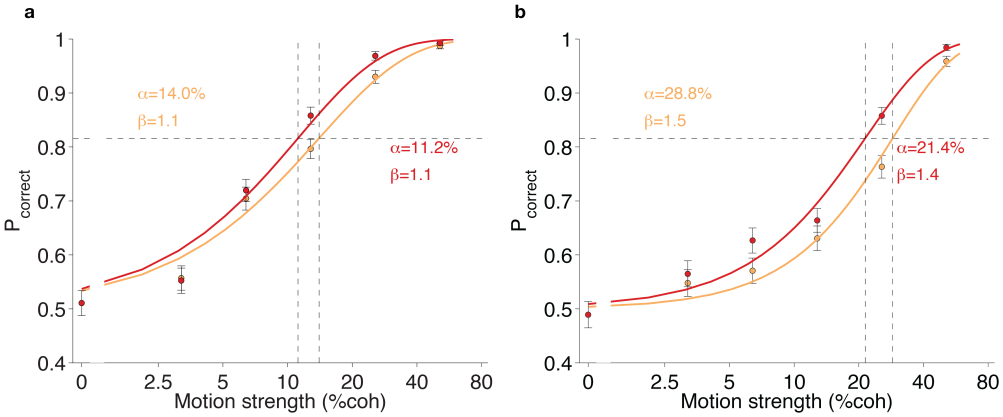

Figure 2.5: **Behavioral performance - Variable duration task (no delay). a)** Psychophysical performance for Monkey H in the variable duration task with no delay. Percentage correct is plotted as a function of net motion coherence (calculated for both directions). Data points for long (red) and short (orange) stimuli are fit separately by a Weibull curve. **b)** Same as **a)** for Monkey F.

After data collection was concluded in the fixed duration task, monkeys performed a variable duration task, which required a modest amount of retraining to obtain excellent behavior. For this new version of the task, the stimulus duration was randomly selected on each trial (200-1000 ms, median 435 ms), and for the vast majority of sessions (no delay variant) the delay period eliminated, requiring subjects to report their decision immediately after stimulus offset. While the best strategy for the motion discrimination task is always to integrate as many stimulus samples

as possible, due to the noisy nature of the stimulus, the results shown so far have not confirmed the monkeys were indeed doing that. One of the advantages of using a variable duration stimulus is the ability to compare performance for different ranges of stimulus duration. The behavioral results for the variable duration show that both subjects performed better for longer stimuli suggesting additional visual evidence was integrated to improve decisions (Figure 2.5). This effect tapered off with performance saturating between the 3rd and 4th quartile of stimulus duration (not shown) suggesting that both monkeys used additional evidence provided by longer stimulus durations, but only up to a certain point. This is also compatible with results found in previous studies (Kiani and Shadlen, 2009). The main advantage of the variable duration task is the ability to query the subject as soon as the stimulus is terminated. However, this advantage comes at the cost of not having the convenient temporal separation between evidence integration (dots period), action planning (hold period) and action execution (post-go period) afforded by the fixed duration task. For this reason, and only for monkey H, we ran a hybrid version that had the same duration for dots stimulus as the variable duration task (200-1000 ms) and the same delay period of the fixed duration task (400-900). We called this version "variable duration with delay" and will use it as a control for the other 2 tasks in Chapter 3.

Besides describing discrimination performance as function of stimulus strength in the dots task we also quantified the relationship between reaction time (RT) and stimulus strength (Figure 2.6 and Figure 2.7). Since none of the task versions used in our study are self-paced but are instead under the control of the experimenter (the subject always has to wait for the go cue), the reaction times quantified are not classical reaction times but instead "post go cue" reaction times. Nevertheless, this metric allows us to compare the readiness of the subject to report its decision as a function of stimulus difficulty and also across task versions. While RTs vary from subject to subject, in both cases (and both tasks) the median values are only slightly longer than the average for much simpler instructed reach tasks (Churchland and Shenoy, 2007b). This observation suggests that, on most trials, the monkeys are well prepared to report their decision once the go cue is presented. Interestingly there is

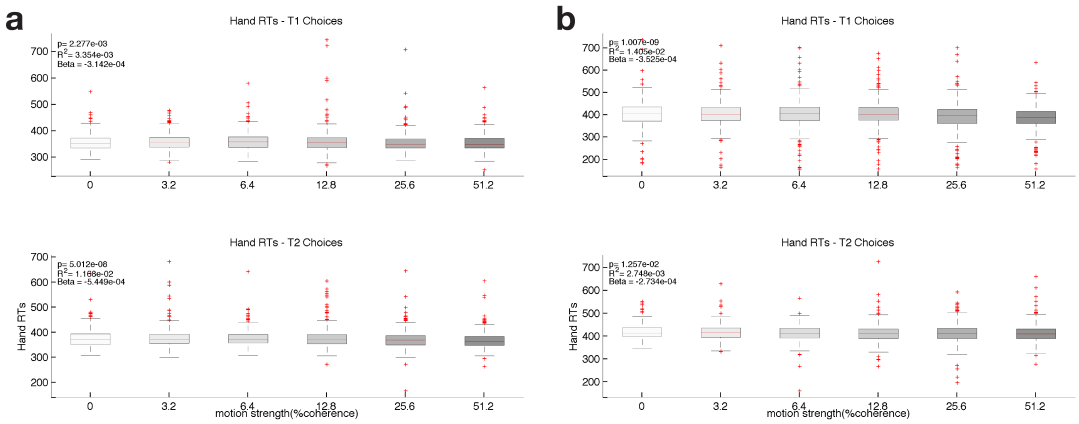

Figure 2.6: **Hand RT as a function of coherence - Fixed Duration. a)** Hand Reaction Times for left choices (top) and right choices (bottom) as a function of stimulus coherence for Monkey H. Box shows median RT (red) and 25th and 75th percentile and whiskers show most extreme data points not considered outliers. Red crosses show outliers. Inset denotes the results of a linear regression of RT on coherence. **b)** Same as **a)** for Monkey F.

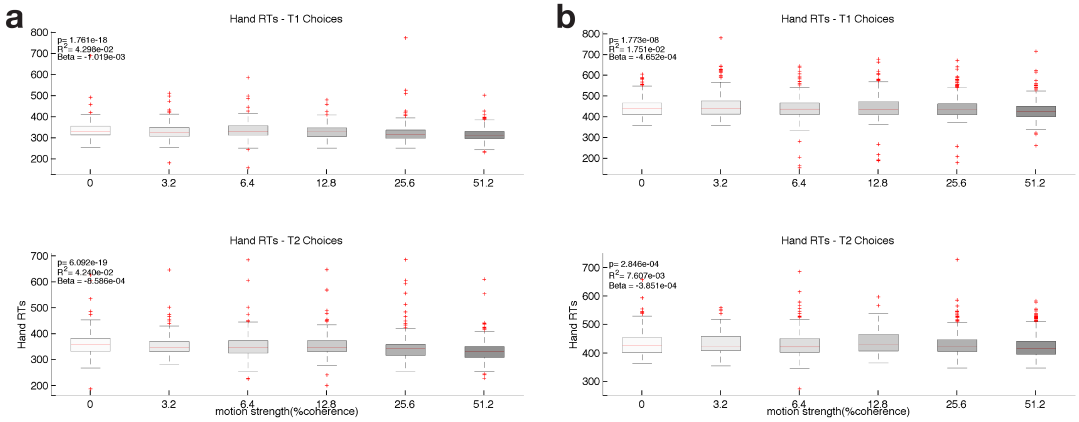

Figure 2.7: **Hand RT as a function of coherence - Variable Duration. a)** Hand Reaction Times for left choices (top) and right choices (bottom) as a function of stimulus coherence for Monkey H. Box shows median RT (red) and 25th and 75th percentile and whiskers show most extreme data points not considered outliers. Red crosses show outliers. Inset denotes the results of a linear regression of RT on coherence. **b)** Same as **a)** for Monkey F.

a small but highly significant effect of coherence on RT: easier trials are associated with slightly shorter RTs when compared to harder trials. This effect is present for all monkeys, task versions and directions of reach and, even though its magnitude is only ∼20-30 ms, it could be a signature of higher confidence in the decision for easier trials. Because these RTs don't correspond to the time of commitment to a choice

(plus a motor delay) making strong statements about their origin becomes difficult. To our surprise, the RTs for a given monkey and direction of reach were very similar between the fixed duration task (Figure 2.6) and the variable duration task(Figure 2.7). This result shows that even when the stimulus presentation is terminated at an unpredictable time, the subjects do not require additional time to commit to a decision, once the go cue is presented.

2.2.2 Diversity of responses of individual neurons in PMd and M1

We recorded neural activity in PMd and M1, using 2 chronically implanted 96-channel Utah arrays, while the subjects performed each of the motion discrimination task (Figure 2.1).

Consistent with recent studies in PMd (Cisek and Kalaska, 2005) we found very diverse responses on a single cell level in this area, which we believe reflect the multiple functions being implemented there. Importantly, we found cells with strong peri-movement activity (Figure 2.8). These cells, had very low firing rates during the entire trial up until around the response period, at which point their firing rates increased sharply and peaked right around the beginning of the arm movement. In some cases these cells were very strongly tuned to reach direction, and thus choice, (Figure 2.8 a) while other cells were broadly or weakly tuned (Figure 2.8 b). Finding these cells also constituted an important sanity check: it confirmed that we were recording in patches of PMd strongly correlated with arm movement execution. Finding and establishing stereotaxic coordinates for these locations in cortex (for array placement) was not trivial, even when recording responses with single electrodes during palpation and manipulation of the arm. Locating the arm-related regions of PMd was an absolute requirement for us to have any chance of finding decision-related activity in the somatomotor system during our task (in which decisions are reported through an arm movement). Had the arrays been erroneously implanted in a different region of the topographic motor map, we would never have found relevant task-related activity let alone decision-related activity. Since the Utah arrays were implanted chronically,

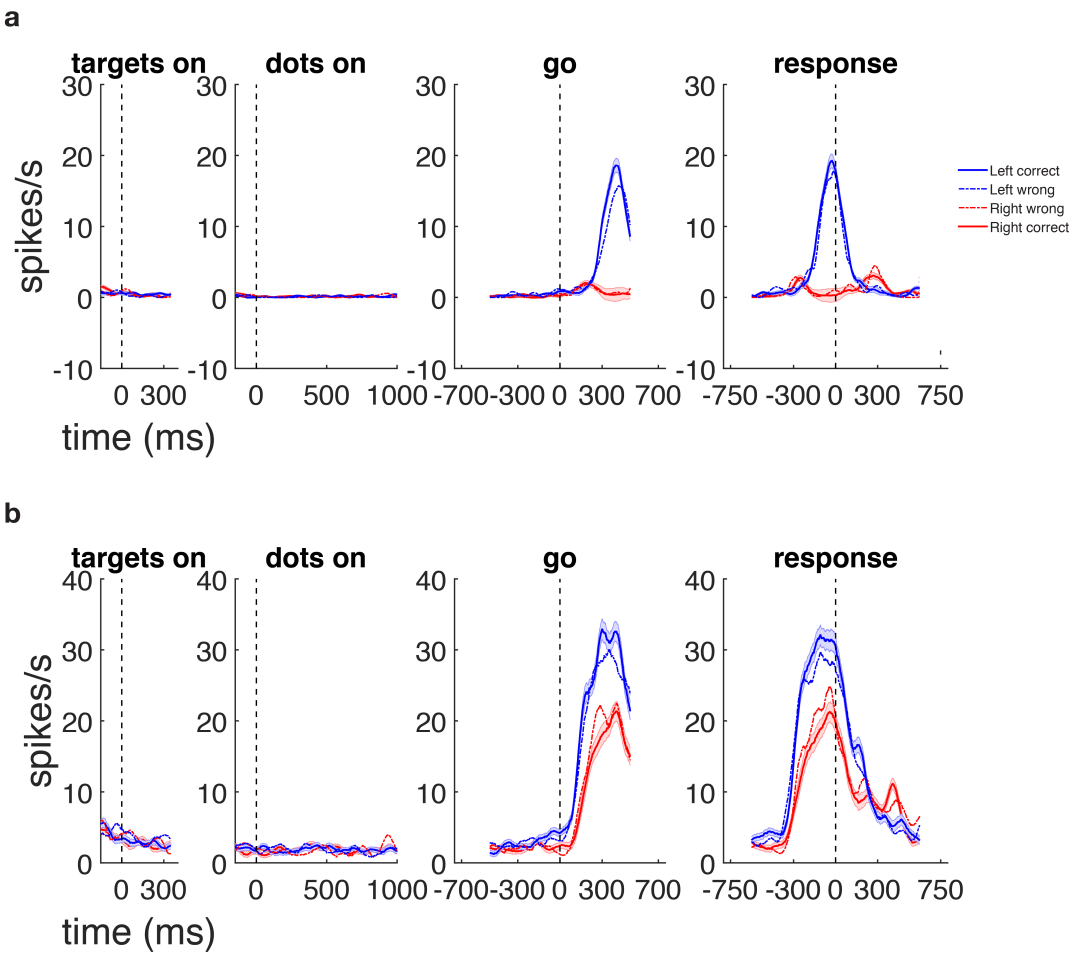

Figure 2.8: **Single neuron responses in PMd - peri-movement activity a)** Neural activity of a well isolated single neuron in PMd. Activity is aligned to 4 events in the task: targets onset, dots onset, go cue and response. Solid red (blue) lines show average activity level for +/- s.e.m. for correct right (left) choices. Dashed lines show incorrect choices to the target of corresponding color: red for right and blue for left. **b)** Same as **a)** for a different PMd cell recorded during the same session.

there was no flexibility to change its location once they were implanted, further raising the stakes for finding the right patches of cortex.

Finding cells with strong peri-movement activity tuned for reach direction was crucial for this project, but it was also insufficient. Had this been the only kind of cells we found, we would have only confirmed the classic view of premotor cortex: that it is post-decisional and hence responsible for planning and executing movements after other parietal or frontal areas have carried out the decision formation process. For-

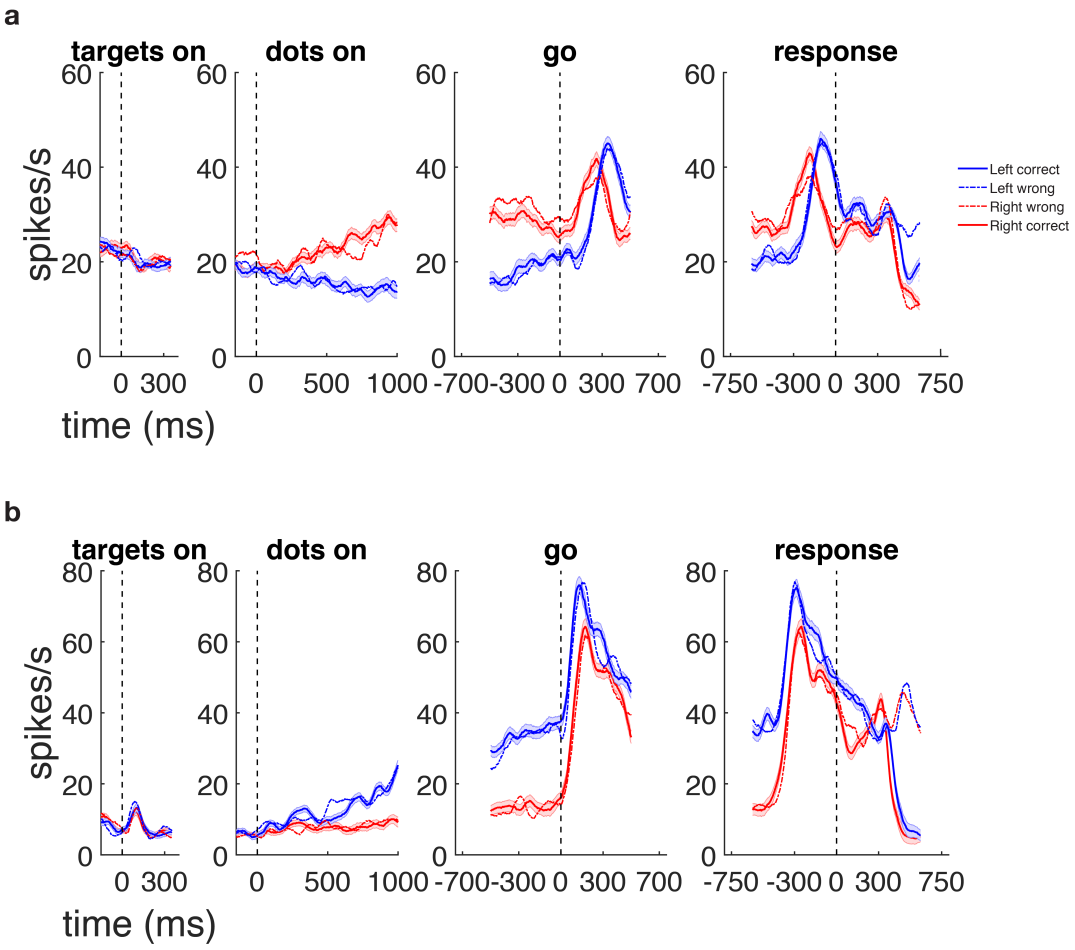

Figure 2.9: **Single neuron responses in PMd - early choice predictive activity** **a)** Example of a single neuron with strong choice predictive activity early in the dots period (separation between red and blue traces). The same choice preference (right) is kept but weakened in the delay period leading up to the go cue. **b)** Another neuron with early choice predictive activity with opposite (left) choice preference. For this cell the predictive activity is strengthened throughout the delay period. Same color convention as Figure 2.8

tunately, however, our expectation that cells with very short latency decision-related activity existed in PMd was confirmed. For both neurons illustrated in Figure 2.9, neural activity is modulated by the upcoming choice of the monkey ∼200-250 msec after onset of the random dot stimulus. Modulation with choice increases throughout the dots period: a hallmark of decision-related activity as the subject acquires more evidence and becomes increasingly confident about the upcoming choice.

As the trial unfolds the patterns of these two example PMd cells become more

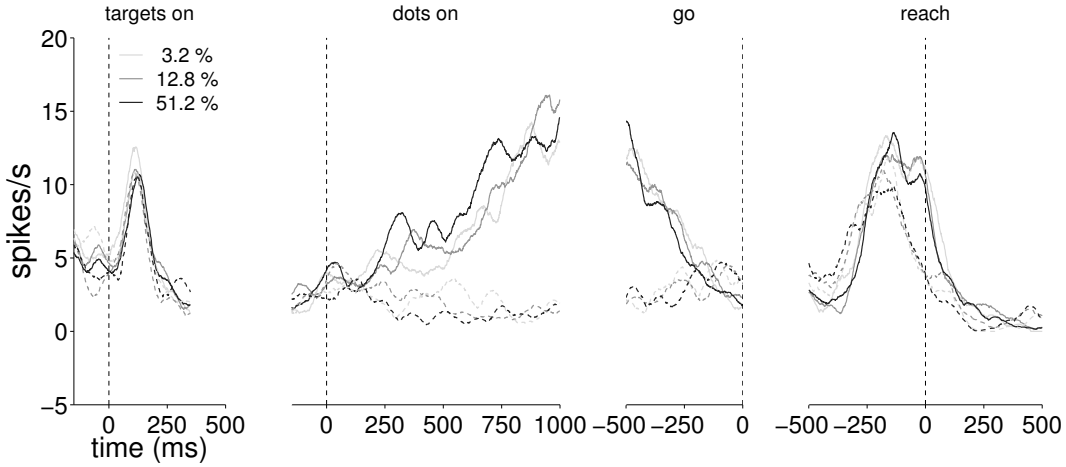

Figure 2.10: **Example neuron in PMd with coherence dependent choice predictive activity during dots** Example neuron with short latency choice predictive activity that depends on the difficulty of the stimulus during the dots presentation. Notice the larger separation between the dark lines (high coherence trials) compared to the light lines (low coherence trials). Different shades of grey from dark to light represent 3 different coherence levels: 51.2%, 12.8% and 3.2%, respectively. Dashed lines correspond to right choices and dashed lines to left choices. Only correct trials were plotted.

complex with modulation sometimes increasing (Figure 2.9 b) or decreasing during the delay period leading up to the go cue (Figure 2.9 a). Even around the time of reach the patterns aren't as simple as those seen in Figure 2.8: The cell in Figure 2.9 a) has two firing rate peaks of similar magnitude one for each reach direction that occur at different timepoints while the cell in Figure 2.9 b) peaks for both directions at the same time but with different and time-varying magnitude.

In Figure 2.10 the ramping activity during dots is strikingly resemblant of LIP response patterns in the same epoch and task (Shadlen and Newsome, 2001): the magnitude of slopes for both choices was larger for high coherences than low coherences. This is another hallmark of decision-related activity that we expected to be present in PMd. For this particular neuron however the activity during the delay and response periods is significantly less choice predictive and therefore less interpretable in the context of decision formation. This diversity of response properties across cells and even within cells across epochs highlights the fact that there is no such thing as a canonical PMd neuron ((Churchland and Shenoy, 2007a; Churchland et al., 2010)):

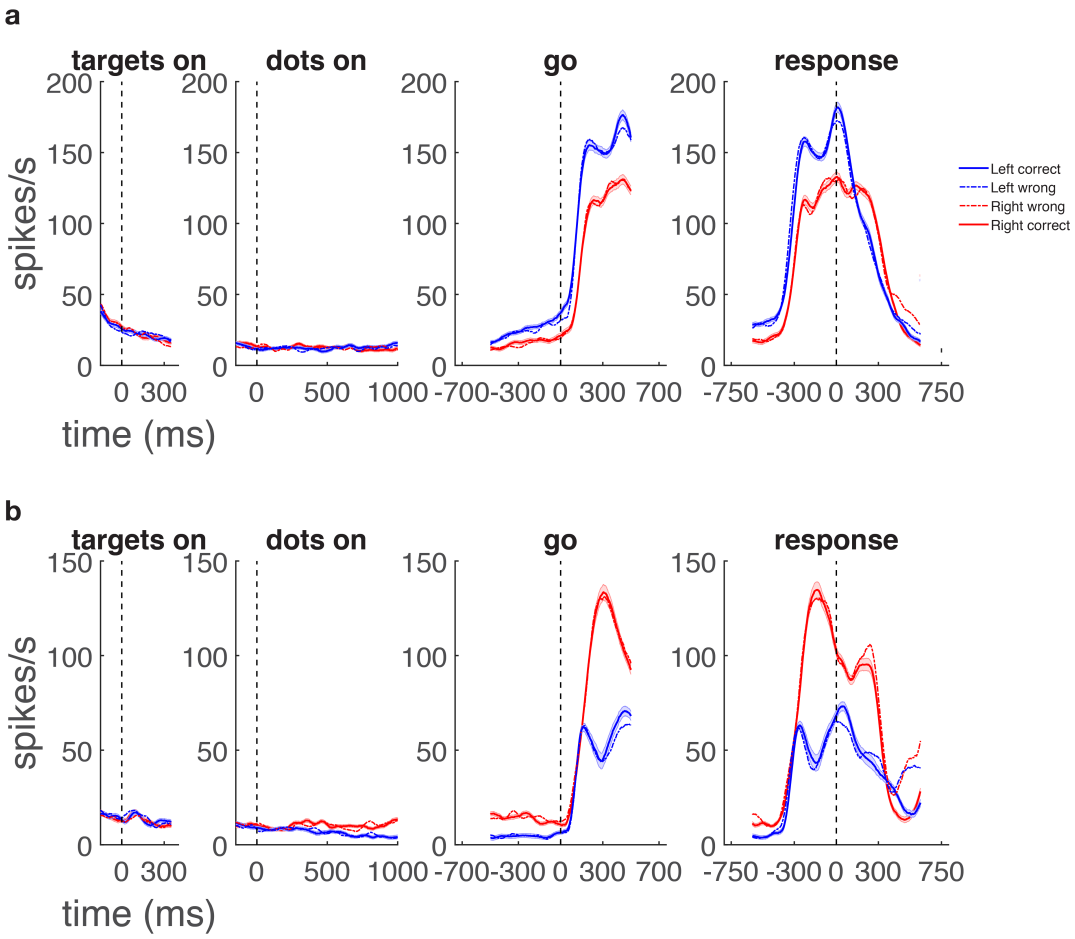

Figure 2.11: **Multi-unit responses in M1 - delay and peri-movement choice predictive activity a)** Multi-unit response with slightly choice predictive activity during the delay, increasing in the period leading up to the response. Multi-unit activty was similar to single unit activity aside from the higher firing rates. **b)** Multi-unit with opposite choice preference to **a)** and slightly earlier predictive activity. Same color convention as Figure 2.8

they all combine different motifs of activity to different extents some of which are more easily interpretable in the context of the task than others.

Nevertheless, some response features were conserved across almost all cells: in error trials responses were much more similar to those of correct trials that led to the same choice than those of the same stimulus that led to the opposite choice. In other words the cell response in an error that led, for instance, to a left choice was much more similar to responses for correct left choices than for correct right choices even for the same stimulus. This is a differentiating feature between decision related

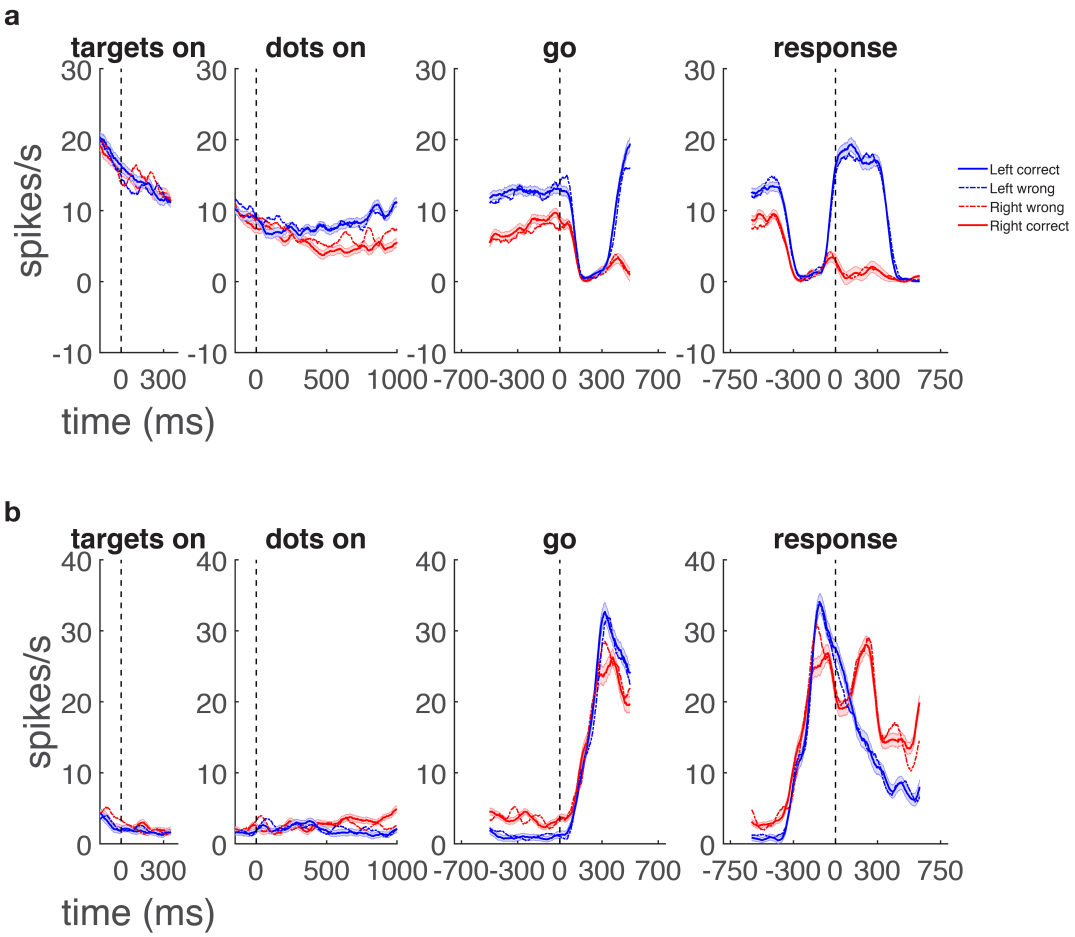

Figure 2.12: **Single neuron responses in M1 - early and delay choice predictive activity a)** M1 neuron with early choice predictive activity during the dots period. Predictive activity was strengthened during the delay period after which it was completely suppressed right before movement initiation. **b)** Single cell with later and opposite choice preference during dots. The choice preference is maintained during the delay period and reversed right before the response. Cells with predictive activity during dots were less frequent but still present in M1. Same color convention as Figure 2.8

areas and sensory areas in which responses go with the stimulus and not the ultimate choice of the subject.

While we had the expectation of finding decision-related signals in PMd, our expectations for M1 were much more conservative and we would not have been surprised if we had mostly found cells with peri-movement activity and maybe some with sustained choice predictive activity during the delay period. Nevertheless, comparing

and contrasting the responses of the two brain areas in a cognitive setting was a worthwhile endeavour on its own due to the lack of literature in the field. We did indeed find single and multi-neuron signals with peri-movement and delay period activity that were only selective for choice later in the trial (Figure 2.11). To our surprise though we also found cells in M1 with some choice predictive activity during the dots period (Figure 2.12) some from very early on in the trial. Similarly to PMd, some of the cells had complex activity patterns later in the trial such as suppression (Figure 2.12 a)) and reversal in preferred direction (Figure 2.12 b)) after the go cue.

In summary both PMd and M1 contained cells whose activity patterns went beyond the canonical peri-movement neurons, some of which had choice predictive activity with latencies and profiles similar to those reported in the oculomotor system (LIP and FEF).

2.2.3 Choice predictive activity in individual neurons across the trial

In the previous section we briefly described the diversity of cell responses in PMd and M1. That is a theme that will have implications in much of our work. Still, it is the knowledge that some neurons carry strong short latency choice predictive signals that justifies studying decision-formation signals in these areas. If it weren't for those it would not be possible to claim these areas are tracking or possibly implementing the decision formation process.

To thoroughly and systematically quantify the strength of the choice predictive signals, and thus obtain a more complete picture of this effect across areas and across the trial, we calculated the average difference in firing rate between correct right and correct left choices for each neuron at different points during the trial (Figure 2.13). To assess the statistical significance of this difference we implemented a Wilcoxon rank sum test that tests the hypothesis that median firing rates for the two choices are identical and rejects it at $p<0.001$. For the example dataset shown in (Figure 2.13 a), at dots offset, 27.5% of cells in PMd were significantly modulated for choice while the same was true for 25.5% of cells in M1. While their firing rate modulations

with choice were not huge (under 20 spikes/s) they were very significant and together they comprise a sizable fraction of the population. Its worthwhile recalling we are not performing any pre-selection of neurons, and due to the nature of our recording system (Utah arrays), we have no control over the types of units we are likely to collect. Thus, we obtain an unbiased sample of neuron responses in these brain areas.

As the trial unfolds, choice predictive signals become stronger and more pervasive with 58.2% of cells in PMd and 47.9% of cells in M1 showing significant modulation at the time of the go cue (Figure 2.13 b). Cells with modulation larger than 20 spikes/s can now be found in both areas. The same trend holds when analysing the time of the arm movement where now 64.3% and 55.3% of cells are significantly modulated in PMd and M1, respectively. This increase in the number of modulated cells is expected given the motoric nature of these areas as shown by strong and mostly directionally tuned responses at the time of the arm movement. Importantly, across all time points and both areas there are neurons tuned for both left and right choices. This observation is in stark contrast with those reported for the oculomotor system where contralateral movements are extremely dominant over ipsilateral movements.

The purpose of this analysis was not to determine exact percentages of modulated cells, as these will change from dataset to dataset and monkey to monkey, but to characterize the main effects of choice on neural activity:

- $\sim$1 out 4 units in both PMd and M1 are modulated by the end of the dots presentation, reassuring us this is a widespread signal from early in the trial.
- For both areas the percentage of units involved in representing choice increase as the trial unfolds and approaches the response time, confirming their roles in motor planning and execution.
- Both choices are well represented by different sets of neurons across all time-points, providing a great opportunity to understand decision formation, memory and motor execution for both the ipsilateral and contralateral sides of the recorded hemisphere.

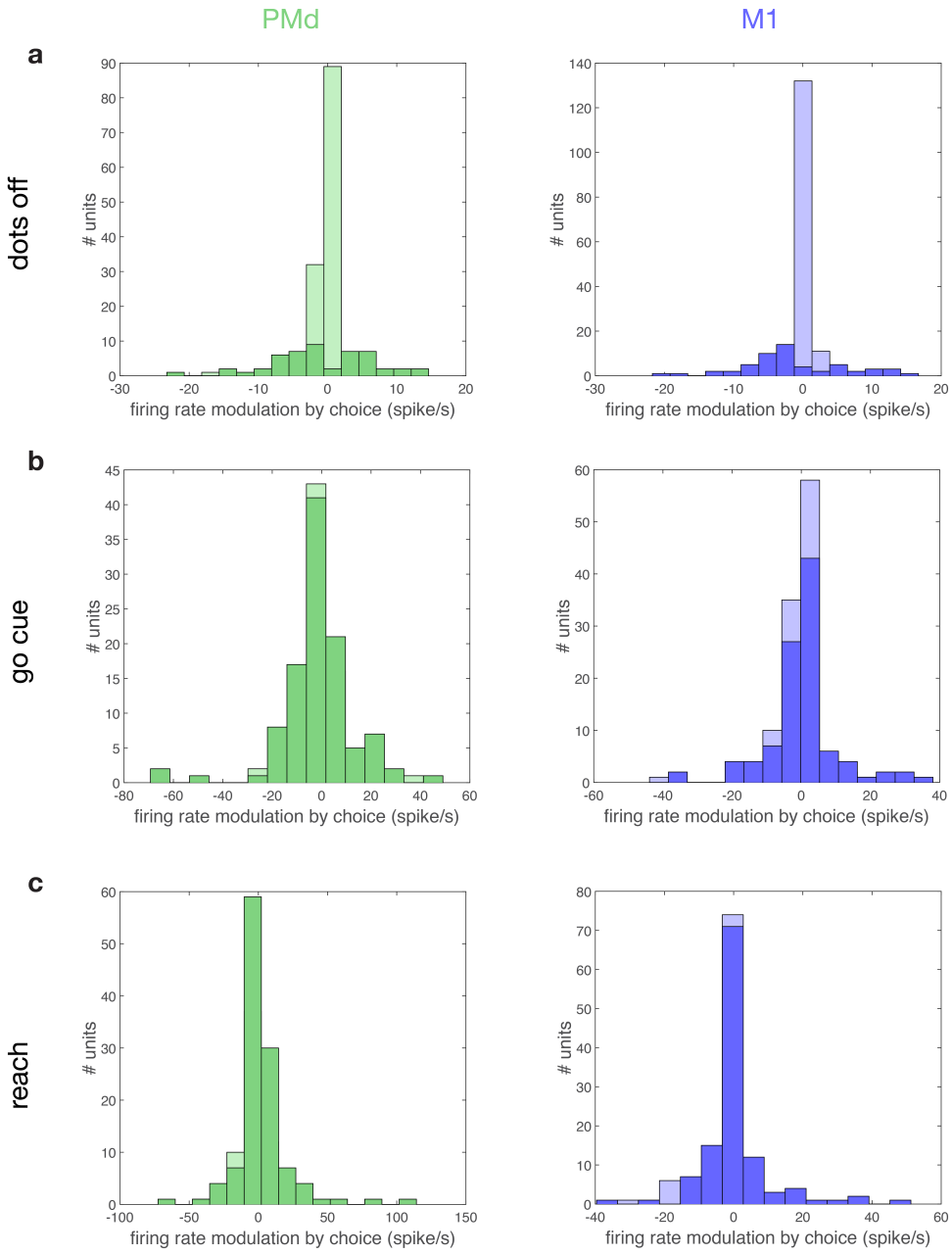

Figure 2.13: **Choice modulation across the trial for PMd and M1 a)** Distribution of firing rate modulation with choice modulation at the end of dots presentation for PMd (left) and M1 (right). Modulation is defined as the firing rate difference between correct right and correct left choices. **b)** Same as **a)** but for the go cue timepoint.**c)** Same as **a)** for the reach initiation timepoint.

2.3 Discussion

In this chapter we demonstrated the successfully training of two monkeys to perform a variant of the classical motion discrimination task, in which a decision is reported with an arm reach. This task has been a tried and true paradigm for studying decision formation processes unfolding over time in the oculomotor system. By modifying the response modality we made it suitable to study the same processes in the somatomotor system. In parallel, we successfully implanted 2 Utah arrays over PMd and M1 allowing us to simultaneously record up to ∼100 neurons each while the subjects perform the task. We found very diverse responses in both areas with some neurons conforming to the canonical peri-movement response profiles (Figure 2.8) and others resembling ramping neurons in LIP or FEF (Figure 2.10). The rich choice predictive signals, that we interpret as a signature of the decision process arise early on in these areas and become stronger and more pervasive as the trial unfolds. In the face of such diverse responses, the classical approach in systems neuroscience would have been to devise indices as an attempt to classify cells in different groups. Despite having improved our understanding of many brain circuits in the past, this approach is limited in its scope and falls short of providing a thorough understanding of the computations being implemented. The only exceptions to this caveat happen when the recorded cells are incredibly homogeneous or clearly fall into discrete and interpretable categories. Even a brief inspection of the presented PSTHs shows how mixed signals are across and within cells and how PMd and M1 would not fall in the latter exceptional case. From here on our approach was to instead embrace the diversity of responses and leverage the simultaneity of our recordings to analyze the dynamics of the decision process on single trials. While the yield of this approach in terms of improving our population-level understanding of decision-making can be immense, the methods required to achieve it are much more sophisticated and extra care is required when analysing results. We will expand on this framework and present its results in Chapter 3.

3

Single-trial population activity in PMd and M1 is consistent with DV representation

In Chapter 2 we provided a general description of diverse cell responses in PMd and M1 and also an account of the distribution of choice predictive activity across cells and across the trial. These results established the presence of decision-like signals in some cells in PMd and M1 but did not quantify their strength or dynamics.

In this chapter we go beyond the classical quantification of *average* decision-related signals and dive into single trial analysis. The motivation is simple: decision-making is an internal process whose output, behavior, only comes in most cases after the cognitive operations are done with. Still, we know from experience and from the data that even the same stimulus presentation can lead to different outcomes, especially in difficult trials. Moreover, even if the outcome is the same, the (neural) path that leads to it can vary substantially from trial to trial. Averaging individual cell or population responses over many trials masks this variability, which may provide crucial clues concerning the neural mechanisms that underlie evolution of the decision.

Obtaining reliable single trial estimates of a decision state is only possible by combining the information conveyed by many cells simultaneously. Due to the quasi-Poisson nature of spiking statistics, a single spike train is too noisy to detect precise changes in a decision variable or neural state over the course of a single trial. We

therefore combined information across a population of neurons by applying a linear classifier for choice that weights information from each spike train in proportion to its effectiveness in predicting the eventual choice at the end of the trial. We recalculate weights at successive temporal intervals during the trial so that our prediction of choice can be reliable even if cells switch choice preference during the course of the trial.

Having determined a reliable decision-state estimate on single trials, we answer several important and novel questions about the decision signals present in PMd and M1:

1. How early in the trial does choice prediction accuracy rise above chance in PMd and M1?

2. How high does prediction accuracy become during the stimulus presentation? And during the delay?

3. Are signals in PMd and M1 compatible with the representation of a decision-variable?

4. How do these signals differ between the two areas?

The answers to these questions will provide a more quantitative and unbiased picture of the strength and features of the decision signals in PMd and M1.

Author contributions: Diogo Peixoto, Roozbeh Kiani and William Newsome designed the statistical analyses. Diogo Peixoto ran the experiments to collect the data, implemented the analysis and generated the figures presented in this chapter.

3.1 Methods

3.1.1 Logistic regression

For each session the responses of all neurons in 90% of the trials were fit with a logistic model (equation 3) that attempted to separate rightward (T_1) and leftward

(T_2) upcoming choices. The logistic model was fit in 150 ms windows, advanced in 20 ms steps over the entire trial duration.

$$P(T_1 \,|\, r) = \frac{1}{1 + e^{-\beta_0(t) + \sum_{i=1}^{n} \beta_i(t) \times r_i(t)}} \tag{3.1}$$

Where β_0 is an intercept term, $\beta_i(t)$ are the classifier weights (one for each neuron and time window) and $r_i(t)$ are the z-scored summed spike counts for each neuron and time window.

The remaining 10% of the trials were tested using the previously trained model and its accuracy was recorded. The same process was followed 10 times for each window (10-fold cross-validation) and the percentage of correctly predicted choices recorded. This process was repeated for consecutive windows displaced by 20 ms and yielding a prediction accuracy trace for each session and brain area.

An L1- regularization technique (LASSO) was used to constrain the norm of the beta coefficients fitted by the model to prevent over-fitting (Kiani et al., 2014). The lambda parameter that determines the strength of the penalty for the L1 norm was calculated for the 150 ms window preceding the go-cue by sweeping through 25 potential values and selecting the value with lower deviance by running 10 fold cross validation. This lambda value was then used for the model for all time points.

Finally, the difference in accuracy between correct and error trials as a function time (during stimulus presentation) was calculated for each dataset and coherence. For each time point, coherence, brain area, and monkey we tested if this difference was significant by performing a two-tailed t-test corrected for multiple comparisons ($p<0.05$ Holm-Bonferroni correction).

3.1.2 Decision Variable

When performing logistic regression on the population activity, the set of weights associated with each neuron form the hyperplane that best separates leftward and rightward choices for the corresponding time window (150 ms width at a time). For each trial and time point, the distance of the population state to this hyperplane is

given by the model choice log odds i.e. it corresponds to models certainty about the upcoming choice of the monkey.

$$DV = \frac{P(T_1 \,|\, r)}{P(T_2 \,|\, r)} = -\beta_0(t) + \sum_{i=1}^{n} \beta_i(t) \times r_i(t) \tag{3.2}$$

We use this distance as a proxy for a Decision Variable (DV) and study its dynamics as a function of stimulus difficulty and trial epoch.

3.1.3 DV Slope Analysis

To analyze the dependency of our putative decision variable on the stimulus strength we first average the DV values for each coherence level and choice using correct trials only. Then we take the absolute value of the difference in DV between right choices and left choices within each coherence level. Finally we truncate these traces at 500 ms and fit them with a tri-linear curve. We fix the first slope as zero since the neural activity is not informative about upcoming choice for the first 100 ms of stimulus presentation and keep the 2nd and 3rd slope as well as the transition times as free parameters. All free parameters were fit to minimize squared error. We used the value of the 2nd slope to quantify the |DVdiff| initial rate of rise. The curves were fitted independently for each dataset and stimulus strength.

3.1.4 RT analysis

To predict Reaction Time (RT) based on neural activity we performed Ridge regression on the z-scored firing rates of all units within a 150 ms window. For each window a different model was trained for each reach direction (left and right) on 90% of the correct trials that lead to the corresponding choice. Then the RTs on the remaining 10% of the trials were estimated using the trained model and the units firing rates. We performed this same process 10 times for each window (10-fold cross validation) and obtained a set of estimated Reaction Times. We then performed a linear regression between the estimated and the observed reaction times for all trials and recorded the R-squared value. Finally we slid the window by 20 ms and repeated the process

until all relevant epochs of the trial were tested. The adequate Ridge parameter was estimated independently for each dataset and reach direction for the window comprising [200, 350ms] after the Go cue, where the RT signal tended to be strongest. The estimation was performed using 10-fold cross validation over 20 potential values. The value corresponding to the smallest testing error was chosen and used to regularize the linear model in every window.

3.1.5 Unit dropping

For the unit dropping analysis we fit a logistic model (equation 3) to data obtained in the last 50 ms of dots presentation using 10-fold cross validation, just as before. The lambda regularization parameter however, was in this case fit to the same 50 ms epoch we would test (again using 25 potential values and 10 fold cross validation). The set of beta coefficients of the model corresponding to the lowest deviance lambda parameter were then chosen and ranked by magnitude. We removed from the data the unit with highest beta coefficient and re-trained and re-tested the model using 10-fold cross-validation and recorded the accuracy. This process was repeated 70 times until the 70 units with highest beta coefficients were all dropped in descending order.

3.2 Results

3.2.1 Populations of cells in PMd and M1 predict choice on single trials with low latency and high accuracy

Building on the results shown in chapter 2, our goal was to attain a more comprehensive understanding of the decision formation process on *singletrials*. Moving from the traditional single cell averaged activity framework to a single-trial population activity framework required a deliberate conceptual and methodological leap. To accomplish this, we trained a logistic classifier to separate trials ending in rightward and leftward choices based on features of the simultaneously recorded activity from tens to hundreds of units (both single-neurons and multi-units) from each area. The classifier

was trained on 150 ms windows aligned to different epochs of the trial and tested using 10-fold cross validation. This analysis was performed on individual sessions and separately for each area. We started by analysing the results for the fixed duration task due to its simplicity and ease of comparison with previous studies (Shadlen and Newsome, 2001). The first question we tackled was: how early in the trial does choice prediction accuracy rise above chance in PMd and M1?

We started by analysing the period around the targets onset and observed choice prediction accuracy is at chance levels (Figure 3.1) indicating that no choice predictive signals are being captured. This is an important sanity check for both our method and the neural activity we are recording. It implies that prior to onset of the visual stimulus the monkeys are asked to discriminate, neural activity does not convey any information about the choice the monkey will ultimately make at the end of the trial. This would not be the case if the subjects were pre-planning from early on and on some trials systematically disregarded the dots motion when making their decision. Thus, this observation alone will lend more confidence to the interpretation of the signals that we do capture during the stimulus presentation period. When aligned to stimulus onset choice predictive activity also starts at chance levels for both monkeys but quickly becomes significant 180-200 msec later for PMd and 255-280 msec later for M1. The slight difference between PMd and M1 is consistent across sessions and monkeys. These latencies for both areas (and especially for PMd) place them within the same range of latencies for decision-related signals reported for LIP Shadlen and Newsome (2001); Roitman and Shadlen (2002); Meister et al. (2013).

This was a surprising observation even after having seen some neural responses that seemed to show short latency choice predictive activity. Most importantly, it militates against the idea that premotor and motor cortex are only responsible for the kinetic and kinematic aspects of movement preparation and execution: if that was the case there would be no reason for choice predictive activity to be present in these areas from so early in the trial, when the monkeys knew they had 1000 msec of dots and at least 400 msec of delay period before the operant response would be cued. Even more impressive than the short latencies observed, was the fast rise in prediction

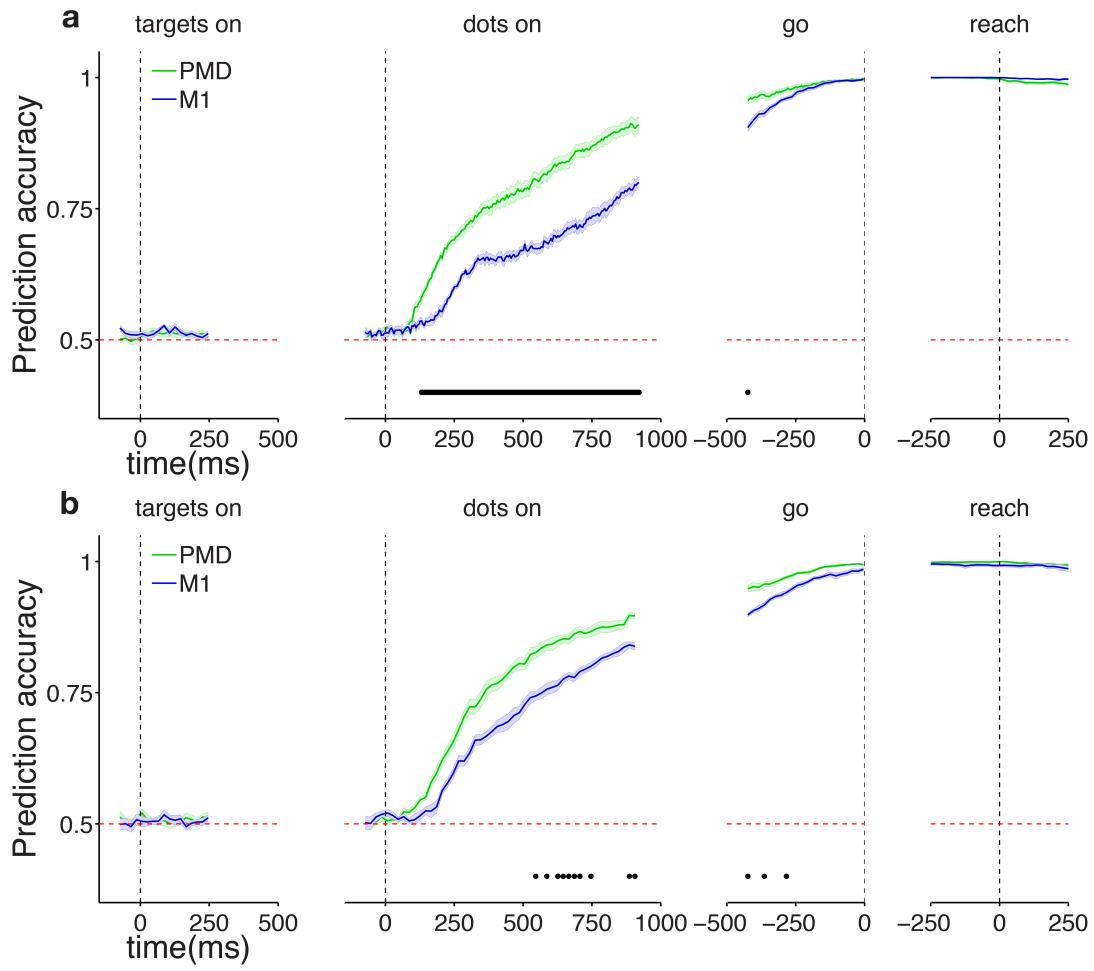

Figure 3.1: **Neural population choice prediction accuracy on single trials. a)** For each session the responses of all neurons in 90% of the trials within a 150 ms window were fit with a logistic model that attempted to separate left and rightward upcoming choices. The remaining 10% of the trials were tested using the previously trained model and its accuracy was recorded. The same process was followed 10 times for each window (10-fold cross-validation) and repeated for consecutive windows displaced by 20 ms, yielding a prediction accuracy trace for each session and brain area. a) Average prediction accuracy over time ± SEM for PMd (M1) are plotted in green (blue). Black dots denote time points for which the prediction accuracy was significantly different between the two areas ($p<0.05$ Holm-Bonferroni correction for multiple comparisons). Choice prediction accuracy quickly departs from baseline after stimulus presentation (around 180/ 255 ms for PMd/M1 pj0.01) and reaches very high values well before movement initiation (91% / 83% for PMd/M1 at the end of the dots epoch). **b)** Same as **a)** for Monkey F. Latencies and average choice prediction accuracy at stimulus offset for Monkey F are 200/280 ms and 90%/84% for PMd/M1, respectively.

accuracy during the stimulus presentation. Prediction accuracy rises steadily for both areas, reaching 90% - 91% for PMd and 83% - 84% for M1 at the end of the stimulus presentation period. These are very high values considering (i) they are obtained through cross-validation, (ii) we are only recording from a relatively small sample of neurons in these areas (iii) they exceed those previously reported for prearcuate cortex using similar recording and analyses techniques (Kiani et al., 2014).

As expected from (pre)motor areas, choice prediction accuracy keeps rising during the delay period until the go cue is presented, at which point the difference between PMd and M1 has largely vanished. This same observation is true for the peri-movement period during which choice prediction is virtually perfect due to the strong and tuned motor signals present in both areas.

3.2.2 Choice predictive activity is compatible with the neural representation of a decision variable

Short latency, highly reliable choice predictive activity suggests close engagement of these areas in the decision process but similar results could be obtained simply by having highly reliable binary classification (left vs right) informed by an upstream area where the decision formation process is actually being formed/tracked. While we cant rule out the participation of upstream areas (frontal and/or parietal) we can analyse features of the predictive activity observed in PMd and M1 and compare them to the expected features of signals carrying decision related activity. One such feature predicted by drift diffusion models (Mazurek et al., 2003) and extensively reported in oculomotor structures (Shadlen and Newsome, 2001; Roitman and Shadlen, 2002) is the dependency of choice predictive activity on stimulus difficulty: choice predictive activity on easier trials should rise faster and attain higher values compared to harder trials due to the difference in strength of visual evidence favoring one choice. Sorting the same trials that went into our logistic classifier analysis by stimulus strength confirms this feature: choice prediction accuracy rises faster and reaches higher values during stimulus presentation for easier trials in both areas although the separation between conditions seems qualitatively stronger in PMd than M1 (Figure 3.2 vs Figure

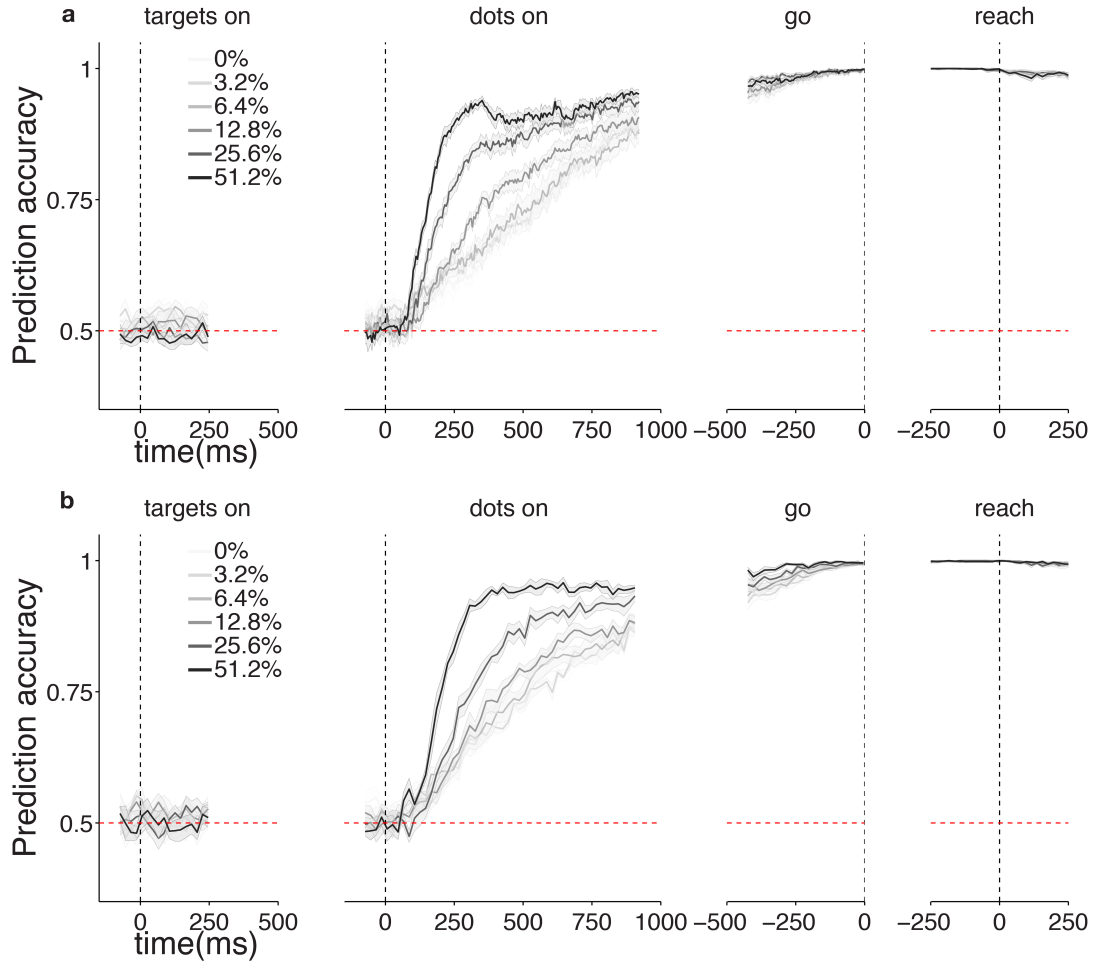

Figure 3.2: **Average choice prediction as function of stimulus difficulty - PMd.** Average choice prediction as function of stimulus difficulty. **a)** Results for Monkey H. Easy stimuli are represented in darker tones while harder stimuli are plotted in lighter tones and shading corresponds to ± SEM. Same data as in Figure 3.1, except prediction accuracy is calculated individually for each stimulus difficulty for PMd. **b)** Same as **a)** for Monkey F.

3.3). The separation between conditions is clearer during the first half of the dots period, becoming smaller as the trial unfolds. During the delay and peri-movement there is very little or no separation by stimulus difficulty, which suggests that by the end of the delay period, in the vast majority of trials, a categorical decision has already been made.

To quantitatively compare the effect of stimulus strength on predictive activity

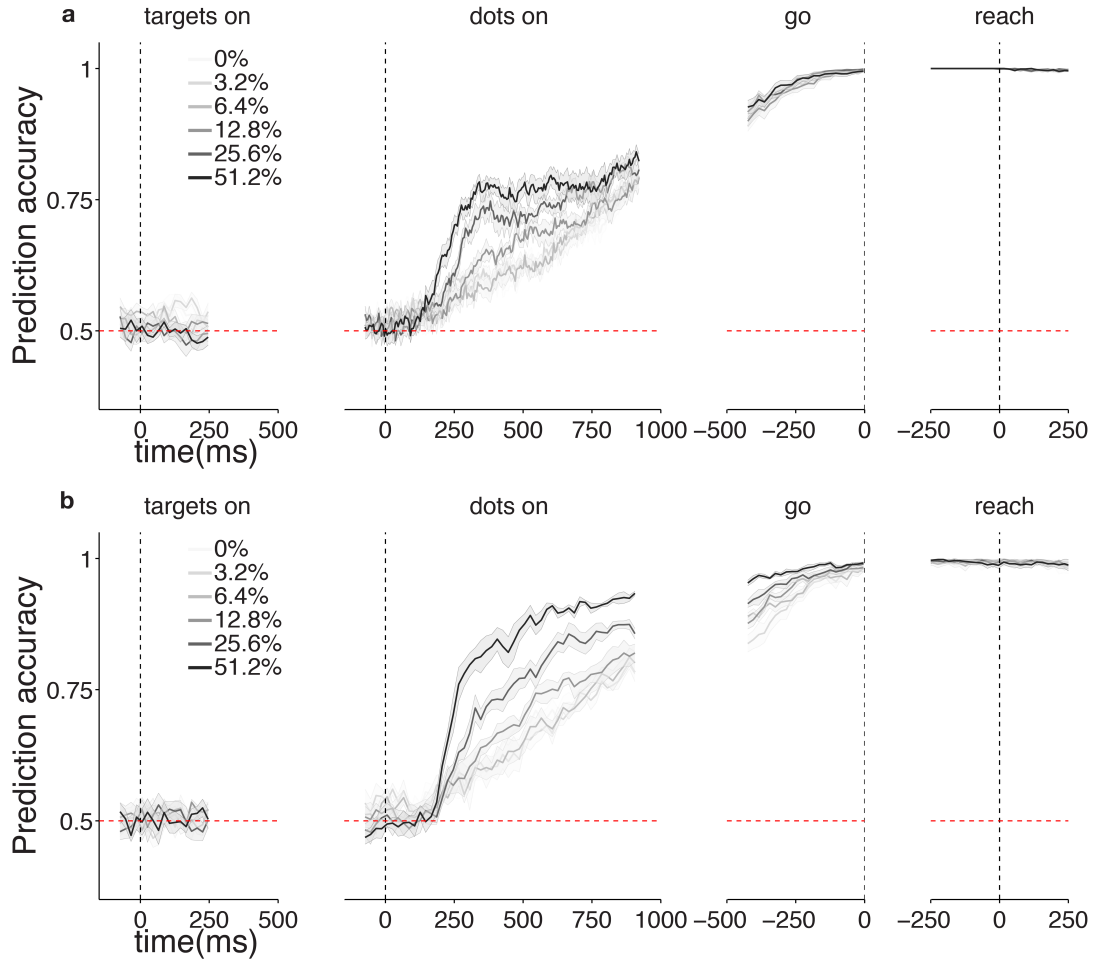

Figure 3.3: **Average choice prediction as function of stimulus difficulty - M1.** Average choice prediction as function of stimulus difficulty. **a)** Results for Monkey H. Easy stimuli are represented in darker tones while harder stimuli are plotted in lighter tones and shading corresponds to ± SEM. Same data as in Figure 3.1, except prediction accuracy is calculated individually for each stimulus difficulty for M1. **b)** Same as **a)** for Monkey F.

between the two areas we sought a finer metric. When fitting the logistic regression model, we are effectively assigning weights to each neuron based on how reliably they separate the two choices. The set of all weights defines a hyperplane in neuronal space that is our classifying boundary. At any given timepoint in a particular trial, the pattern of neural activity across the population can be defined as a point in neural space. The distance of this point to our classifying boundary informs us of the confidence of the model on the prediction: the further from the boundary, and thus

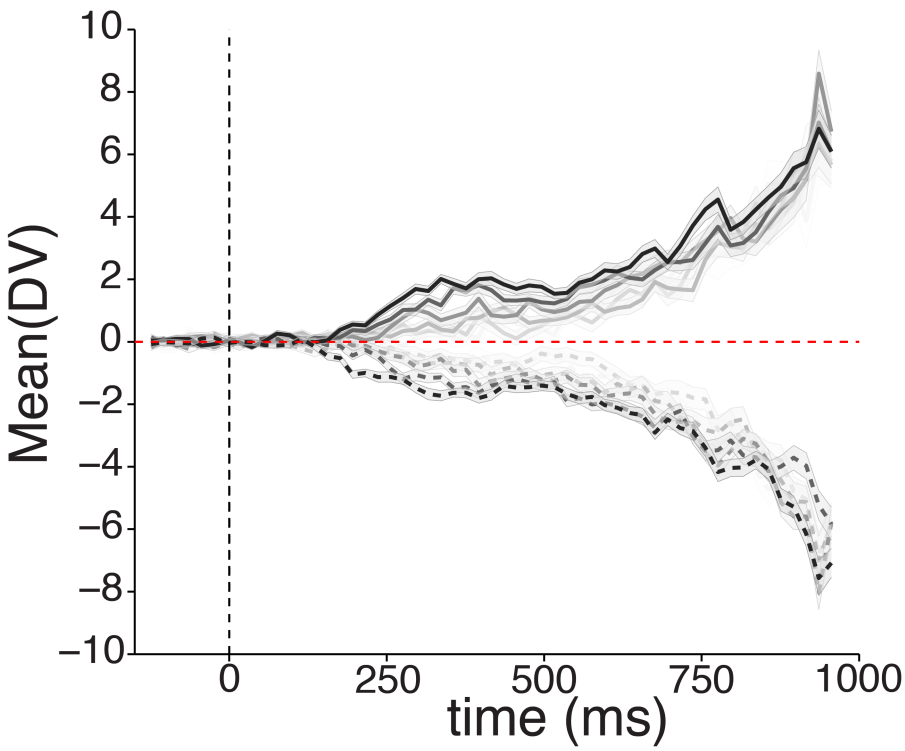

Figure 3.4: **Decision variable as function of stimulus difficulty.** Average decision variable during the dots presentation as a function of time and stimulus coherence. Traces show average prediction over the time with darker tones corresponding to easy stimuli and lighter tones to harder stimuli. Dashed lines represent average rightward choices and dotted lines average leftward choices ± SEM (shaded areas). Results for one example dataset from Monkey H PMd. Only correct trials were analysed and plotted. As expected from Figure 3 b, DV also depends on stimulus difficulty in a lawful manner.

the larger the distance, the higher the confidence of the model on its estimate of the eventual choice of the animal. In fact, in the case of logistic regression the distance to the boundary is equivalent to the models log odds of choosing right vs choosing left. Similarly to previous studies (Kiani et al., 2014) we interpret this distance as the model decision variable and use it as a proxy for the commitment state of the animal towards a given choice. Because the decision variable is continuous, unlike predicted choice which is binary, and can differ even between correctly predicted trials, it constitutes a finer metric for quantifying commitment state and its dependency on stimulus difficulty. Importantly, and having set a convention for positive values for right choices and negative values for left choices, we recapitulate for the decision

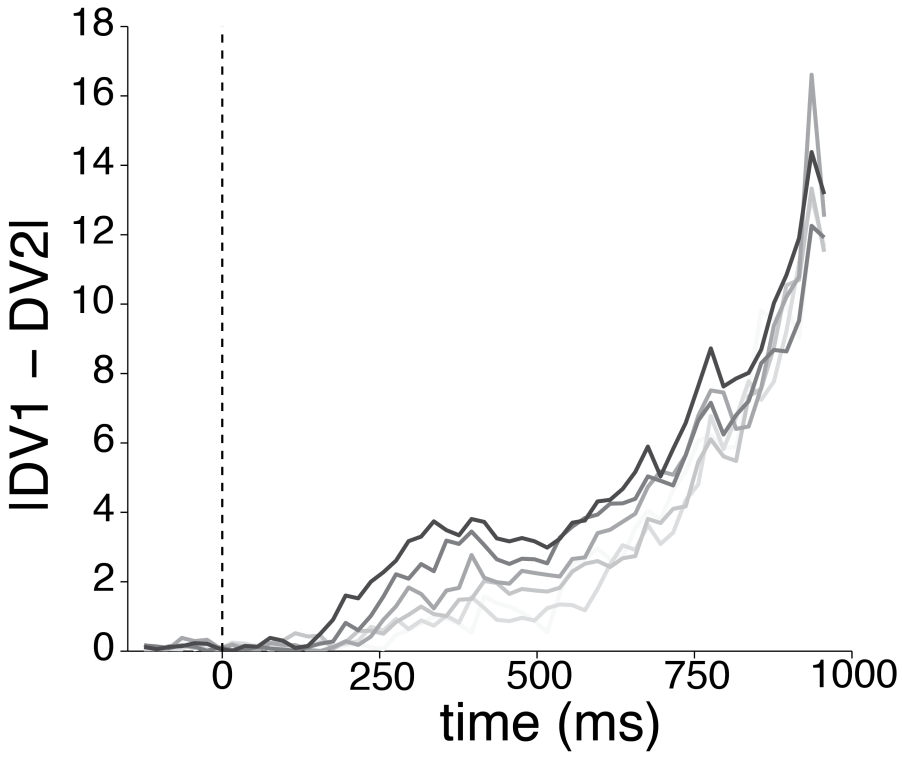

Figure 3.5: **Decision variable difference as function of stimulus difficulty.** Absolute difference in DV (|DVdiff|) as a function of stimulus difficulty. Traces show the average absolute difference in DVs for rightward and leftward choices. Same data and color convention as Figure 3.4 . We used this variable to quantify the stimulus difficulty effects seen in Figure 3.4

variable the same effects found for choice prediction accuracy: its magnitude increases with time and with stimulus coherence (Figure 3.4)

To quantify stimulus difficulty effects on the decision variable we collapsed across choices by taking the absolute value of the difference between right and leftward choices within a stimulus coherence level. This metric quantifies the separation between the conditions when the neural data is projected onto the classifier axis. (Figure 3.5).

We then focused on the first portion of the stimulus presentation and quantified the first non-zero slope as predictive activity departs from chance Figure 3.6. This slope informs us of the initial choice related push the neural state undergoes as visual evidence informing the upcoming choice emerges in these brain areas. This was the

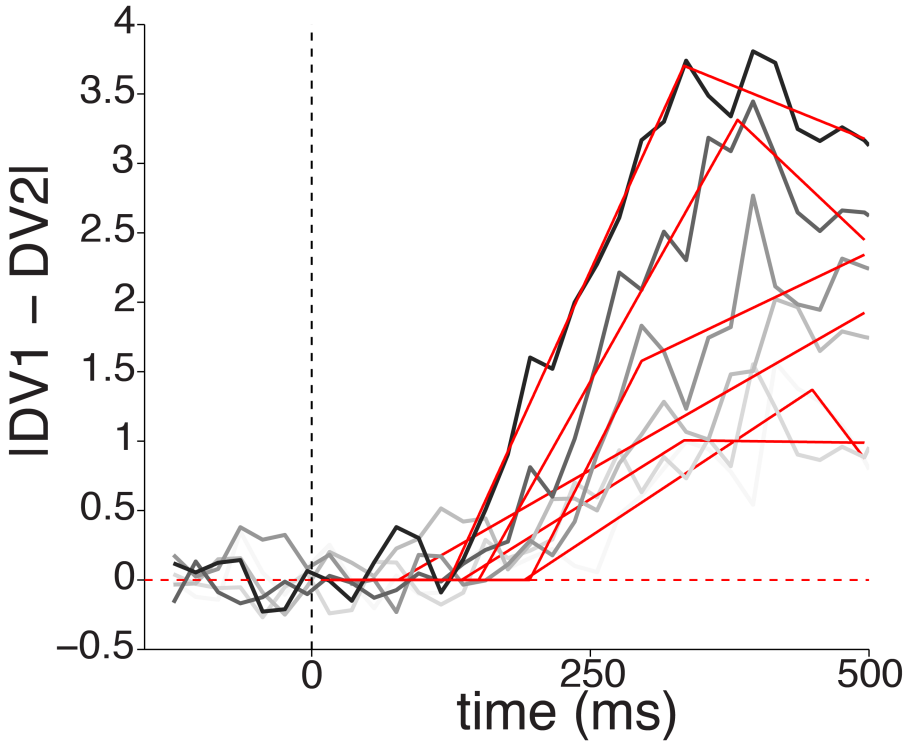

Figure 3.6: **Tri-linear Slope fitting.** We fit the difference in DV with a tri-linear curve in the first 500 ms. We fix the first slope as zero since the neural activity is not informative about upcoming choice for the first 100 ms of stimulus presentation and keep the 2nd and 3rd slope as well as the transition times as free parameters. We use the value of the 2nd slope to quantify the |DVdiff| initial rate of rise. c) One example of the tri-linear fit to |DVdiff|. Same data as in Figure 3.5 truncated at 500 ms of stimulus presentation.

period with stronger stimulus coherence effects, during which we believe the motion energy of the stimulus plays a more substantial role. This impression comes from the fact that behavioral performance does not increase substantially for durations much larger than the median duration ($\sim$ 435 ms). Also, visual inspection of Figure 3.2 and Figure 3.3 shows that coherence effects are stronger in the first half of the stimulus than the second.

Consistent with the representation of an actual decision variable in these areas, higher coherence trials are associated with steeper DV slopes (Figure 3.7). The results are highly significant for both areas but consistently stronger for PMd than M1 (Figure 3.7 vs Figure 3.8).

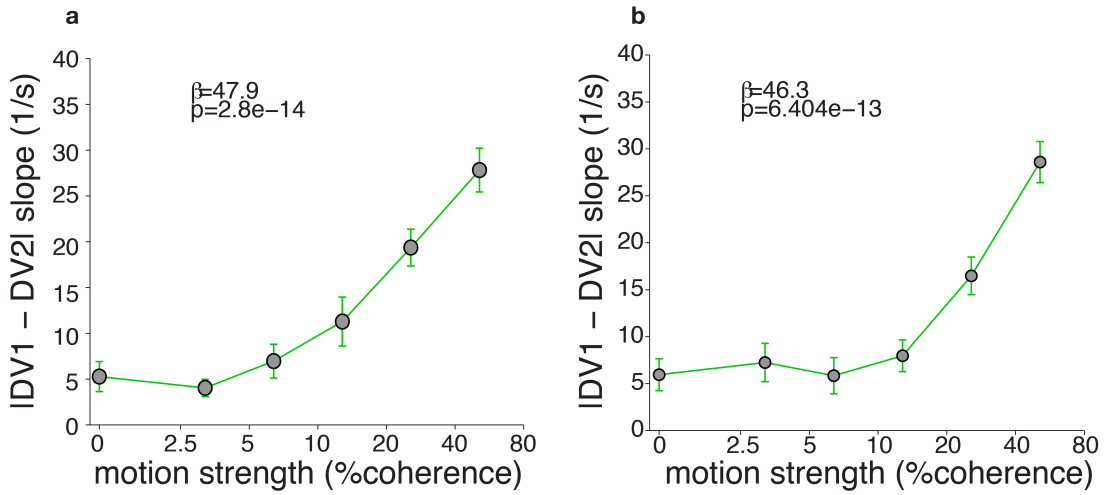

Figure 3.7: **Slope values as function of stimulus strength - PMd. a)** The slopes show significantly higher values for higher coherence (easier stimuli) as one would expect from a brain area representing accumulation of evidence toward a choice. Beta and p-values shown for a linear regression of |DVdiff| on stimulus strength **b)** Same as **a)** for Monkey F.

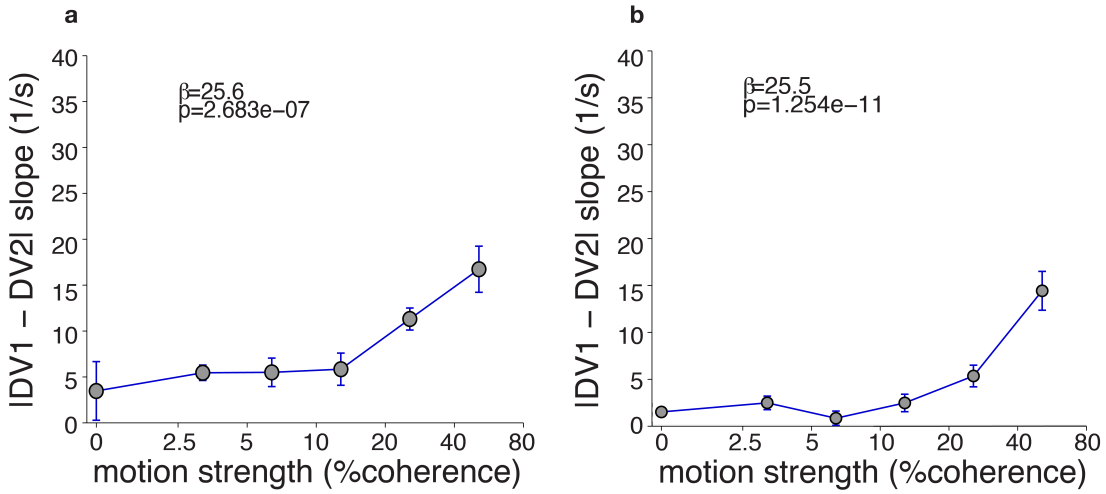

Figure 3.8: **Slope values as function of stimulus strength - M1. a)** The slopes show significantly higher values for higher coherence (easier stimuli) as one would expect from a brain area representing accumulation of evidence toward a choice. Beta and p-values shown for a linear regression of |DVdiff| on stimulus strength **b)** Same as **a)** for Monkey F.

3.2.3 Stimulus duration uncertainty dramatically increases choice predictive activity in both areas

So far we focused on data from the fixed duration task for which the subjects consistently had 1 second of visual evidence to integrate and base their decision on. However, in the real world subjects rarely have information about the precise timing of the source of visual information theyll use to make a choice. For this reason, and once we had terminated data collection on the fixed duration task, we introduced a variable duration task by presenting stimuli of random durations and asking for an immediate decision once the stimulus was terminated. It is worth highlighting that prior to our recordings the monkeys had never been exposed to short stimuli (< 1000 ms). The subjects performed better for longer stimuli (Figure 2.5), confirming they were using additional visual evidence to improve decision accuracy.

Since the subjects had no prior information about the duration of the stimulus on each trial and most trials were short (median 435 ms - see Methods Chapter 2) we were indirectly placing a premium on accurately integrating the first couple hundred ms of dots motion: the first 200 ms of evidence were guaranteed to be shown but from then on stimulus presentation could be interrupted at any point. Knowing PMd and M1 carry decision formation signals under conditions of temporal certainty we asked whether the dynamics of those signals change once the certainty of the stimulus and thus the demands on the subjects changed. To our surprise, the change in predictive activity across the population is dramatic in both areas: even though the latencies are similar in the two task versions (fixed and variable duration), the rise in predictive activity is accelerated under uncertainty conditions leading to much higher values during the stimulus presentation (Figure 3.9). This difference is even more dramatic in M1, which becomes largely indistinguishable from PMd under these conditions. The dynamics of neural activity in these areas during decision-making is thus flexible and dependent on the statistics of stimulus duration.

Importantly, and because we are recording in (pre)motor areas, we wanted to confirm that the acceleration of predictive activity in the variable duration task was

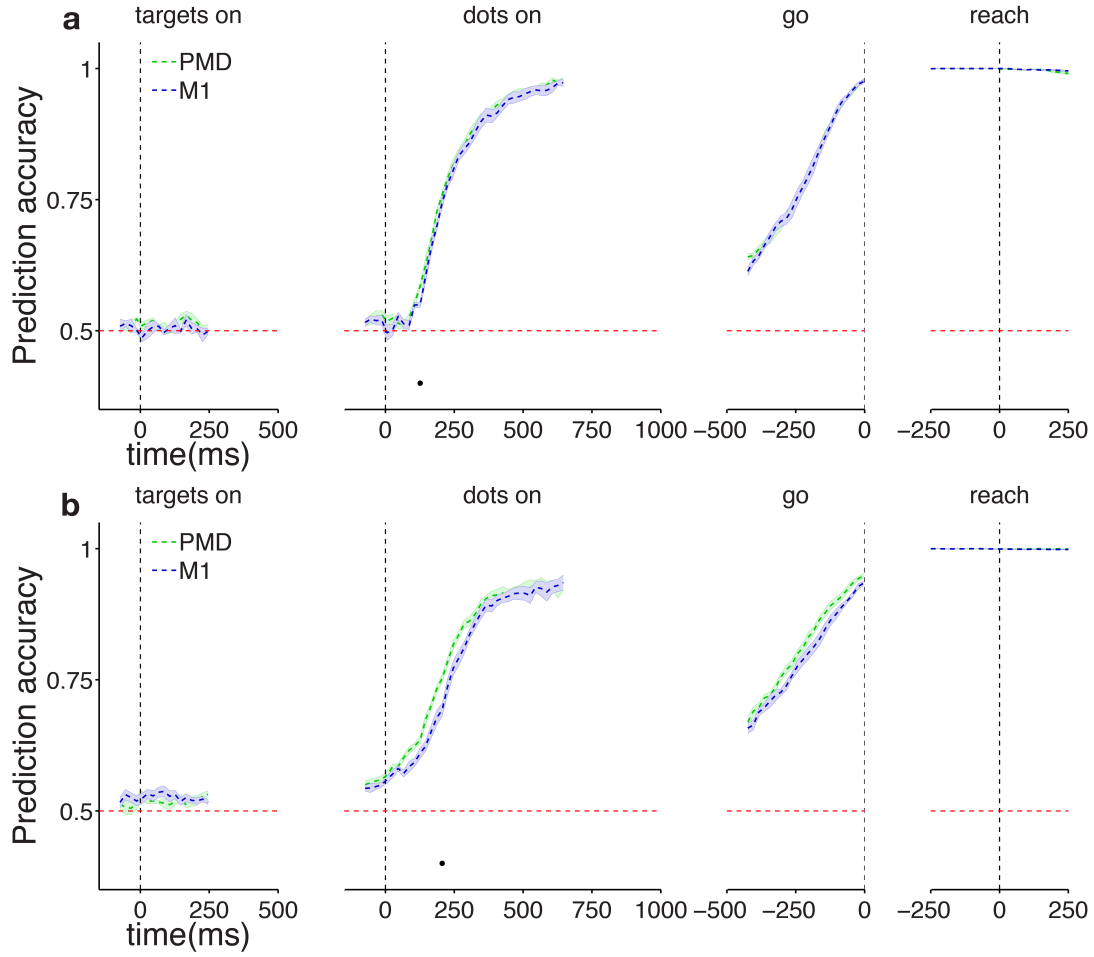

Figure 3.9: **Neural population choice prediction accuracy on single trials - Variable Duration task without delay. a)** Average prediction accuracy over time ± SEM for PMd (M1) are plotted in green (blue). Same conventions as in Figure 3.1. The rise in prediction accuracy after the onset of the dots stimulus is much sharper than in the fixed duration task (Figure 3.1) for both PMd and M1. **b)** Same as **a)** for Monkey F.

not simply a consequence of enhanced motor signals appearing earlier in the trial due to elimination of the delay period. Performing the same slope analysis on the DV from data in this task shows the coherence effects are largely conserved in both PMd (Figure 3.10) and M1 (Figure 3.11) areas despite the accelerated dynamics . In fact and when comparing data within each area across tasks, the shape of the slope trace is very similar (compare dashed and solid traces within the same area and monkey) aside from the vertical shift observed in the variable duration task. This shift is suggestive

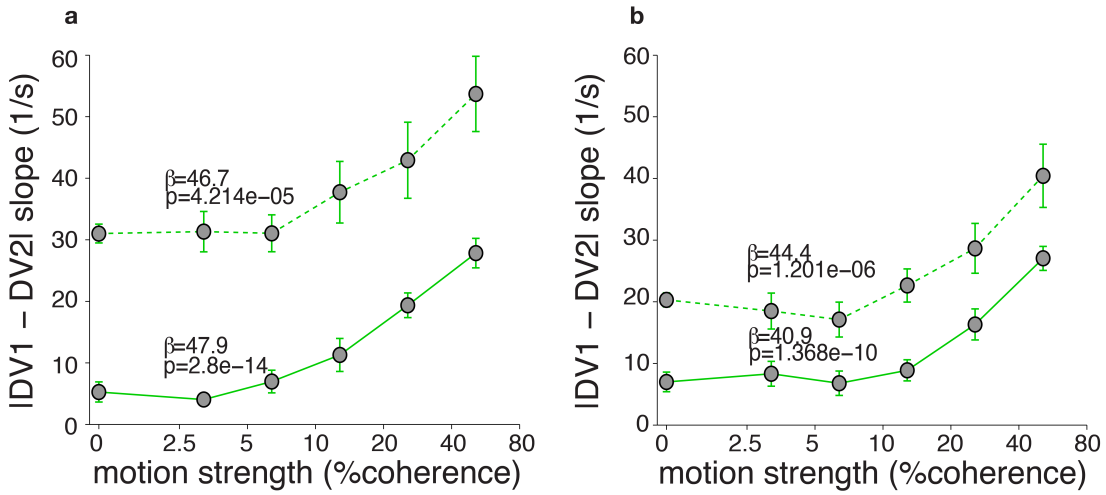

Figure 3.10: **Slope values as function of stimulus strength - PMd. a)** For both the fixed duration task (solid line) and the variable duration task (dashed line) the slopes show significantly higher values for higher coherence (easier stimuli) as one would expect from a brain area representing accumulation of evidence toward a choice. Notice the vertical shift of the traces between the fixed duration (solid line) and the variable duration (dashed line) indicating consistently higher |DVdiff| slopes in the variable duration task. Beta and p-values shown for a linear regression of |DVdiff| on stimulus strength. **b)** Same as **a)** for Monkey F.

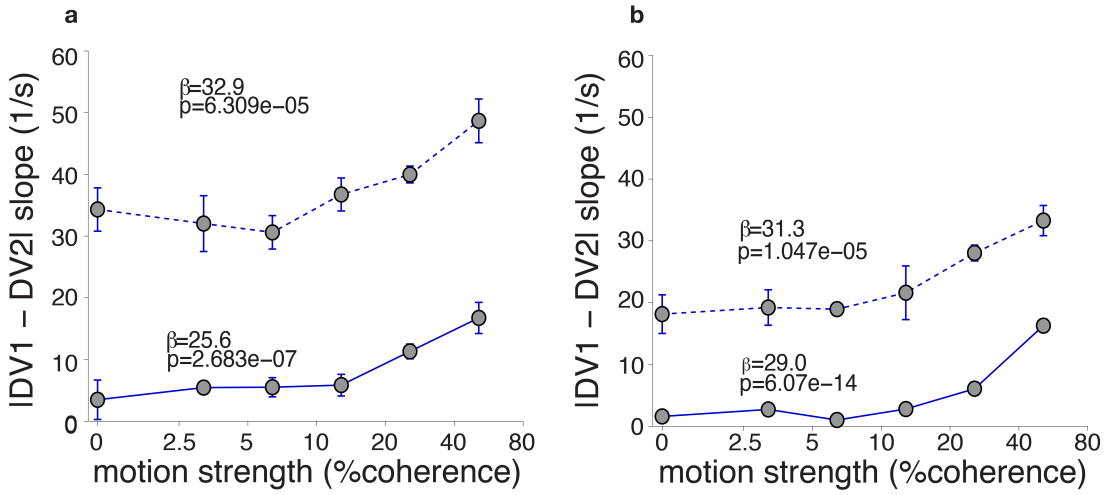

Figure 3.11: **Slope values as function of stimulus strength - M1. a)** For both the fixed duration task (solid line) and the variable duration task (dashed line) we recover the same effects seen in PMd (Figure 3.10). Beta and p-values shown for a linear regression of |DVdiff| on stimulus strength **b)** Same as **a)** for Monkey F.

of a gain adjustment in the integration of evidence under uncertainty conditions.

As a control for the influence of removing the delay period we ran a third version

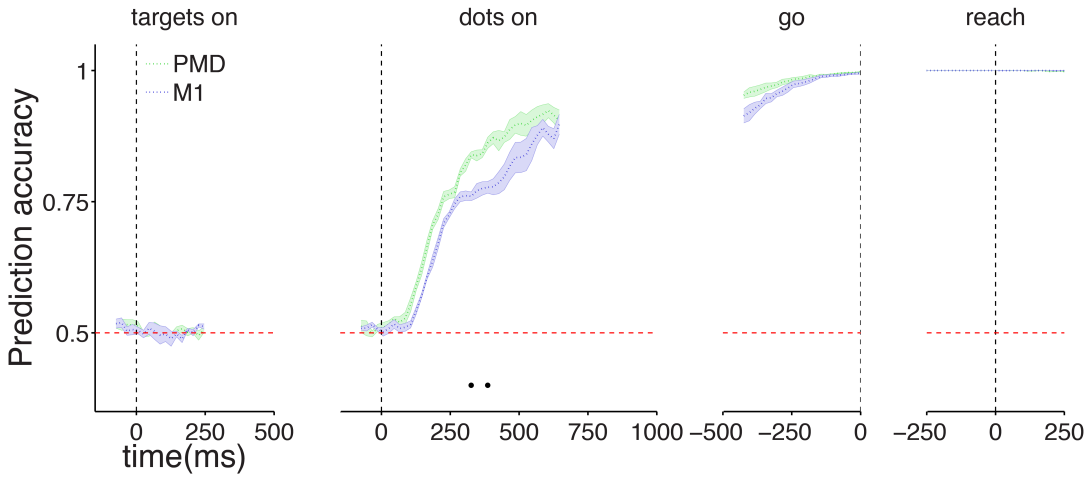

Figure 3.12: **Neural population choice prediction accuracy on single trials - Variable Duration task with delay.** Average prediction accuracy over time ± SEM for PMd (M1) are plotted in green (blue). Same conventions as in Figure 3.1. The rise in prediction accuracy after the onset of the dots stimulus is much sharper than in the fixed duration task (Figure 3.1) for both PMd and M1 even when the delay period is present. Data for Monkey H.

of the task in which the stimulus duration was variable but the delay period was present and equal in length to that used in the fixed duration task. Choice prediction accuracy traces in this task clearly show (Figure 3.12) that the increase in predictive activity is not exclusively due to removing the delay period but are in fact mostly due to the uncertainty about the stimulus duration (compare Figure 3.12 with Figure 3.1 a and Figure 3.9 a)

3.2.4 Increase in predictive activity is not due to motor signals

The preceding analysis shows that the accelerated dynamics under conditions of temporal uncertainly cannot be attributed simply to motor signals that appear earlier in the trial in the absence of a delay period. However, it remains possible that the accelerated dynamics result from a combination of the decision-related activity with motor signals early in the trial. A signature of such motor signals would be a correlation with motor parameters known to be well represented in PMd and M1 (Georgopoulos

et al., 1982, 1989; Afshar et al., 2011). To rule out this possibility we attempted to predict one of those parameters, reaction time, based on neural activity of the exact same units that went into our logistic regression analysis. If we could predict reaction time based on activity fairly early on in the stimulus presentation period, it would imply motor signals had permeated the evidence integration period. To have a reference point and also to rule out this was already the case in the fixed duration task we started by analysing those datasets. The analysis was performed separately for each reach direction to improve the models prediction accuracy, since the RT predictive units (or their relative weights) might be different for the 2 directions of movement. The quality of our prediction of RT was quantified as the fraction of variance of behavioral RTs explained by our neural data using our best predictive model for each time point during the trial. Our results for the fixed duration task show that, as expected, our prediction of reaction time during the early portion of the trial (targets and dots epochs) is indeed very poor (Figure 3.13).

It is only late in the delay period that the fraction of variance in reaction time explained by neural activity starts to slowly rise; the predictions become strikingly more accurate after the go cue, peaking around 400-500 msec. At this point the monkey will have already started his reach on fast trials but not on slow trials which leads to a strong dynamic range in firing rates that correlates with reaction time, leading to the increase in R^2. The peak values for R^2 in this period are higher for M1 than PMd, hinting at a stronger role of the former in implementing movement initiation.

The fixed duration results set a benchmark for what we should expect for the variable duration task. It turns out the results for the variable duration task are remarkably similar (Figure 3.14). If anything, the R^2 values are even lower both during the dots period and just prior to the go cue for the variable duration task compared to the fixed duration task. The same difference between M1 and PMd remains.

Our results show that regardless of task timing, motor parameter representation (as exemplified by reaction time) only becomes strong and reliable in these structures

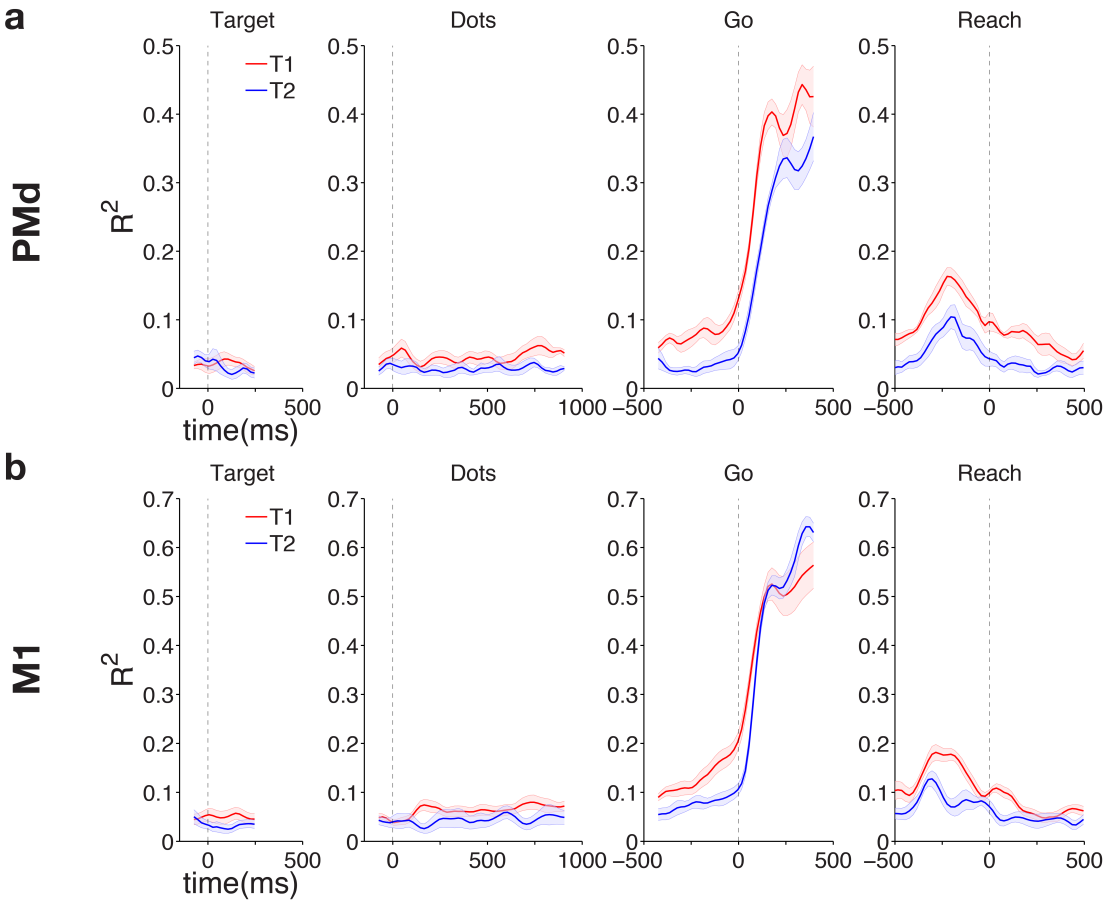

Figure 3.13: **Single trial reaction time prediction in the fixed duration task based on neural activity from PMd and M1.** Fraction of variance explained by a linear model regressing single unit activity in **a)** PMd against reaction time for the fixed duration task. Red traces represent average fraction of variance for rightward choices and blue traces average leftward choices ± SEM (shaded areas). Across the population, neural activity only becomes a reliable RT predictor on or around the time of the go cue. **b)** Same as **a)** for M1.

around and after the time of the go cue and not while the evidence integration is taking place. Thus, the enhancement in choice predictive activity early in the stimulus presentation period during the variable duration task does reflect a change in decision dynamics and not a contamination of motor signals.

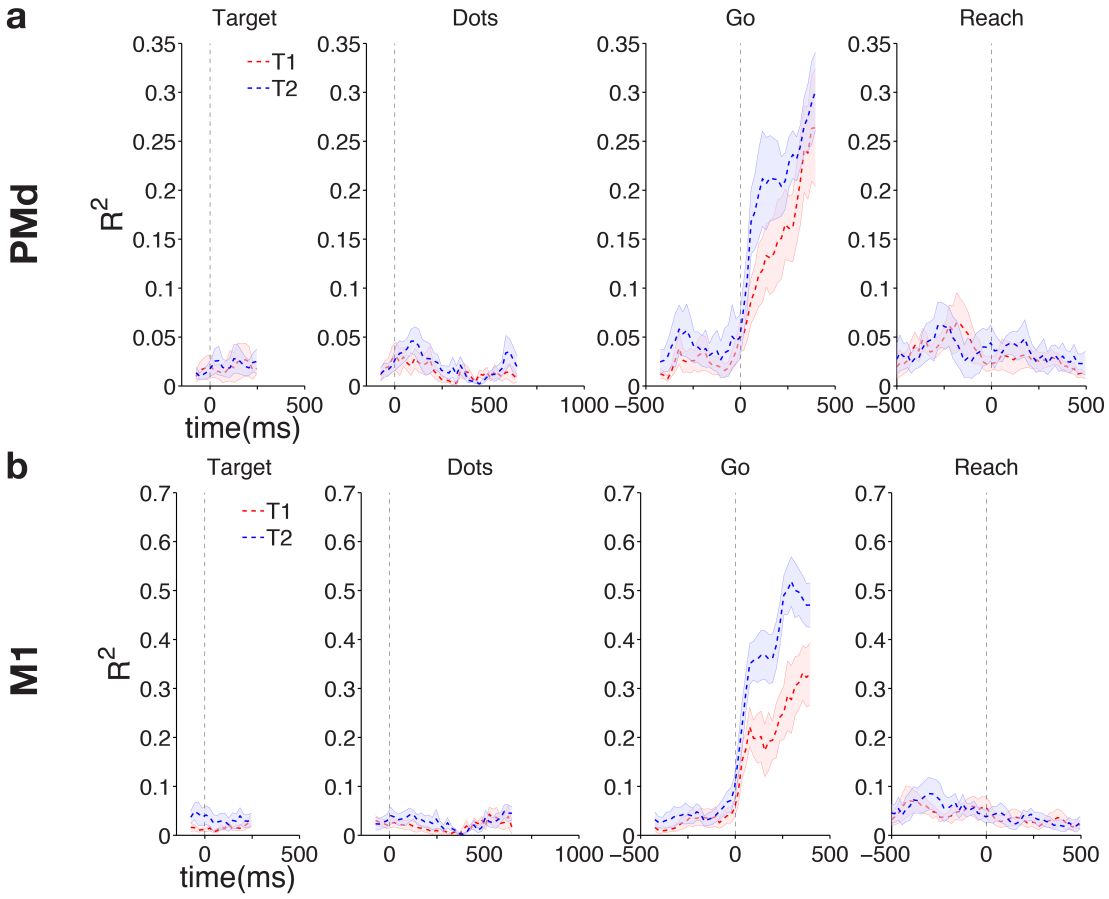

Figure 3.14: **Single trial reaction time prediction in the variable duration task based on neural activity from PMd and M1.** Fraction of variance explained by a linear model regressing single unit activity in **a)** PMd against reaction time for the variable duration task. Red traces represent average fraction of variance for rightward choices and blue traces average leftward choices ± SEM (shaded areas). Across the population, neural activity only becomes a reliable RT predictor on or around the time of the go cue. **b)** Same as **a)** for M1.

3.2.5 Choice signal is well distributed across the population

Finally, we wanted to determine just how robust our choice prediction accuracy was, and whether it relied on signals carried only by a small fraction of cells. If this was the case it could be that the early choice predictive signals were only a small component of what these areas were representing in the context of this task. We already know from chapter 2 that while some cells clearly carry these early signals (Figure 2.9) others have no choice modulation until much later in the trial (Figure 2.8). We also

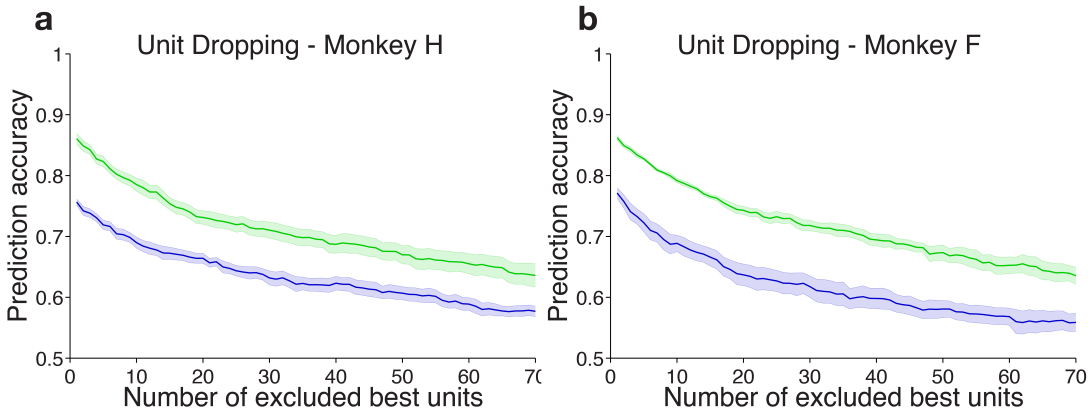

Figure 3.15: **Unit dropping analysis - Fixed Duration. a)** Prediction accuracy curves for PMd (green) and M1 (blue) as a function of the number of best units excluded for the fixed duration task. The decay in performance is very smooth, demonstrating how distributed the choice signal is across many cells. **b)** Same as **a)** for Monkey F.

know the number of units with significant modulation decreases with the size of the modulation for both signs (Figure 2.13). Still, we wanted to directly test just how much our prediction accuracy would be hurt had we not been fortunate to record from the best predictive units. We chose a fixed time point, the end of the dots presentation, for simplicity and because it was a good compromise between a strong signal and one that is still linked in time to the integration of evidence. We then proceeded to rank the units according to how predictive of choice they were at this time and remove them one by one, allowing the classifier to re-adjust the remaining weights (see Methods). Every time a unit was removed from the dataset the prediction accuracy was recalculated using 10-fold cross-validation. The unit dropping curves for the fixed duration task (Figure 3.15),show how predictive accuracy decays smoothly as the best units are removed for both areas and both monkeys. PMd remains more predictive than M1 in all cases, and strikingly both areas still predict choice above chance even after the 70 best units were dropped!

We applied the same analysis to the variable duration task and obtained only up to 10% drop in prediction accuracy for both areas and monkeys (Figure 3.16). This drop in performance is much lower and smoother compared to the fixed duration due to the higher number of strongly tuned units. The curves for PMd and M1 in this

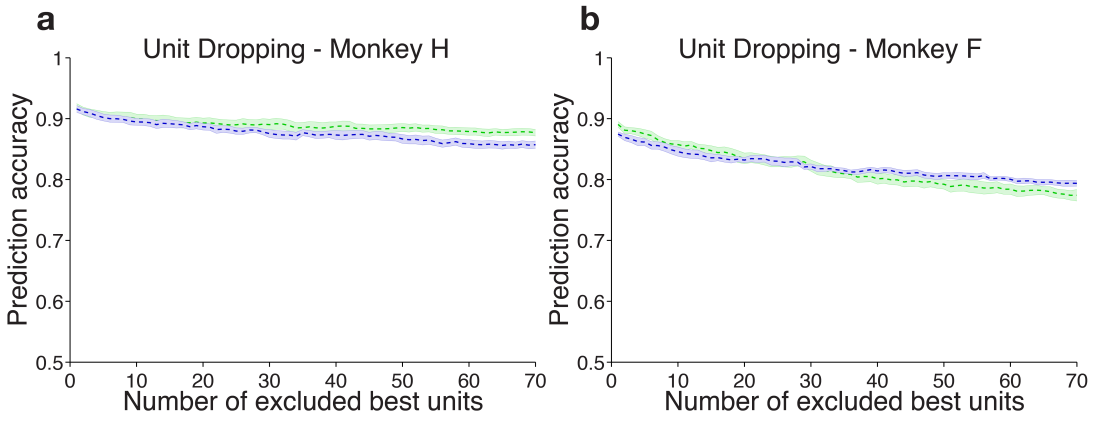

Figure 3.16: **Unit dropping analysis - Variable Duration. a)** Prediction accuracy curves for PMd (green) and M1 (blue) as a function of the number of best units excluded for the variable duration task. The choice signal is even more robust in this task as evidenced by the very small decline in prediction performance. **b)** Same as **a)** for Monkey F.

case remain largely overlapping, strengthening the argument that under conditions of temporal uncertainty the two areas behave very similarly.

3.3 Discussion

At the beginning of this chapter we set out to dive deeply into single trial analysis and obtain a population level description of eventual decision related responses. From our brief analysis in Chapter 2, we knew there was a broad distribution of choice predictive activity across the PMd and M1 populations. Because the responses were very diverse and multiple signals seemed to be represented even on individual units, we decided to quantify the information about the future choice of the subjects across the entire population for each area. Doing so in a cross-validated manner and on single trials provided an accurate measure of what an ideal observer could infer based on the activity of the recorded population. When evaluating the obtained prediction accuracies is important to take a step back and recall we are only monitoring a few hundred of millions and millions of neurons present in motor and premotor cortex. And yet, due to strong signals on individual units and redundancy of responses across even a small population we were able to predict choice above chance

levels just ∼200 ms into the stimulus presentation. In the fixed duration task, that allows better temporal separation between evidence integration, motor preparation and motor execution, the rise in prediction accuracy was steady throughout the stimulus presentation well before the go signal. We were also struck by the reliability of the difference between choice prediction accuracy in PMd and M1 across sessions and across monkeys (Figure 3.1). While we tried to be as consistent as possible placing the arrays in the most likely locations for strong arm related activity in PMd and M1, there is inevitable variability in anatomical features and stereotaxic coordinates from monkey to monkey. Moreover, the arrays themselves cover a significant patch of cortex (4 x 4 mm) and are placed almost edge to edge along the anterior- posterior axis (Figure 2.2), which could have muddled this difference between the two areas. One interesting question we intend to pursue in the future using our existing data is whether this difference between PMd (anterior) and M1 (posterior) is also present at a finer scale. Said, differently is it the case that even *within* each area, anterior units tend to be more choice predictive early on during the dots period than posterior units? Or is there no clear organization within each area with regards to this functional property? Perhaps the most important finding in this chapter was the lawful dependence of choice predictive activity on stimulus difficulty. This feature is one of the hallmarks of decision-related activity and allowed us to confirm activity in these areas (and especially PMd) represents the evolution of the decision process. A very recent study in PMd and M1 claimed that average activity in both these areas is strongly decision-related in an evidence-tracking task in which evidence was provided in discrete steps during the trial (Thura and Cisek, 2014). The researchers argued both the strategy of the subjects and the activity of specific cells in PMd and M1 was better explained by a tracking model with an added urgency signal than an accumulator model. This property could, however, be specific to the task design used in that study. Deeper analysis of our data could allow us to distinguish between these two models in (i) a task that for which the optimal strategy is to integrate visual evidence and (ii) a dataset that allows us to calculate decision states on single trials in a very reliable manner across a diverse population of neurons. While one could argue there

was some precedent to expect decision-related signals in PMd and perhaps in M1 there was very little precedent for the dramatic increase in prediction accuracy when the stimulus duration became uncertain. In fact the only other report of a similar effect, to our knowledge, was the last results figure in (Shadlen and Newsome, 2001). In this study Shadlen and Newsome had performed a very similar task manipulation and verified the firing rate modulation of LIP neurons with choice increased very significantly when short duration trials were added to the task. This effect was interpreted as a consequence of the simultaneous influence of motion evidence integration and temporal expectation of the stimulus duration in LIP activity. We interpret the increase in prediction accuracy as a change of dynamics in the evidence integration process that seems to resemble an adjustment in gain, since the stimulus coherence effects are very well preserved. There is evidence of gain adjustment in LIP even from trial to trial following error responses (Purcell and Kiani, 2016) so it is conceivable the same could happen in PMd and M1 from session to session. However, we can't rule out an adaptable urgency signal that instead of growing over the course of the trial (Thura and Cisek, 2014), is permanently enhanced when the stimulus duration is uncertain. Having, reliable decision variable estimates on single trials should allow for a direct comparison of goodness-of-fit between the two different models" adjusted gain and constant gain with added urgency. Ruling out the presence or enhancement of motor signals early on during the trial was a very important control to our analyses of decision-related activity and confirms that, regardless of the stimulus statistics, the activity we analyse during dots is very different in nature compared to activity around the go cue, when peri-motor signals take over. The rise in prediction accuracy for the variable duration task is also accompanied by the disappearance of clear differences between PMd and M1 during the dots period. While we know these areas are clearly functionally segregated in the fixed duration task and during resting states (Kiani et al., 2015), it will be interesting to determine whether they act more as a unit once stimulus duration uncertainty comes into play. Clustering analysis as well as cross correlation analysis between single trial decision variable traces across the two areas will shed light on this possibility. Finally, the unit dropping analysis confirms choice

signals are robust and distributed across many cells in the population. This observation confirms we weren't just fortunate to record a few very reliable units but indeed decision related signals emerge from a significant portion of these networks.

4

Signal Stability and Diversity in PMd and M1

In the previous chapters we have solely focused on choice signals in PMd and M1. When studying decision formation this is arguably the most relevant signal but not necessarily the only meaningful one represented in premotor areas. In fact, it has been shown (Meister et al., 2013; Mante et al., 2013) that even in areas LIP and PFC other non-decision signals are present. In particular a non-directional coherence dependent signal akin to a "stimulus difficulty" signal and a signed motion coherence signal that was orthogonal to choice, interpreted as momentary evidence, were found. The ability to find these signals was mostly due to the fact that these authors recorded from a more diverse set of neurons in these studies, dropping the selection criteria employed in most previous studies. Using an approach that relied on clever experimental design, a prior study by Bennur and Gold (2011) also identified multiple task-related signals in LIP, notably demonstrating a clear dissociation of abstract, decision-related signals from signals related to action selection.

In the same spirit, we sought to identify a fuller range of task-related signals in PMd and M1 by combining population analyses with an all comers selection policy. Due to the nature of our chronic recordings (Utah arrays), we dont have the ability to select which neurons to record; as consequence we obtain an unbiased pool of neural signals. To these data we applied an analysis method first described in Mante et al. (2013) that attempts to dissociate multiple task-related signals present at the

population level.

In addition to analyzing our own data, we re-analyzed data from the Bennur and Gold study cited above (data provided by courtesy of Prof. Joshua Gold, University of Pennsylvania). Most of the analyses in the published study (Bennur and Gold, 2011) were done at the single neuron level and then averaged. We were interested in applying population methods (Mante et al., 2013) to this interesting data set to understand what insights might be added by the population analysis and to obtain results that would serve as a point of comparison for our PMd and M1 population results.

Another issue we wanted to address in the current study concerned the fact that almost all studies thus far have reported decision-related signals in premotor areas that are well matched to the corresponding motor effector: eye movements for oculomotor areas and arm movements for somatomotor areas. We wanted to know if some of these signals were effector independent or supra-modal. To test this idea we had monkeys perform the fixed duration dots task with both a reach response and a saccadic response within the same session. This approach allows us to directly compare the responses of the exact same populations of neurons in PMd and M1 when using the two different motor responses. A very recent study showed that decision related signals in LIP were largely effector independent while decision-related signals in MIP were significantly reduced (but still present) when eye movements, as opposed to arm movements, were employed as the operant response (de Lafuente et al., 2015). We were interested in testing whether areas PMd and M1 would resemble LIP or MIP in this regard or if decision related signals would not be present at all when using the non-preferred motor response.

Author contributions: Diogo Peixoto collected the data and performed the analyses on the multiplexed signals in PMd and M1. Sharath Bennur and Joshua Gold collected and generously shared the LIP data. Diogo Peixoto re-analysed it with William Newsome's input. Diogo Peixoto performed the experiments for comparing eye and hand related responses in PMd and M1. Diogo Peixoto and Bora Erden designed the analyses and generated the corresponding figures.

4.1 Methods

4.1.1 Colored targets motion discrimination task

The full description of the methods used to collect LIP data while the monkeys performed a modified motion discrimination task can be found in Bennur and Gold (2011). In brief, the researchers trained two monkeys to perform a more sophisticated motion discrimination task in which the decision about the direction of motion in the stimulus was orthogonal to the action selected to report it. This separation was achieved by implementing the following rule: rightward motion is reported by a saccade to a red target whereas leftward motion is reported by a saccade to a green target. By randomizing the location of the colored targets from trial to trial, the decision about the motion direction and the action required to report it become effectively independent. The researchers then used 3 different versions of this same task that differed based on the time when the colored targets were unveiled. In Task 1 both targets started out blue but switched color, one to green and one to red, before the random dots stimulus was presented (Figure 4.1). In Task 2 this color changed happened 400 ms after the start of the random dots stimulus, or halfway through the dots presentation. Finally in Task 3, the color change only occurred in the delay period, 300 ms after the dots had been removed from the screen. This new paradigm enabled the dissociation of neural signals related to formation of the perceptual decision from neural signals related to action selection. The different task versions allowed to study how the perceptual signal is converted into an action signal when the mapping between stimulus and action is revealed at different points in the trial. The different Tasks were run in a block fashion and we analysed all units (56 neurons) for which all 3 tasks had been tested.

4.1.2 Targeted Dimensionality Reduction

Targeted dimensionality reduction (TDR) was a method developed to disentangle neural signals that are mixed at the single cell level but can be dissociated at the

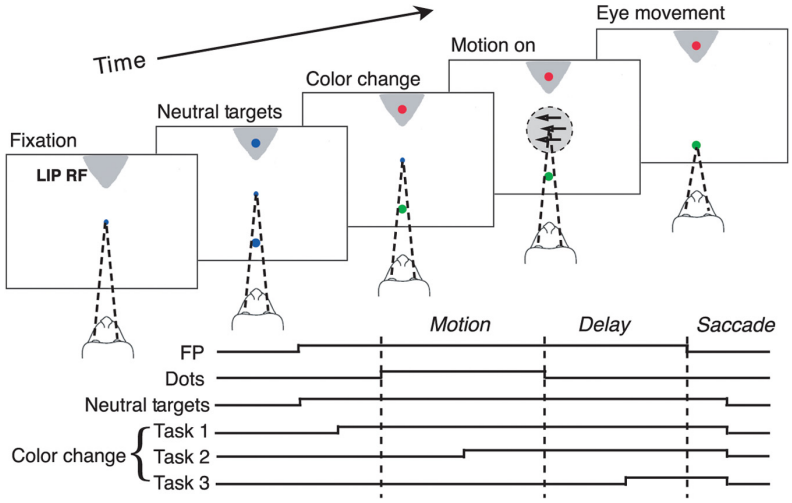

Figure 4.1: **Motion discrimination task with flexible choice mapping.** The trial starts with monkeys fixating on the fixation point on the screen. As soon as the trial starts 2 blue targets appear: 1 in the cell's Response Field and one opposite to it. In Task 1 these targets change to red and green 200 ms before the stimulus is presented. In Task 2 this change happens halfway through the dots period which lasts 800 ms in total and in Task 3 300 ms into the delay period that follows the stimulus presentation. The delay period lasts a total of 500 ms at the end of which the monkey is given a go cue to report its decision by performing a saccade to one of the colored targets.Figure from Bennur and Gold (2011)

population level. It also incorporates a dimensionality reduction step as a form of smoothing or noise reduction. The full description of targeted dimensionality reduction can be found in the Supplements for Mante et al. (2013). The main change to the original method when applied to the LIP data of Bennur and Gold (2011), was the use of different regressors corresponding to different task variables of interest. For this analysis we used Color (context signal - red or green in RF), Response Field (RF) Choice (Target in RF or opposite to RF chosen at the end of the trial) and Signed Motion (stimulus coherence, positive values for rightward motion and negative for

leftward). The time epoch analysed starts 400 ms before the dots onset and ends at the end of the delay period (1500 ms after dots onset). We selected the subset of 56 units for which all three tasks were ran. Spike trains for each trial were smoothed with a 60 ms gaussian kernel. These single trial psths obtained after smoothing, were z-scored individually for each unit.

In summary, the method can be broken down in the following steps:

1. Describe the (z-scored) response of unit i at time t on trial k as the following linear combination of task variables:

$$r_{i,t}(k) = \beta_{i,t}(1) \times Color(k) + \beta_{i,t}(2) \times RFChoice(k) + \beta_{i,t}(3) \times SignedMotion(k) + \epsilon \tag{4.1}$$

2. Calculate the beta values for each regressor, time point t and unit i.

3. Group beta values in vectors for each time point and regressor. These regression vectors now define directions in state space along which task variables are represented.

4. Select regression vectors from the time point for which the norm is maximum.

5. Build Condition-averaged population responses (defined by context, choice, motion and task).

6. Project regression vectors in lower dimensional PCA space.

7. Obtain axis of Color, RF Choice and Signed Motion by orthogonalizing low-D regression vectors.

Regressors:

- Color: +1 Red in RF, -1 Green in RF;
- RF Choice: +1 Chosen Target in RF, -1 Chosen Target out of RF;
- Signed Motion: +1 for 99% coherence to the right, -1 for 99% coherence to the left;

Detailed notes about the implementation of the method:

- After smoothing and z-scoring, the responses of each unit were fit to the linear model described in step 1. The beta values for each regressor were calculated anew for each ms of the epoch considered: [-400,1500] ms aligned to dots onset (equivalent to using 1ms bin width, after smoothing, that we slide by 1ms at a time)

- Condition-averaged responses comprise responses from all units considered in the analysis for one given condition. Conditions were defined by: task version, context (red in RF or green in RF) and signed motion. For a given condition the responses of one unit were averaged across all trials of that same condition. The same procedure was followed for all units. For example for task 1 the population response to + 99% motion, Red in RF, and correct choice would be a matrix with the time course of each units average response for those trials. The matrix dimension would be 56 (# units) x 1900 (# timepoints).

- After building the condition-averaged population responses (for all conditions) we used PCA to estimate the dimensionality of the population responses. We first concatenate the responses of each unit across all conditions and obtain a matrix of size #units $\times$ (#conditions $\times$ #timepoints).We then run PCA on this matrix to obtain the weights for each PC (which relate the directions of maximum variance with the identity of the units in the population). We also determined how much variance each PC explains and plotted the cumulative variance as a function of PC number. For further analysis, we retained the first 12 PC dimensions, which explained greater than $> 70\%$ of the variance so we chose the first 12 PCs for this analysis. The main observations reported here do not depend on critically on the exact number of PCs retained for the analysis. The main purpose of using PCA is to find a lower dimensional space that explains the most significant patterns across the populations but not every single fluctuation. In essence, this is a de-noising step where the main population components are preserved and the noisy components are discarded.

- Finally, the purpose of orthogonalising regression vectors is to find dimensions that explain task variables independently of each other. For instance we might want to orthogonalise Signed Motion to RF choice to look at effects of Signed Motion that are

independent of the choice the monkey makes. The orthogonalisation was performed (sequentially) through QR decomposition and the order we used was: Color (which remains unchanged) RF choice and Signed Motion. We chose to keep Color unchanged since it was the strongest and most stable signal in the neural responses. The order of orthogonalisation matters since (as long as the vectors are not perfectly orthogonal to begin with) only the first vector will remain unchanged and the following vectors will be rotated away just enough to become orthogonal to all the previous vectors.

For the PMd and M1 analyses we used a very similar methodology with the following changes:

- We focused on the dots epoch to best tease apart signals during the evidence integration and thus used data from [-150, 1000] ms aligned to stimulus onset.
- We pre-selected units that have an overall minimum rate of 2 spikes/s during the dots period. This selection should still give us a very unbiased pool of neurons and exclude neurons that are almost completely quiet during our epoch of interest
- Our regressors were Choice (left or right), Signed Motion (just like in the LIP data) and Stimulus Difficulty (unsigned stimulus coherence) akin to the signal described in Meister et al. (2013).
- Since there is no context signal analogous to Color, the orthogonalisation order was Choice, Signed Motion and Stimulus Difficulty.

4.1.3 Dots Task: Eye vs hand

We used a fixed duration version of the motion discrimination task for both reach blocks and saccade blocks. The trials in the reach blocks were identical to those described in Chapter 2 (Figure 4.2 a)). For the saccade blocks however, the front plate of the primate chair was closed preventing the subject from reaching out or touching the screen. Up until the go cue the monkey was required to hold fixation on the fixation point, just as in reach trials. As the name suggests, for saccade trials

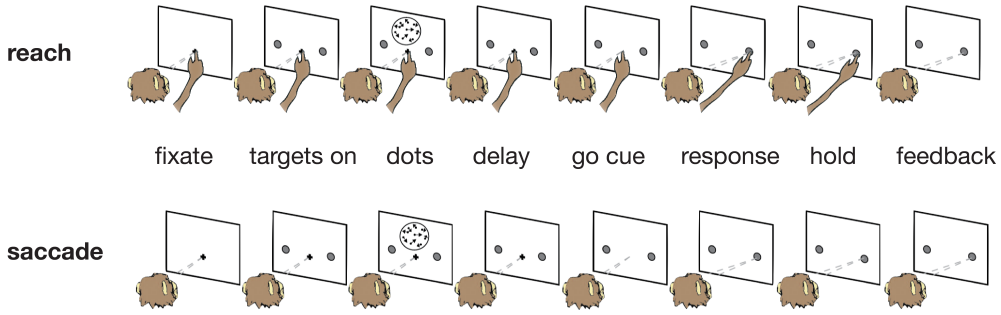

Figure 4.2: **Motion discrimination task with two different operant responses.** Top panel: fixed duration task with arm reach as the operant response, as described in Chapter 2. Bottom panel: fixed duration task with saccadic eye movements as the operant response. The timing of the events in the task was exactly the same. In both versions eye fixation was required from the beginning of the trial until the go cue was presented.

the monkey was asked to report its decision with a saccadic eye movement towards one of the two targets after the go cue was presented (Figure 4.2 b)). Both arms were inside the chair, and the ipsilateral arm was restrained, but we cant rule out the possibility that the subjects performed very small, habitual arm movements during the saccade blocks. From our visual inspection, however, the monkeys sat calmly in the chair when performing the saccade task and switched seamlessly from reach blocks to saccade blocks as soon as the front plate of the chair was closed. For these reasons we find it very unlikely that small arm movements could explain our findings (below) that choice signals were present in PMd during this task. In a given session for this experiment, we typically did one reach block followed by one saccade block. The number of trials was usually very similar for both blocks ($\sim$500 trials each). The significant advantage afforded by our chronic array recordings was the opportunity to compare the same units under the same behavioral conditions across both motor effectors. The methods for the choice modulation analysis and for the logistic regression were previously described in Chapters 2 and 3, respectively.

4.2 Results

4.2.1 Multiplexed signals in LIP

The analyses on the LIP data were performed separately for each task. We'll start by analysing results from Task 1, then 2 and 3 and finally comparing the results across tasks. In Task 1, color, signed motion and RF choice are well represented in the population (Figure 4.3 a) as shown by the percentage of cells whose activity is significantly correlated ($p< 0.01$) with these task variables. Color is the strongest signal (Figure 4.3 a, b: highest % of significant betas and largest norm) and has a very short latency after the onset of the colored targets. The advantage of plotting vector norm instead of percentage of significant betas lies in not having to choose an arbitrary cutoff for significance. This metric captures the overall magnitude of a signal across the population and allows for comparison between regressors. Its downside is that even noise levels of signal representation (like baseline) have non-zero norms. The RF choice signal only starts to rise $\sim$ 400 ms after the motion onset but, as expected, keeps getting stronger throughout the trial. This latency is longer than what we would normally expect for LIP neurons especially since the mapping between motion direction and action is known before the stimulus presentation begins. Interestingly, the signed motion signal begins rising 200 ms after the motion onset (the expected latency for LIP) and lasts throughout most of the delay period, long after the motion offset and long after the color signal appears in this task. These observations suggest that this signal is not just directly tied to the stimulus presentation and is consistent with author's interpretation of a perceptual decision signal.

In a previous iteration of this analysis we included an additional regressor which we named RF motion (stimulus coherence supporting evidence towards RF target or opposite to RF target, defined as Color $\times$ Signed Motion). RF motion combines color and signed motion information and as a consequence its onset requires both pieces of information to be present on the screen. We had included RF motion as a regressor because we felt intuitively that once the color cue appeared, at least some of the

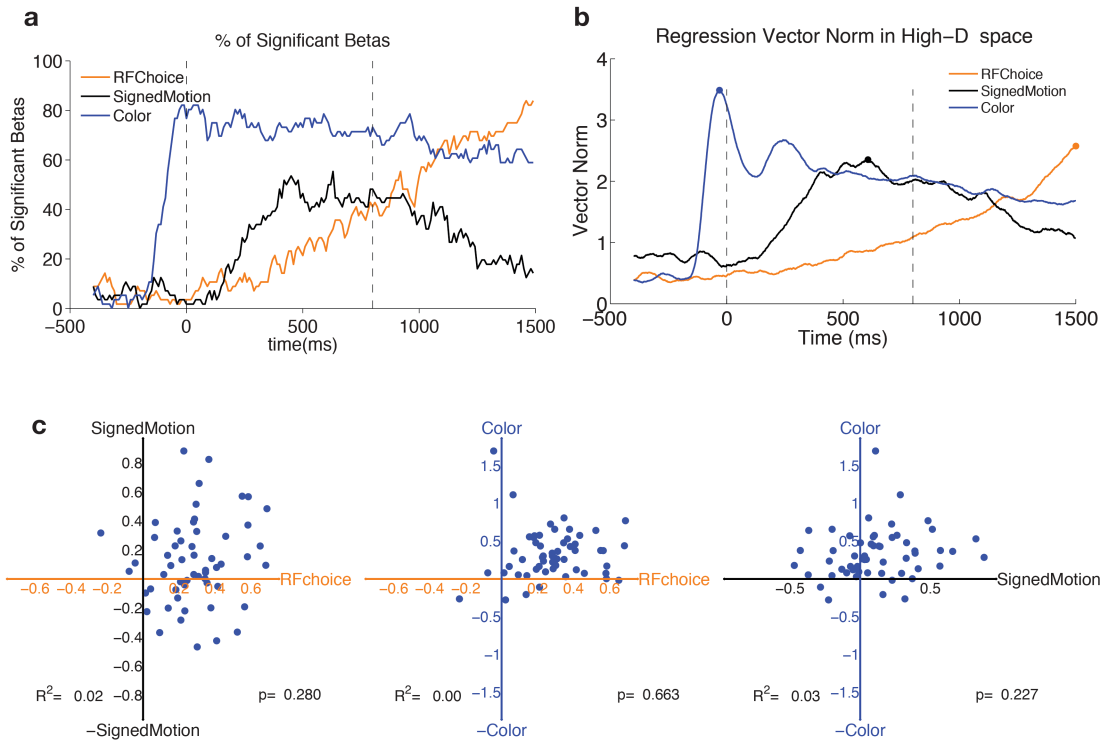

Figure 4.3: **Choice, Stimulus Motion and Color representations in LIP - Task 1. a)** Percentage of cells whose activity is significantly correlated with Choice, Stimulus Motion or Color throughout the dots presentation. **b)** Norm of the 3 regression vectors for Choice, Stimulus Motion and Color throughout the dots presentation. **c)** Correlation between all pairs of regressor values for each neuron (blue dots).

incoming motion information would be integrated directly toward a plan to move the eyes to the appropriate target. Basically this intuition turned out to be wrong, with RF motion being represented by only a small fraction of cells and having a very low norm. For this reason and to avoid using an irrelevant regressor in our analysis, it was removed from our linear model. Nevertheless, we are still puzzled why the LIP appears to continue with a categorical direction calculation when it could be planning the eye movement directly.

After choosing the time point for which each signal is strongest (highest beta norm Figure 4.3 b)) we examined the relationship between beta coefficients for different pairs of regressors on a cell-by-cell basis. There are no strong correlations between beta coefficients for different regressors (Figure 4.3 c)). This result shows that, for instance, knowing how well a cells activity is correlated with choice is not very predic-

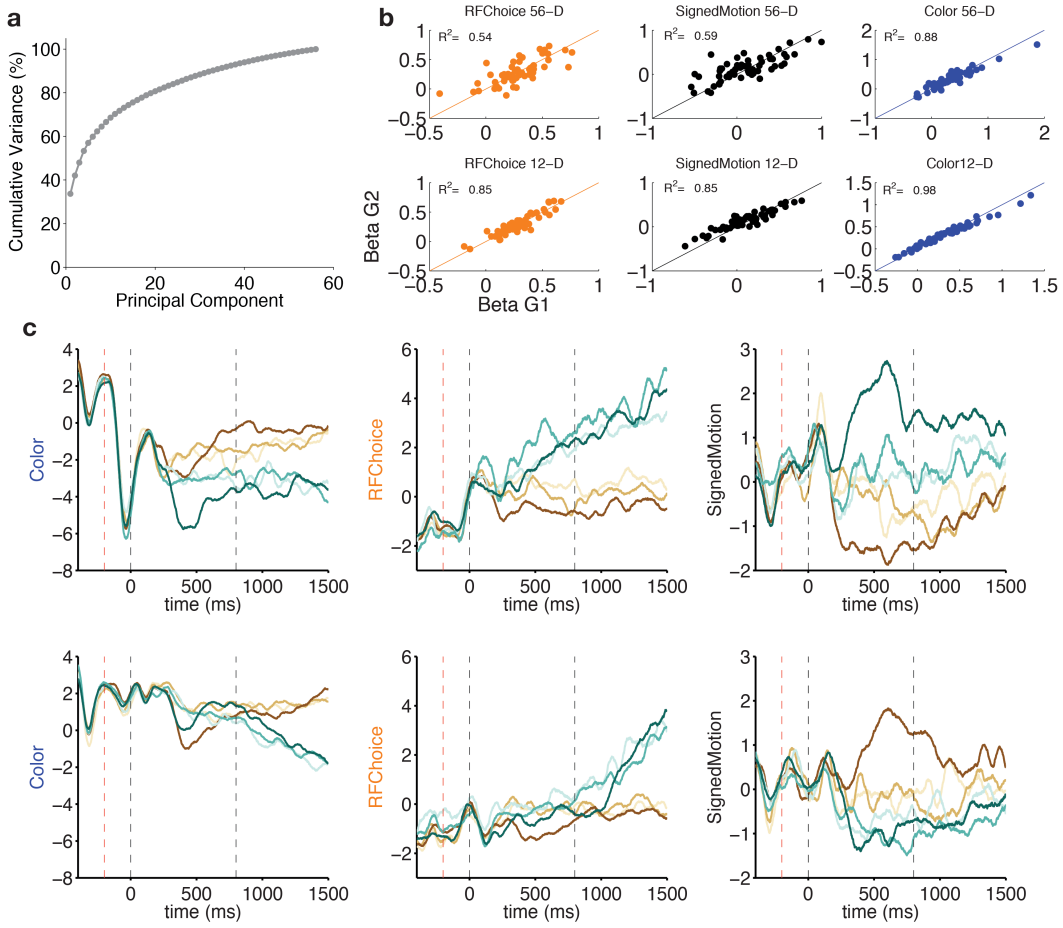

Figure 4.4: **High and low dimensional signal representation in LIP - Task 1. a)** Cumulative variance explained as a function of principal component number after performing PCA on the population data during the dots period. **b)** Regression value consistency for 3 factors in High (top row) and Low (bottom row) dimensional spaces. For each neuron trials were randomly assigned to two disjoint groups and regression values calculated independently. Scatter plot shows correlation between regressor values for each trial group (x and y axes) and each neuron (solid dots). **c)** Projection of condition-averaged population data on the three task-relevant axes defined: Choice, stimulus motion and color.Top row corresponds to context 1 (red in RF) and bottom row corresponds to context 2 (green in RF). Green traces correspond to Tin choices while brown traces correspond to Tout choices. Responses for different stimulus coherences are plotted as different shades of the same color with higher coherences corresponding to darker shades. Black dashed lines indicate the onset and offset of the dots stimulus and red dashed lines indicate the onset of the coloured targets. Only correct trials were used to compute the condition averages.

tive of how well it will be correlated with motion coherence. Still, as we'll see later, it doesn't exclude the possibility of effects of one signal leaking into another regressor

dimension, i.e. a non-significant correlation between beta vectors does not guarantee perfect orthogonality between them.

For this subset of 56 cells, 12 principal components are enough to account for a large fraction ($> 70\%$) of the population variance (Figure 4.4 a)), indicating that despite mixed selectivity, the population response is fairly low dimensional. We assessed the reliability of the beta coefficients by calculating them using disjoint sets of trials. Projecting the beta coefficients onto the low dimensional space de-noises the beta coefficients for Color, Signed Motion and Choice, improving their reliability as demonstrated by a substantial increase in the R-squared values for beta coefficients calculated using two separate sets of trials (Figure 4.4 b)).

A primary goal of TDR is to visualize the population activity over time along axes of interest, which in our case are state space directions that co-vary with task variables. The population activity is defined by the condition-averaged psths for all cells considered as defined in the methods. The axes are a set of orthogonal vectors based on the regression vectors we obtained. These vectors are orthogonalized using QR decomposition and define our beta basis. In this particular analysis we first establish the Color regression axis and keep it fixed since it is the strongest and most stable signal in the neural population. We then orthogonalize RFchoice to the Color. Thus the RF choice axis should be thought of as the component of choice-related activity that is not accounted for by the color axis (this becomes important below). We then orthogonalize signed motion to both Color and RF Choice to obtain a component that covaries with the stimulus coherence and direction independently of the color context and eventual choice. The 3 resulting orthogonal vectors are what we call our beta basis. When projecting the population activity onto the final beta basis (Figure 4.4 c) we can verify that along our color axis there is not only a strong color signal (compare traces between top-left and bottom-left panels after the color cue onset) but there are also choice components along the color axis as evidenced by the separation between green and brown traces (Tin and Tout choices)) in the top-left and bottom-left panels. Along the RF choice axis (Figure 4.4 c second column) we observe a clear separation between Tin and Tout choices as expected, but the latency of the

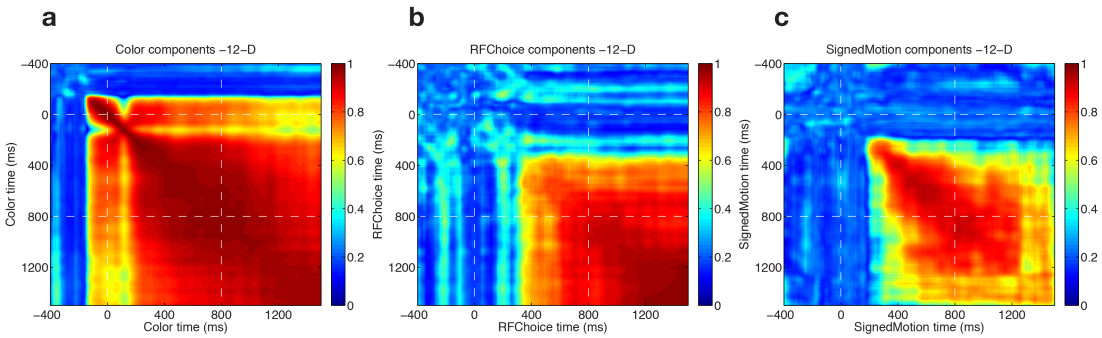

Figure 4.5: **Signal stability in LIP throughout the dots presentation and delay period - Task 1. a)** Heat map of Color vector similarity across time. For each time point the vector for Color was determined and normalised independently. The dot product for all pairwise combinations of timepoints is depicted in the heat map. Hot colors correspond to high dot products (strong alignment) and cool colors to low dot products (weak alignment). **b)** Same as **a)** for the Choice vector. **c)** Same as **a)** for Stimulus Motion vector.

choice signal was longer than expected for LIP, especially for context 2 (lower panel, column 2; green target in RF). For task 1 all ambiguity about the contingency between stimulus direction and the correct saccade target is resolved prior to dots presentation, and we would therefore have expected an onset latency for the choice signal of 200 msec as in most previous studies in LIP. The projection of population activity along the signed motion axis (Figure 4.4 c third column) shows a good separation between leftward and rightward motion stimuli, especially for strong coherences. Importantly these effects are still present to a lesser extent several hundred msec after the dots offset, suggesting that this is not a momentary stimulus-driven signal, as in Mante et al. (2013), but instead represents something closer to the integrated motion signal.

After their initial rise, both color and RF choice are very stable signals in the lower dimensional space as indicated by the square-like structure in the heat map of Figure 4.5 a and b). This implies that the neural ensembles that carry these signals are relatively constant over time. Signed motion is still fairly stable even after the motion offset (Figure 4.5 c), although the perceptible diagonal structure in this plot hints at some change over the timecourse of the trial in the ensembles that carry the signal.

Importantly, color and RF choice are not orthogonal signals at the population level

(Figure 4.4 c: compare brown and green traces in the top-left and bottom-left panels). For this reason the orthogonalisation order used to obtain the final beta basis is not trivial. Since color is the earliest and strongest signal we chose to keep it unchanged and orthogonalized RF choice and Signed Motion to it. Had we not orthogonalized in this order, we would have seen a substantial choice signal (related to the color of the RF target) prior to onset of dots motion. This raises the strong possibility that the initial transient color signal is in fact a pre-potent saccade planning response due to the animals extensive prior training on red saccade targets. There are hints in the data that the early color signal is different from the late color signal (Figure 4.5 a) top left, focus on the projection between the color components at t=-100 ms and t = 1400 ms for example and compare it with the hot square pattern we find from ∼200 ms to 1400 ms). In addition the overwhelming preference for the red target (Figure 4.3 c: center panel, notice how almost all cells have a positive y-value) and the fact that the choice signal seems to arise later in the context in which the green target is in the RF (Figure 4.4 c center-bottom panel) lend support to this possibility.

The same exact analyses shown for Task 1 were applied to Tasks 2 and 3. In essence most of the main features of the signals described for task 1 are conserved for tasks 2 and 3 with the expected time shifts caused by the different timing of onset of the red/green target colors.

Color is still a very strong, short latency signal in tasks 2 and 3 (Figure 4.6 a,b and Figure 4.9 a,b), with a sharp rise in magnitude after the colored targets onset. Also similarly to Task 1, Choice ramps up steadily until the operant saccade occurs, but with much longer latencies and slower rises than expected from prior studies of LIP (Figure 4.6 a,b and Figure 4.9 a,b).Signed Motion follows a similar time course in all 3 tasks lasting into the delay period and suggesting integration of evidence both in the presence and absence of the visual stimulus and colored targets on the screen (Figure 4.6 a,b and Figure 4.9 a,b).

The dimensionality of the data does not seem to dramatically depend on the timing of task events and remains low for Tasks 2 and 3 (Figure 4.7 a and Figure 4.10 a). Projecting the population activity into the low dimensional (de-noised) space

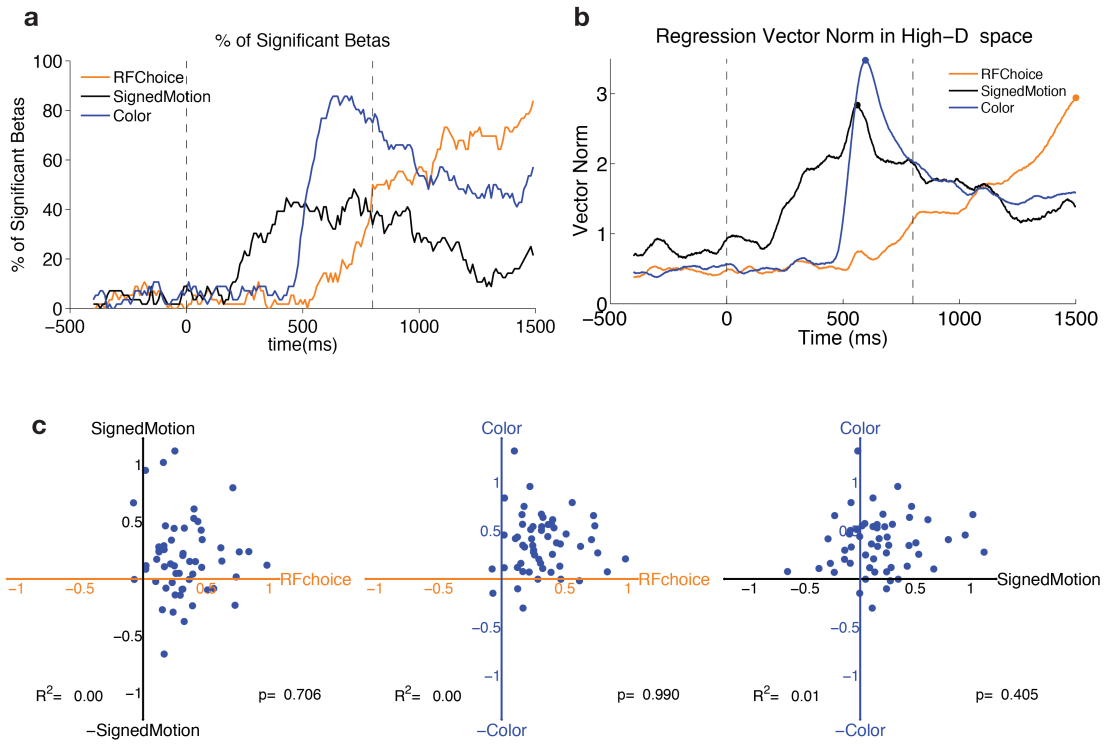

Figure 4.6: **Choice, Stimulus Motion and Color representations in LIP - Task 2. a)** Percentage of cells whose activity is significantly correlated with Choice, Stimulus Motion or Color throughout the dots presentation. **b)** Norm of the 3 regression vectors for Choice, Stimulus Motion and Color throughout the dots presentation. **c)** Correlation between all pairs of regressor values for each neuron (blue dots). Conventions as in Figure 4.3.

yields much more consistent, replicable beta coefficients in these tasks as well (Figure 4.7 b and Figure 4.10 b).

While most pairwise correlations between different beta values remain fairly small for Tasks 2 and 3 (Figure 4.6 c and Figure 4.9 c), the correlation between Color and Signed Motion for Task 3 is now statistically significant. This is a departure from the results for the other two tasks that becomes more clear when comparing the population projections in the Beta axes (Figure 4.7 c and Figure 4.10 c): while for Task 2 there is still some separation by choice on the color axis, for Task 3 the color axis captures motion signals throughout the dots and delay periods.

In terms of stability the results are remarkably consistent across all tasks:

- Color is extremely stable from its onset.

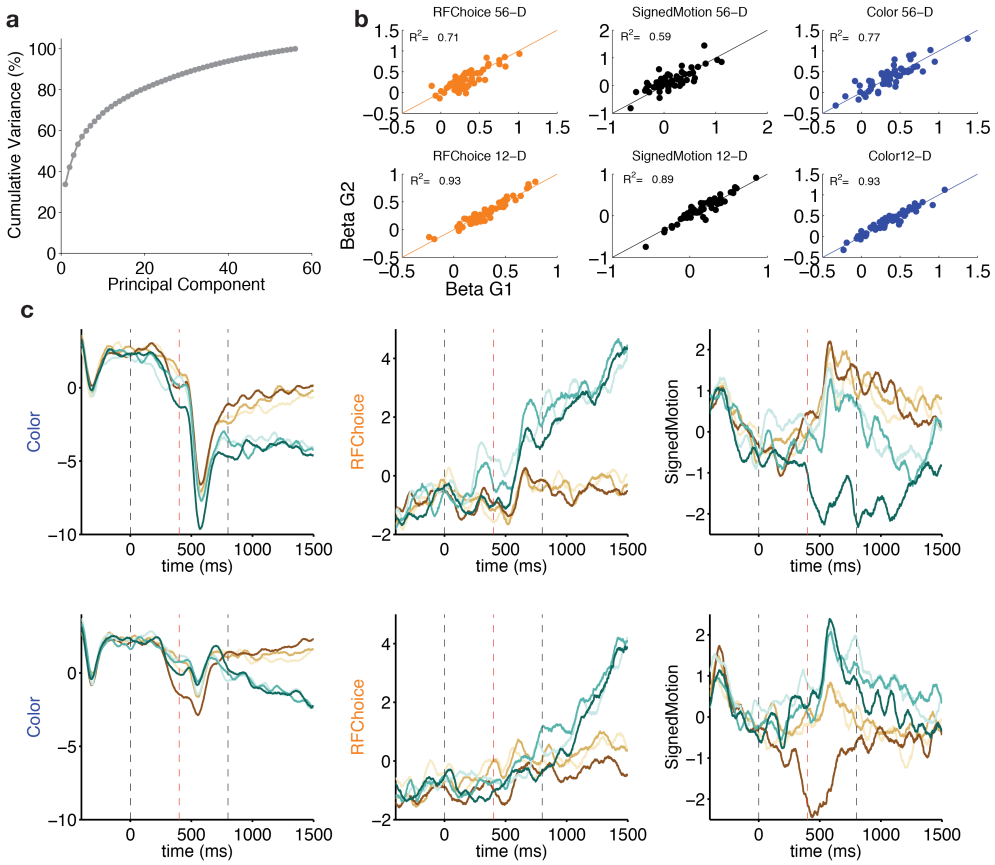

Figure 4.7: **High and low dimensional signal representation in LIP - Task 2. a)** Cumulative variance explained as a function of principal component number after performing PCA on the population data during the dots period. **b)** Regression value consistency for 3 factors in High (top row) and Low (bottom row) dimensional spaces. For each neuron trials were randomly assigned to two disjoint groups and regression values calculated independently. Scatter plot shows correlation between regressor values for each trial group (x and y axes) and each neuron (solid dots). **c)** Projection of condition-averaged population data on the three task-relevant axes defined: Choice, stimulus motion and color.Top row corresponds to context 1 (red in RF) and bottom row corresponds to context 2 (green in RF). Only correct trials were used to compute the condition averages. Conventions as in Figure 4.4.

- Choice is also very stable after it develops at the end of dots/delay period for task 2/3 with a 300-400 ms delay after the colored targets presentation.

- Signed motion is fairly stable throughout the dots presentation and most of the delay period, although its nontrivial diagonal structure hints at malleable representation of motion over time.

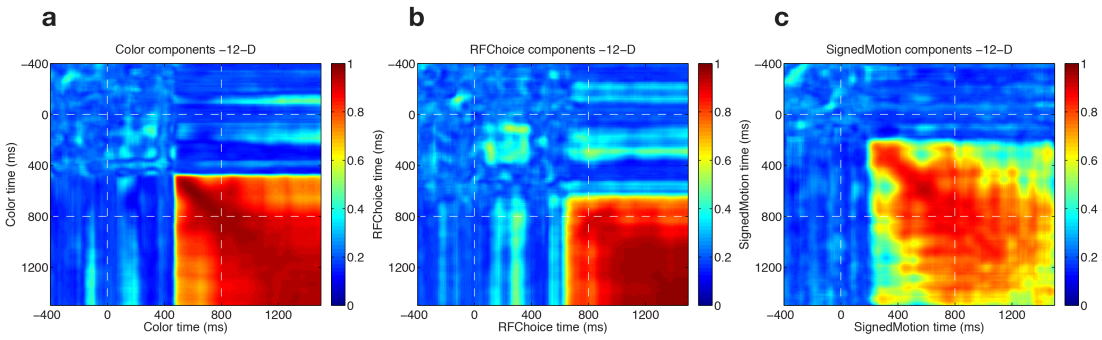

Figure 4.8: **Signal stability in LIP throughout the dots presentation and delay period - Task 2. a)** Heat map of Color vector similarity across time. For each time point the vector for Color was determined and normalised independently. The dot product for all pairwise combinations of timepoints is depicted in the heat map. Hot colors correspond to high dot products (strong alignment) and cool colors to low dot products (weak alignment). **b)** Same as **a)** for the Choice vector. **c)** Same as **a)** for Stimulus Motion vector. Conventions as in Figure 4.5.

Having extensively explored the representation of the Color, Choice and Signed Motion signals within each task, we were very interested in analysing these signals *across* tasks. Due to the different timing of the Color signal in the different tasks, the transformation from integrated evidence to choice was only possible at different times in the trial for the 3 tasks. For this reason, it could be the case that different ensembles of neurons represent these same signals on the different tasks. This possibility was not addressed in Bennur and Gold (2011), and we believed our combination of regression at the population level and dimensionality reduction was a great tool to tackle it.

To visualise the stability of the signals across tasks and over time we generated the same type of heat maps as before (in low dimensional space), except now the regression vectors are compared across tasks.

The Color representation is remarkably stable across tasks (Figure 4.12 a) despite the vast difference in timing. The only exception is a transient period in Task 1 around 150 ms after the dots presentation. To some extent the same can be said about the RF Choice representation across tasks despite its slower onset when compared to Color (Figure 4.12 b). The RF choice vector is very stable between tasks 1 and 2 and less so between 1 and 3 and 2 and 3. This is due to the fact that the RFChoice signal in Task 3 increases in magnitude and becomes stable only at the very end of

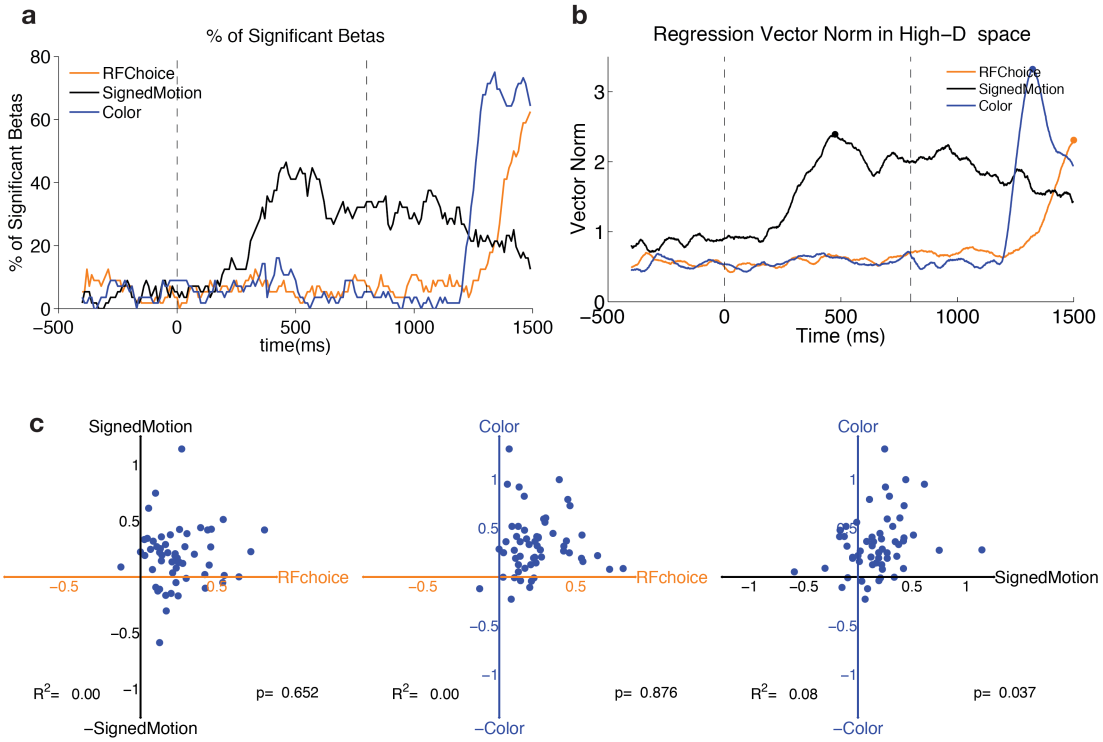

Figure 4.9: **Choice, Stimulus Motion and Color representations in LIP - Task 3. a)** Percentage of cells whose activity is significantly correlated with Choice, Stimulus Motion or Color throughout the dots presentation. **b)** Norm of the 3 regression vectors for Choice, Stimulus Motion and Color throughout the dots presentation. **c)** Correlation between all pairs of regressor values for each neuron (blue dots). Conventions as in Figure 4.3.

the analysed period.

Perhaps the most interesting signal comparison across tasks was the one for the Signed Motion signal. In Task 1 the stimulus information could be immediately mapped to choice while in Task 3 it had to be held in memory until the mapping was unveiled. Yet, we had seen a robust representation of this signal within each task and both during the dots period and the early delay period. It turned out that regardless of the task timing the Signed Motion is locally stable across tasks just as it was within each task (Figure 4.12 c). The effect is not quite as strong for comparisons with task 3 given the signals own limited stability at the end of the trial.

While the dimensionality reduction step in TDR greatly reduces noise in the regressor vectors, we wanted to make sure that the observed stability was not simply a byproduct of an excessive dimensionality reduction. To do so, we analysed the

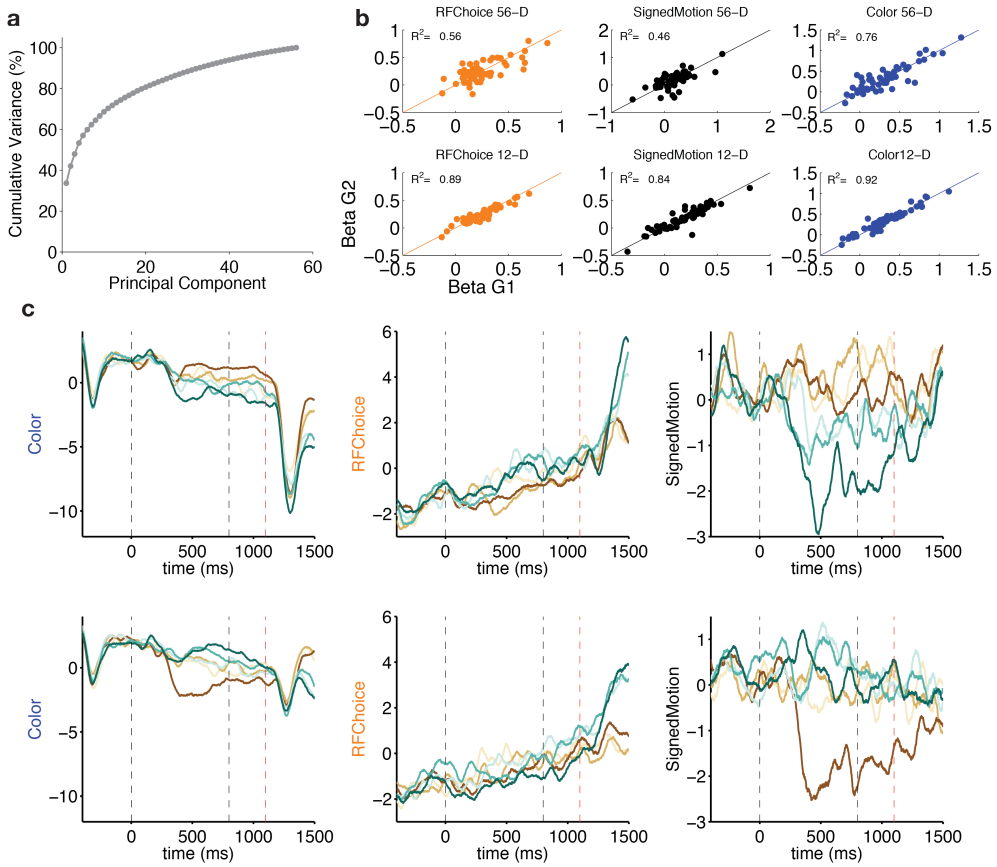

Figure 4.10: **High and low dimensional signal representation in LIP - Task 3. a)** Cumulative variance explained as a function of principal component number after performing PCA on the population data during the dots period. **b)** Regression value consistency for 3 factors in High (top row) and Low (bottom row) dimensional spaces. For each neuron trials were randomly assigned to two disjoint groups and regression values calculated independently. Scatter plot shows correlation between regressor values for each trial group (x and y axes) and each neuron (solid dots). **c)** Projection of condition-averaged population data on the three task-relevant axes defined: Choice, stimulus motion and color.Top row corresponds to context 1 (red in RF) and bottom row corresponds to context 2 (green in RF). Only correct trials were used to compute the condition averages. Conventions as in Figure 4.4.

original regressors in the full dimensional space and compared them across tasks. The stability of the Color signal as expressed by the original Beta values is even more striking especially when taking into account that the time points at which they are calculated vary from -30 ms for Task 1, 600 ms for Task 2 and 1300 ms for Task 3 (Figure 4.13 a). The beta values for Choice are also very stable although in this case they are calculated at the end of the trial for all tasks (Figure 4.13 b). The correlation

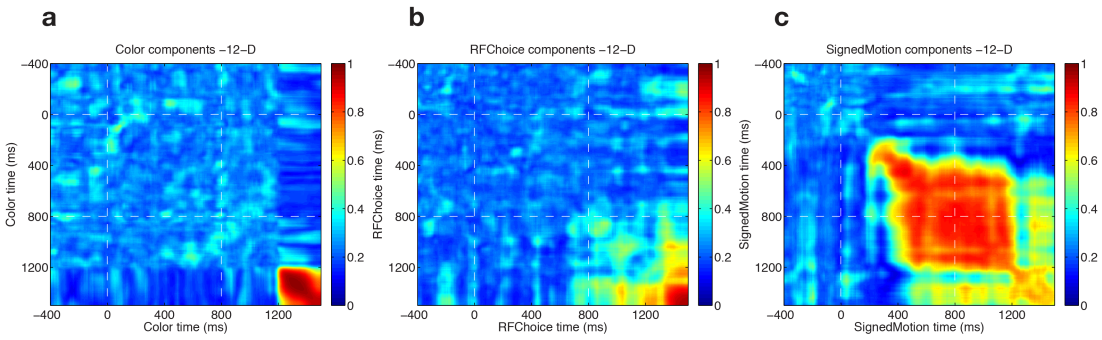

Figure 4.11: **Signal stability in LIP throughout the dots presentation and delay period - Task 3. a)** Heat map of Color vector similarity across time. For each time point the vector for Color was determined and normalised independently. The dot product for all pairwise combinations of timepoints is depicted in the heat map. Hot colors correspond to high dot products (strong alignment) and cool colors to low dot products (weak alignment). **b)** Same as **a)** for the Choice vector. **c)** Same as **a)** for Stimulus Motion vector. Conventions as in Figure 4.5.

between individual betas is still very significant for Signed Motion although not as strong as the other signals (Figure 4.13 c).

In summary, individual neurons in LIP are selective for different combinations of motion, choice and color as described in Bennur and Gold (2011).Motion selectivity does not depend on the timing of the color cue and has a much shorter latency than choice even in Task 1. This is a place where we thought TDR might yield a different result from Bennur and Gold. We guessed that the RFmotion signal might take up variance after the targets turned red/green, showing the signed motion signal to be momentary motion evidence as in Mante et al. (2013). This turned out to not be the case. Signed motion really is a persistent, perhaps integrated, signal that persists after offset of the motion stimulus, as suggested by Bennur and Gold. Choice has a slower time course than expected from the literature, especially in Task 1. As previously stated we speculated whether the initial color signal is a proxy, or prepotent choice signal due to extensive initial training with red targets, but we didn't find enough conclusive evidence in this regard.

LIP does not seem to represent accumulation of evidence supporting a plan to saccade to/away from the RF in this task (i.e. the RF motion signal is negligible, even after the red/green targets appear). As stated in Bennur and Gold (2011), both

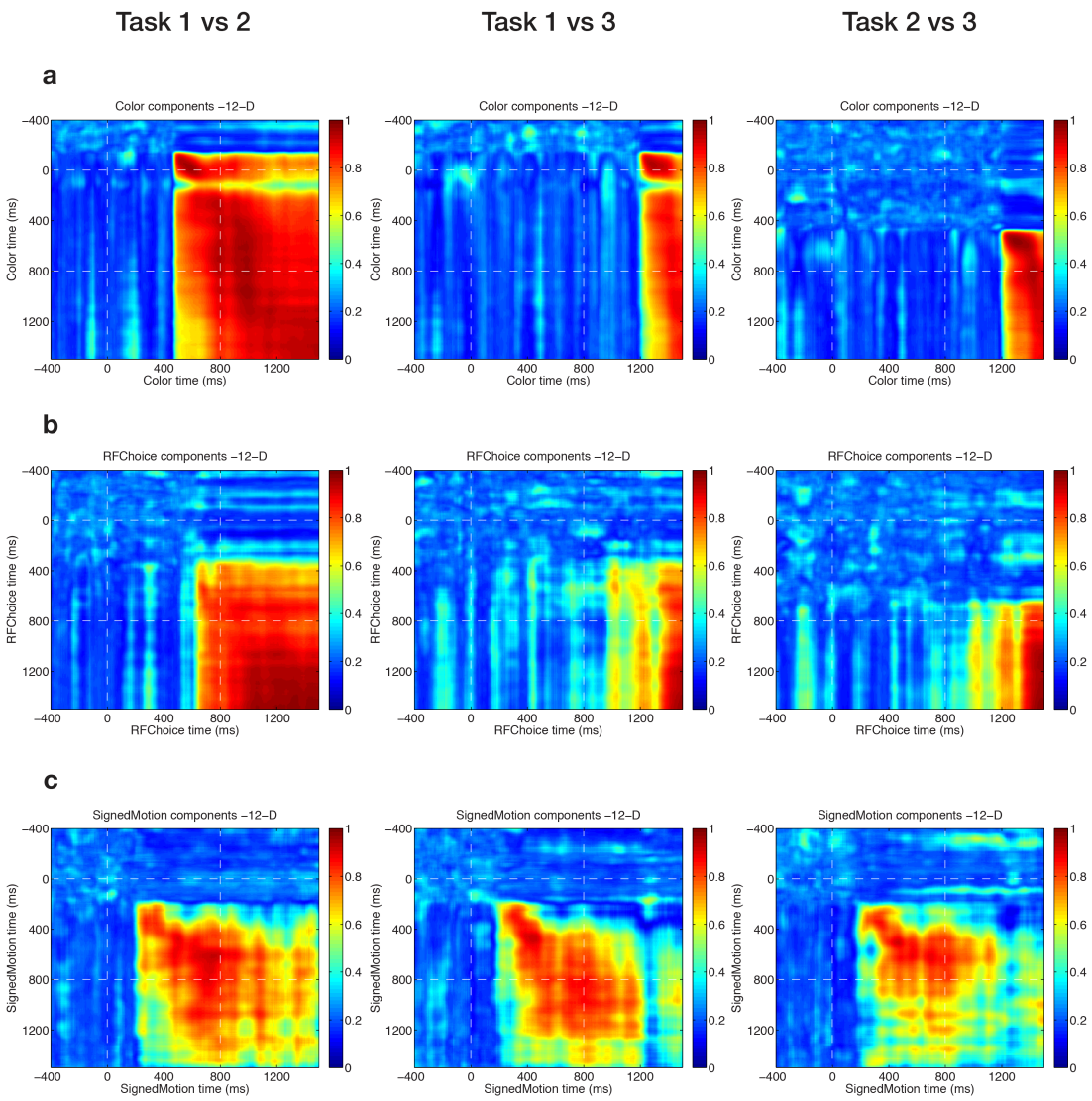

Figure 4.12: **LIP signal stability throughout the dots presentation and delay period across all tasks. a)** Heat map of Color vector similarity across time. For each time point the vector for Color was determined and normalised independently. The dot product for all pairwise combinations of timepoints is depicted in the heat map. Hot colors correspond to high dot products (strong alignment) and cool colors to low dot products (weak alignment). Task 1 vs Task 2 (left), Task 1 vs 3 (center) and Task 2 vs 3 (right) are shown. **b)** Same as **a)** for the Choice vector. **c)** Same as **a)** for Stimulus Motion vector.

the signed stimulus coherence (possibly integrated motion per se) and the categorical choice exist simultaneously in the population activity and are represented by different combinations of cells.

New contributions:

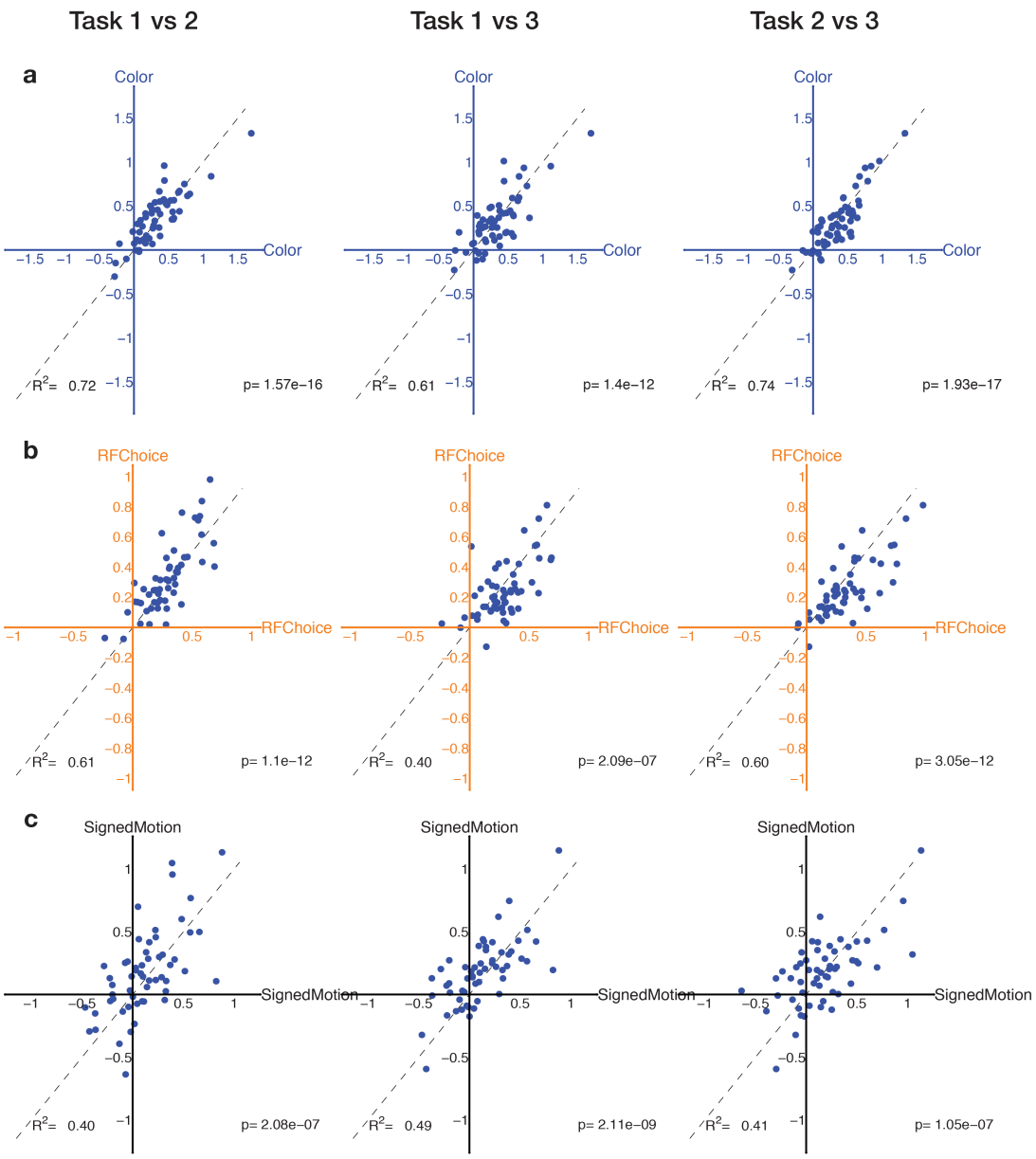

Figure 4.13: **Stability of task-relevant dimensions in LIP across all tasks.** **a)** Scatter Plots of regression values of individual cells in high dimensional space, for each pair of tasks. Beta values are calculated for each task at the time point in the trial signal is strongest (beta norm is maximum). Task 1 vs Task 2 (left), Task 1 vs 3 (center) and Task 2 vs 3 (right) are shown. **b)** Same as **a)** for the Choice vector. **c)** Same as **a)** for Stimulus Motion vector.

- The population data is fairly low dimensional, with 12 PC dimensions accounting for $> 70\%$ variance.

- Color and Choice are represented by non-orthogonal combinations of cells for

all 3 tasks.

- Choice and Color signals are extremely stable over time, whereas Signed Motion is only locally stable.

- The Signed Motion signal follows a similar time course for all three tasks, lasting well into the delay period, and survives orthogonalisation to Color and Choice (despite a significant projection onto Color in task 3).

4.2.2 Multiplexed signals in PMd and M1

In the previous section we analysed LIP data in a task designed to separate the motion integration process from the action selection process. In this section we apply a very similar analysis to our PMd and M1 data that was collected in a task in which those signals are tightly mixed from an experimental perspective: integrated rightward motion should always lead to a right choice and integrated leftward motion should always lead to a left choice. This analysis will also allow for a comparison between PMD and M1 signals beyond choice. We chose the fixed duration task with delay since this version was the closest in terms of timing to the task used in Bennur and Gold (2011). More specifically we wanted to directly tackle these questions:

- Is the population data in PMd and M1 low dimensional, similarly to LIP and PFC (Mante et al., 2013)?

- Is choice the only task relevant signal or is the coherence and the difficulty of the stimulus also represented in both PMd and M1? If the latter, are these signals represented by similar or independent ensembles of neurons?

- What is the stability of the signals represented in these areas? Do the same neurons carry them through the entirety of the stimulus presentation or is there a hand-off of information between different ensembles?

Just like in Bennur and Gold (2011) and Mante et al. (2013) we used Choice and Signed Motion as regressors but in our study, unlike in those tasks, there was only a

single context so there was no analogue to a Color signal. The third regressor we analysed was stimulus difficulty (stimulus coherence magnitude) known to be represented in some neurons in LIP (Meister et al., 2013). Also similarly to Mante et al. (2013) we focused only on the evidence integration period and tried to tease out the integrated choice signal from an eventual momentary motion evidence representation. We also did include a baseline period to serve as a control in terms of regressor magnitude for the dots presentation period. When applying our regression model to PMd data (Figure 4.14 a) we can verify that all regressors have a meaningful representation although their magnitude and timecourse differ dramatically. As expected from our logistic regression results shown in Chapter 3, choice increases in magnitude over time in a very gradual but consistent way being the strongest (for the epoch considered) at the end of the dots presentation. In contrast Signed Motion peaks ∼350 ms after the dots onset, then decays slowly throughout the remainder of the dots presentation. Stimulus difficulty peaks even earlier at ∼260 ms after the dots onset, but decays very sharply after reaching its peak (Figure 4.14 b).

Interestingly, and like in PFC Mante et al. (2013), the Signed Motion and Choice signals are significantly correlated in PMd (Figure 4.14 c, left panel). Although we made no attempt to orthogonalize these signals through experimental design like in Bennur and Gold (2011), it did not have to be the case that neurons that carry choice information would also carry signed motion information with a congruent preference. In contrast, pairwise correlations between Difficulty and Choice and Difficulty and Signed Motion point to a random combination of selectivity in individual neurons for these pairs of regressors (Figure 4.14 c, middle and right panel).

The same analysis of M1 data recorded during the same session shows that the choice signal has a very similar profile to that in PMd, both in terms of percentage of cells with a significant effect and the size of the vector norm (Figure 4.15 a,b). For M1, however, Signed Motion is clearly weaker and more transient; stimulus difficulty never departs from baseline levels, informing us that unlike in PMd this signal is not meaningfully represented in M1 (Figure 4.15 b). The correlation between Choice and Signed Motion remains the only significant one although it is much weaker in M1

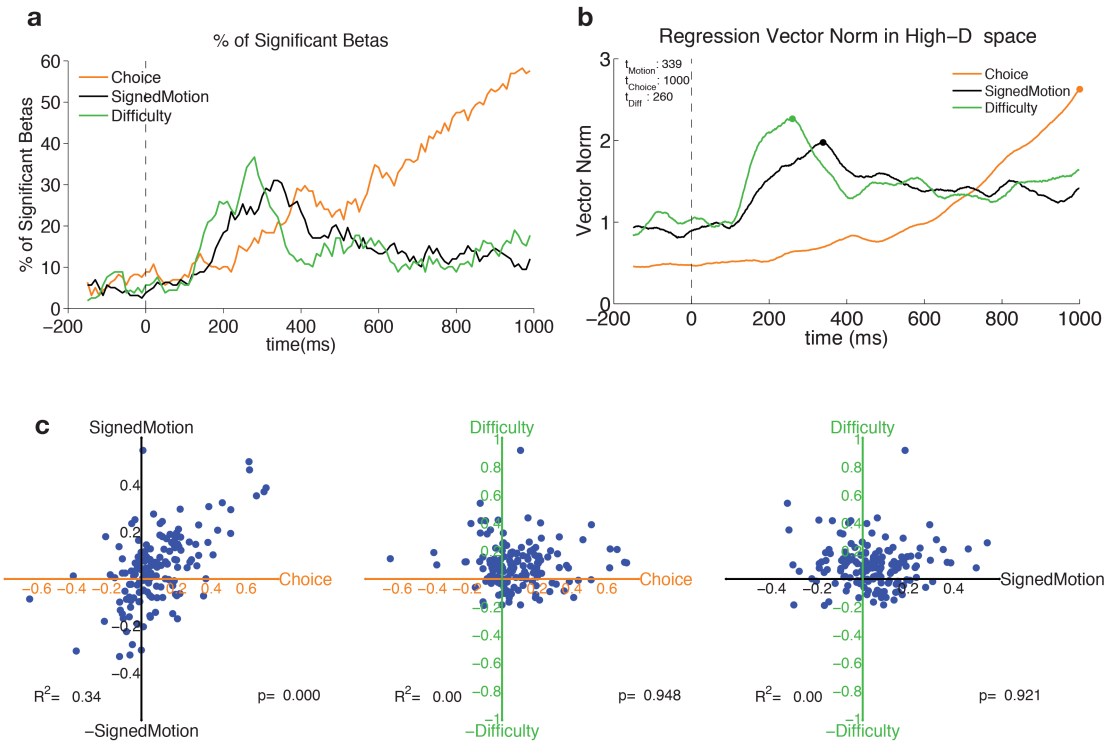

Figure 4.14: **Choice, Stimulus Motion and Stimulus Difficulty representations in PMd. a)** Percentage of cells whose activity is significantly correlated with Choice, Stimulus Motion or Stimulus Difficulty throughout the dots presentation. **b)** Norm of the 3 regression vectors for Choice, Stimulus Motion and Stimulus Difficulty throughout the dots presentation. Timepoint (inset) denotes the time aligned to the dots presentation for which the norm of each vector was maximum. **c)** Correlation between all pairs of regressor values for each neuron (blue dots).

than in PMd ($R^2 = 0.04$ vs 0.34 respectively).

The PMd dataset shown here was composed of 158 units (between neurons and multi-units), almost three times the number of neurons in the LIP data and yet it was still very low dimensional (Figure 4.16 a). Using only 12 PCs we are still able to capture 72%; de-noising the regressors by discarding the higher PC dimensions yields much more consistent vectors compared to the full dimensional space (Figure 4.16 b). A major payoff of applying TDR is the ability to visualize the entire population activity projected onto meaningful axes defined by the experimenter. Starting with Choice we can observe an increasing separation between right and left choices starting at $\sim$ 200 msec matching our Logistic Regression time course (Figure 4.16 c left panel). Between 250 msec and 500 msec the strength of the choice signal is clearly modulated by

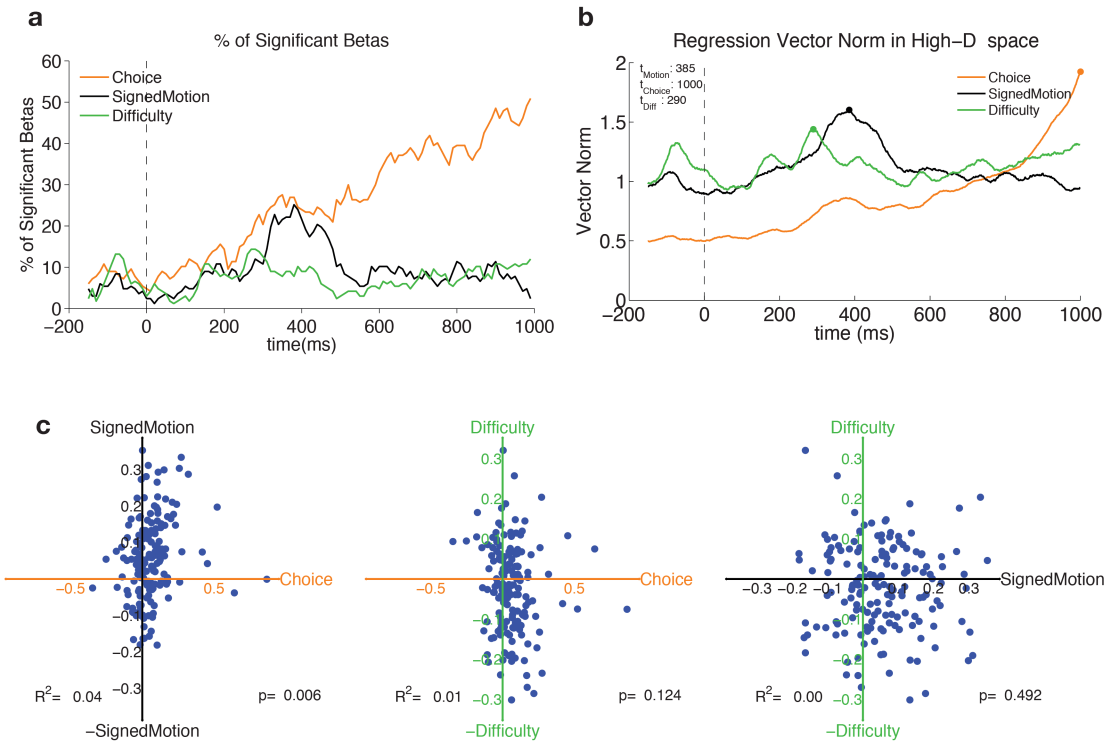

Figure 4.15: **Choice, Stimulus Motion and Stimulus Difficulty representations in M1. a)** Percentage of cells whose activity is significantly correlated with Choice, Stimulus Motion or Stimulus Difficulty throughout the dots presentation. **b)** Norm of the 3 regression vectors for Choice, Stimulus Motion and Stimulus Difficulty throughout the dots presentation. Timepoint (inset) denotes the time aligned to the dots presentation for which the norm of each vector was maximum. **c)** Correlation between all pairs of regressor values for each neuron (blue dots).

the strength of the visual evidence, especially for rightward choices. This observation confirms the separation by stimulus difficulty observed for the Logistic Regression results in Chapter 3 and might arise due to the significant overlap between the Choice and Signed Motion vectors. It could have been indeed, that most of the variance caused by the stimulus coherence effects on the neural responses was absorbed by the choice axis. It turned out however that after orthogonalizing the Signed Motion axis to the Choice axis, a robust representation of stimulus coherence and direction was preserved (Figure 4.16 c, middle panel). A similar result had been obtained in PFC (Mante et al., 2013), and this signal was interpreted as "momentary evidence" that represented the stimulus features but did not influence choice. The main difference between that result and ours for PMd has to do with its time course: while in PFC

this signal was fairly transient peaking early into the dots period, the signal in PMd (despite its early peak) persisted, maintaining a clear separation between conditions until the end of the dots presentation.

Finally, the Stimulus Difficulty signal was also present and carried a meaningful amount of variance, peaking ∼235 msec into the dots period and rapidly decaying afterwards (Figure 4.16 c, right panel). This signal could possibly be associated with the uncertainty about the stimulus direction or the likelihood of obtaining reward at the end of the trial. Whatever its role this signal is clearly present in PMd (as also reported for LIP (Meister et al., 2013)) and expands the repertoire of cognitive signals present in this area.

M1 activity in this task is similarly low dimensional (66% of variance captured by the first 12 PCs) (Figure 4.17 a) and projecting the regressors into low dimensional space also yields more consistent directions (Figure 4.17 b). However, both in low dimensional and full dimensional space, the values for Signed Motion and Difficulty are more noisy in M1 than they were in PMd (compare R^2 values), pointing towards a weaker representation of these signals in this area. The Choice axis separates both choices with the expected time course and but with much weaker coherence dependence compared to PMd (Figure 4.17 c, left panel). The orthogonal Signed Motion signal peaks around the same time as PMd's but is now much more transient, decaying quickly in the second half of the dots presentation (Figure 4.17 c, middle panel). Finally and unlike in PMd, the Difficulty signal is extremely noisy and not easily interpretable (Figure 4.17 c, right panel). Even at its peak it only accounts for a very small percentage of variance indicating stimulus difficulty is not well represented in M1.

This is a striking difference between PMd and M1 and it is consistent across datasets and monkeys. It is tempting to interpret this difference as a result of a more cognitive role for PMd and a more motoric role for M1 but that would be an oversimplification. We were already surprised in Chapter 3 by the fact that M1 represents the decision process fairly well in a stimulus dependent manner especially if the stimulus duration is uncertain, conferring it a cognitive role in this task. Teasing

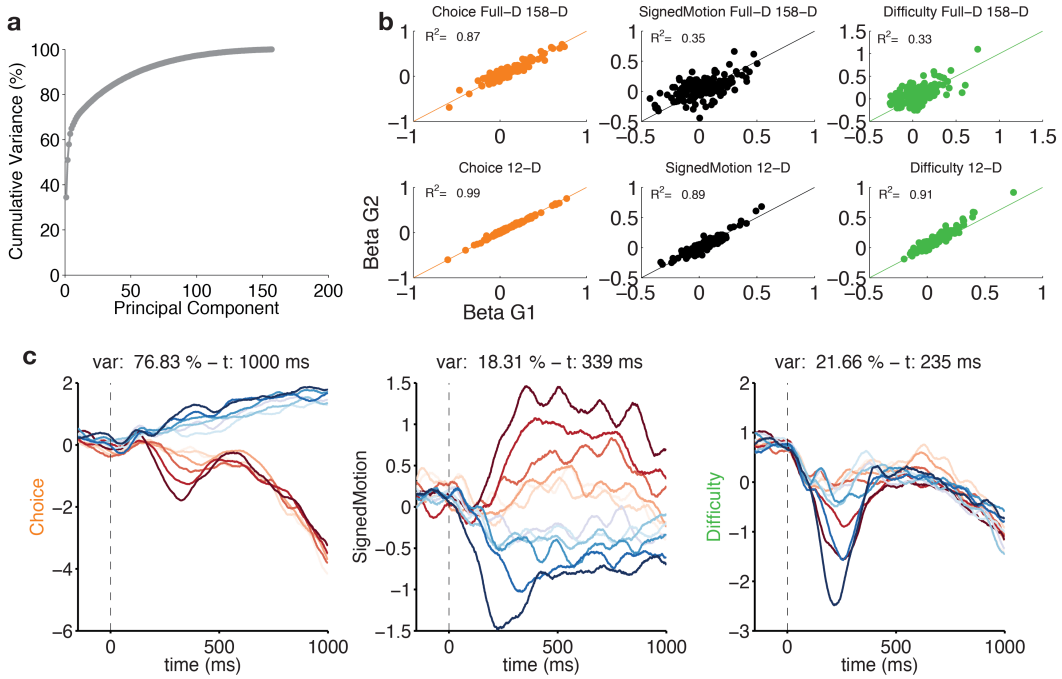

Figure 4.16: **High and low dimensional signal representation in PMd. a)** Cumulative variance explained as a function of principal component number after performing PCA on the population data during the dots period. **b)** Regression value consistency for 3 factors in High (top row) and Low (bottom row) dimensional spaces. For each neuron trials were randomly assigned to two disjoint groups and regression values calculated independently. Scatter plot shows correlation between regressor values for each trial group (x and y axes) and each neuron (solid dots). **c)** Projection of condition-averaged population data on the three task-relevant axes defined: Choice, stimulus motion and stimulus difficulty. Red (blue) traces correspond to right (left) choices at the end of the trial. Stronger color saturation corresponds to higher stimulus strength. Only correct trials were used to compute the condition averages.

these differences apart would require further direct investigation using tasks that directly test decision uncertainty or reward expectation, which is beyond the scope of the current study.

Another major payoff of applying TDR is the ability to evaluate the stability of the representation of each variable through time during a trial. We took advantage of this approach in the previous section when analysing LIP data and now apply it to PMd and M1.

As in LIP the representation of Choice is very stable in both PMd and M1, confirming that the same ensembles of neurons carry choice predictive activity in a stable

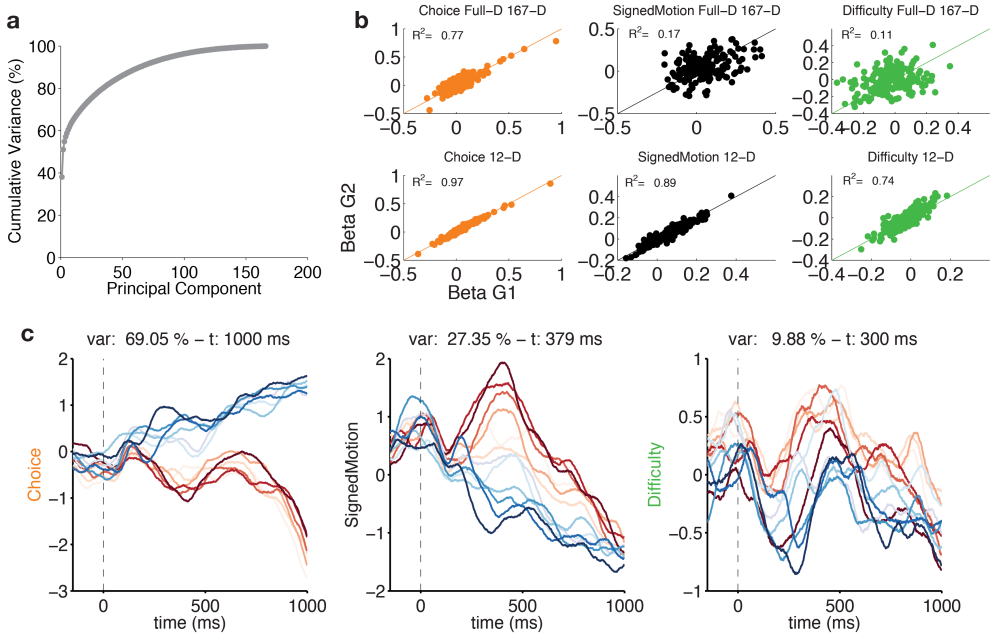

Figure 4.17: **High and low dimensional signal representation in M1. a)** Cumulative variance explained as a function of principal component number after performing PCA on the population data during the dots period. **b)** Regression value consistency for 3 factors in High (top row) and Low (bottom row) dimensional spaces. For each neuron trials were randomly assigned to two disjoint groups and regression values calculated independently. Scatter plot shows correlation between regressor values for each trial group (x and y axes) and each neuron (solid dots). **c)** Projection of condition-averaged population data on the three task-relevant axes defined: Choice, stimulus motion and stimulus difficulty. Red (blue) traces correspond to right (left) choices at the end of the trial. Stronger color saturation corresponds to higher stimulus strength. Only correct trials were used to compute the condition averages.

manner at different time points throughout the dots presentation (Figure 4.18 a and Figure 4.19 a). In contrast Signed Motion is locally stable in PMd in the first half of dots and more stable (but also weaker) in tha second half of the dots (Figure 4.18 b). In M1 this signal is even more transient and only stably represented from *sim*250-550 msec into the dots period (Figure 4.19 b). Finally stimulus difficulty is locally stable for PMd from ∼150-400 msec into the dots period with a second and separate period of stability from ∼450 msec until the end of the stimulus presentation. This result suggests two separate components to the stimulus difficulty each of them stable within its own period and hints at a hand-off of information from one ensemble of neurons

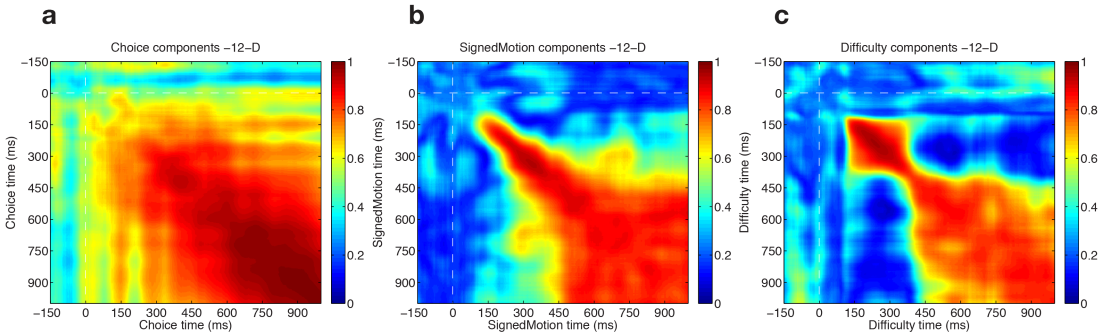

Figure 4.18: **Signal stability in PMd throughout the dots presentation. a)** Heat map of Choice vector similarity across time. For each time point the vector for Choice was determined and normalised independently. The dot product for all pairwise combinations of timepoints is depicted in the heat map. Hot colors correspond to high dot products (strong alignment) and cool colors to low dot products (weak alignment). **b)** Same as **a)** for the Stimulus Motion vector. **c)** Same as **a)** for Stimulus Difficulty vector.

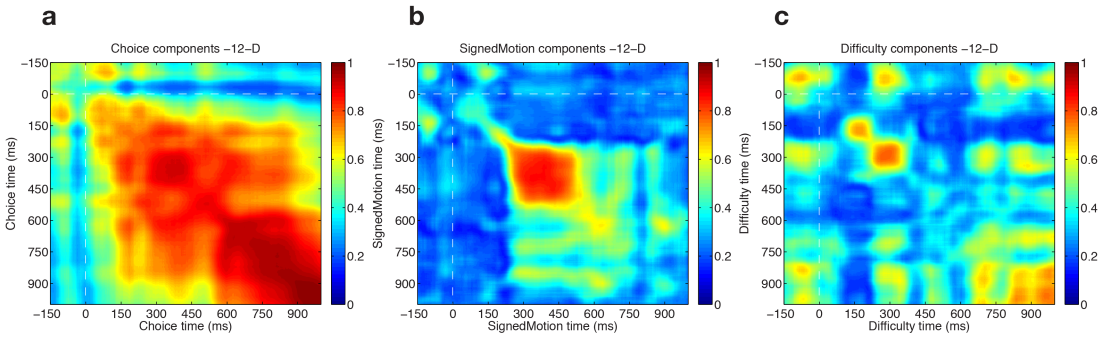

Figure 4.19: **Signal stability in M1 throughout the dots presentation a)** Heat map of Choice vector similarity across time. For each time point the vector for Choice was determined and normalised independently. The dot product for all pairwise combinations of timepoints is depicted in the heat map. Hot colors correspond to high dot products (strong alignment) and cool colors to low dot products (weak alignment). **b)** Same as **a)** for the Stimulus Motion vector. **c)** Same as **a)** for Stimulus Difficulty vector.

to another. In M1 the representation of stimulus difficulty is so weak that the axis that tries to best represent it constantly changes from one timepoint to another.

In summary, by applying TDR to our existing PMd and M1 datasets our main findings were the following:

- The population data is low dimensional, with 12 PC dimensions accounting for 72%/66% of the variance for PMd/M1.

- Signed Motion and Choice are represented by non-orthogonal combinations of cells for both PMd and M1.
- Choice is extremely stable over time, whereas Signed Motion is only locally stable.
- The Stimulus Difficulty signal is only represented in PMd and seems to be formed by two components: a strong and fairly transient component from from ∼150-400 msec and weak but stabler component from ∼450 msec until the end of the dots presentation .

4.2.3 Reaching vs looking: response modality effects on choice signal representation

Having demonstrated the presence and analysed the dynamics of the choice signals in PMd and M1 in a reaching task in Chapter 3 we wanted to determine whether these signals were supra-modal or completely reliant on the monkey planning and executing an arm reach to report its decision.

To distinguish between these two scenarios we asked the monkeys to report their decision with an arm movement in one block of trials, and with a saccadic eye movement in another block of trials. While it has been shown that visual signals can reach PMd with a very short latency (Song and McPeek, 2010) and relative eye and hand position can affect PMd's activity (Pesaran et al., 2006), very little is known regarding the presence choice signals in premotor areas when a non-preferred motor effector is being used. While we purposefully targeted an arm related region of PMd and M1 it could still be the case that decision signals are formed in parallel across effectors and brain regions such that decision signals are present even when the non-preferred response is used. This seems to be the case in parietal cortex and especially so in LIP (de Lafuente et al., 2015).

We took advantage of our chronic recordings that allow us to directly compare the responses of the exact same units in block of reach trials vs a block of saccade trials.

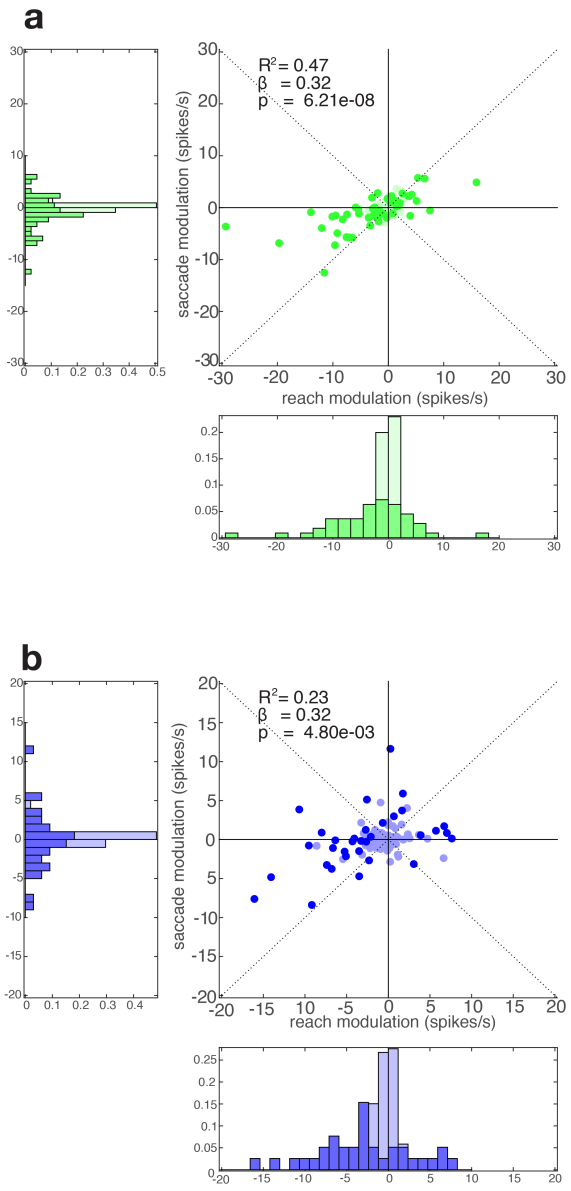

Figure 4.20: **Choice modulation at the end of dots across motor effectors, for PMd and M1. a)** Distribution of firing rate modulation with choice modulation at the end of dots presentation for PMd with reach (horizontal histogram) and saccade (vertical histogram). Modulation is defined as the firing rate difference between correct right and correct left choices. Scatter plot shows the correlation between the modulation values for the two motor effectors, for each unit. Inset shows the parameters obtained for a linear fit of saccade modulation as a function of reach modulation. Significant values of modulation for each effector are shown in bright green and non-significant ones in light green **b)** Same as **a)** for M1

We started by analysing the firing rate modulation with behavioral choice for all

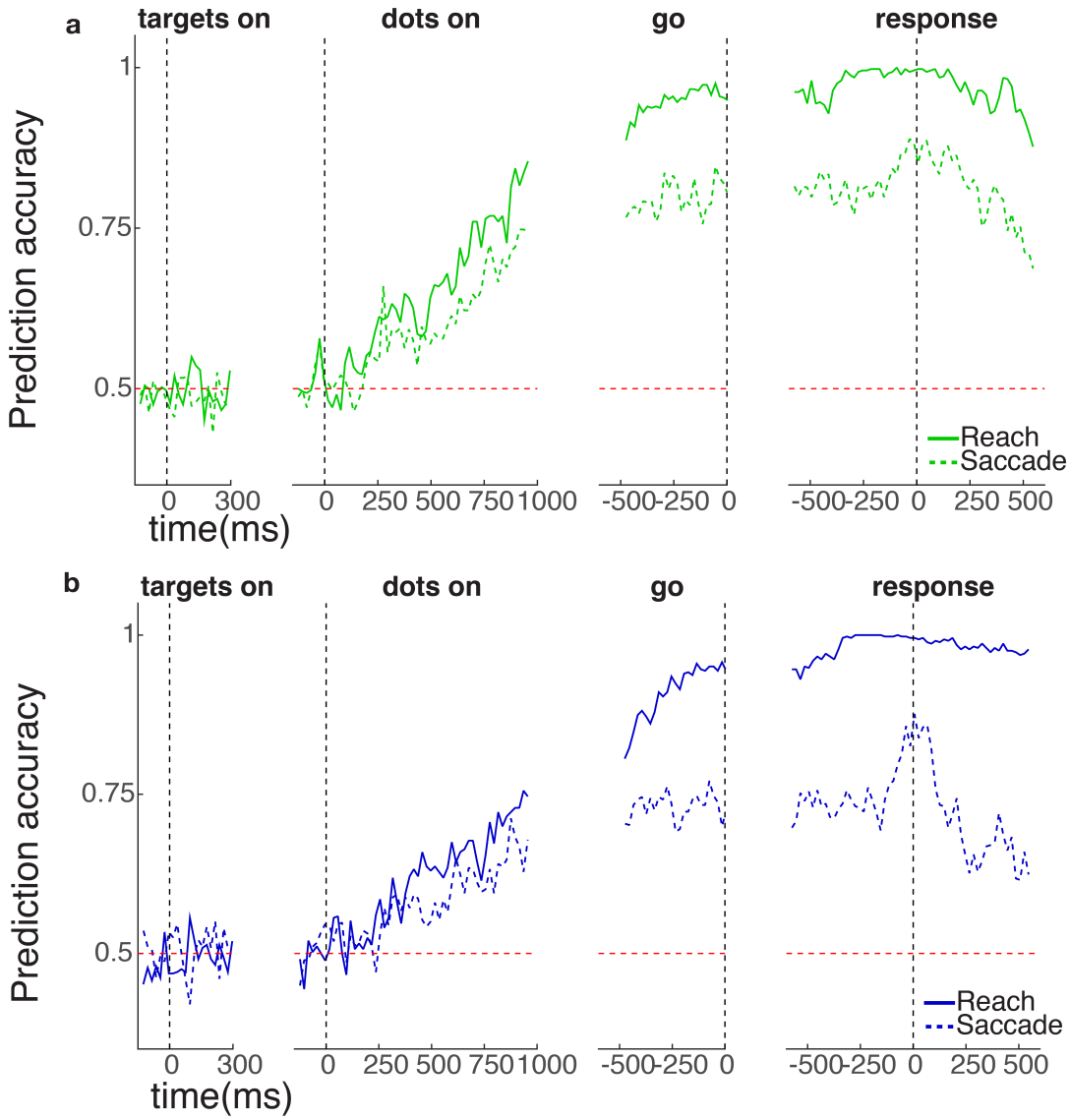

Figure 4.21: **Population choice prediction accuracy for PMd and M1 across motor effectors. a)** Choice prediction accuracy aligned to target onset, dots onset, go cue and response time for PMd for an individual dataset. Solid lines correspond to a reach block and dashed lines to a saccade block recorded in the same session **b)** Same as **a)** for M1. Results for one example session (with one block of reach trials and one block of saccade trials) in which PMd an M1 data were recorded simultaneously.

recorded units. For simplicity we fixed a timepoint, the end of the dots presentation for which we expect good prediction accuracy in the reaching trials. For PMd and M1 the fraction of significantly modulated cells in the reach trials for the example dataset was 19% and 28%, respectively. In contrast the fraction of choice modulated

cells for PMd and M1 during saccade trials was 8% and 13%.

Since we are recording the exact same units in both blocks of trials we can directly correlate the choice modulation in reach trials with the choice modulation in saccade trials. We discovered that this correlation is very significant in both areas (Figure 4.20) and stronger in PMd ($R^2 = 0.47$ vs 0.23 for PMd vs M1, respectively). Importantly, when modelling the modulation for saccade as a linear function of the modulation for reach we obtain a slope that is between 0 and 1 (0.32 for both areas) showing that, on average, the choice modulation sign is conserved and it's magnitude reduced by roughly one third. This result tells us that even when the monkey is not allowed to execute a reach, choice predictive activity is present although attenuated in PMd and M1 and congruent with choice predictive activity for reach trials.

To quantify the amount of choice information throughout the trial and compare it between motor effectors we performed logistic regression to predict the final choice of the monkey based on neural activity from PMd and M1 (separately). This analysis takes full advantage of our simultaneous recordings and allows us to compare the strength of the choice signal across time, brain areas and motor effectors. The models were fit separately for each brain area and block of trials (1 block for reach and 1 block for saccade). Within each area, the number of units was exactly the same for both blocks and the number of trials within each block was comparable (446 trials for reach and 490 trials for saccade) allowing for a fair comparison of the different models' results.

For both brain areas and effectors, choice prediction accuracy rises steadily during the dots presentation remaining higher for PMd than M1 and higher for reach than saccade trials (Figure 4.21). Within each area, the difference between saccade and reach trials was smaller than we anticipated: even though on average the choice modulation was cut to a third in the saccade block, the loss in choice prediction accuracy at the end of dots was only 11% for PMd (85% vs 74%) and 7% for M1 (75% vs 68%). This effect resembles the loss of decision-related activity in MIP for saccade trials (de Lafuente et al., 2015) although the difference between effectors does not seem as dramatic for PMd or M1. Later in the trial, during the delay period, this

difference grows larger, reaching 15% for PMd (95% vs 80%) and 22% for M1 (94% vs 72%) at the time of the go cue. This result is not entirely surprising since the subject is not allowed to reach in saccade block trials causing absence of the strongly choice predictive motor preparation. The same trend is maintained after the go cue with a 15% difference for PMd (99% vs 85%) and 12% for M1 (99% vs 87%) at the response time.

Taken together these analyses suggest there are indeed supra-modal decision-related signals in PMd and M1 during the stimulus presentation period even though these signals are slightly attenuated for saccade trials. The fact that this difference grows larger later in the trial is compatible with our interpretation that decision-related signals present during the stimulus presentation are gradually transformed into motor preparation signals during the delay period which are more effector-specific and thus more attenuated in saccade blocks. While we cant rule out the possibility that the monkeys are still planning/imagining reaches to some extent when performing the task with saccades, that would hardly explain why the loss in prediction accuracy during the delay period is higher during the saccade block. This becomes clear by picturing an extreme case in which the monkeys are planning reaches to the exact same extent in both tasks: in this scenario we expect no difference in predictive activity as we approach the go cue. Only after the go cue and around the time of the response would we expect a large difference in accuracy since the reach isnt actually executed in saccade trials.

4.3 Discussion

In this Chapter we tried to combine several different approaches to thoroughly understand and explore the role of PMd and M1 in the context of perceptual decision-making. This multi-pronged strategy has, in our view, become increasingly necessary when studying complex phenomena in systems neuroscience. Even the understanding of LIP's role in this process keeps evolving and becoming more nuanced more than 20 years after the first study was published (Shadlen and Newsome, 1996).

Our approaches were to analyze and compare responses across:

- Areas by performing comparable population analyses of different datasets;
- Motor effectors by having the monkeys switch between reach and saccade responses to perform the dots task;

4.3.1 LIP results

By re-analysing the LIP dataset we revisited many of the original results first presented in Bennur and Gold (2011)) but we did so from a population standpoint:

- We verified that task variables Choice, Signed Motion and Color are represented by different combinations of cells within each task.
- We identified a representation of the stimulus strength and direction that was independent of when the association between the direction of motion and action was unveiled.

But we also went further and discovered new features in the LIP data. First, despite the diversity of responses and complexity of the task, the population data is fairly low dimensional with 12 PC dimensions accounting for $> 70\%$ of the variance. This observation confirms there is redundancy in the population responses and some motifs are shared across neurons. Second, the Color and Choice signals, despite being represented by different combinations of cells, are not perfectly orthogonal. This implies the representation of one signal will always spill over to the representation of the other signal. This is especially surprising since by design Color and Choice are perfectly independent in this task. Third, we found the representation of Choice and Color to be extremely stable across time, within each task, and also across tasks. Fourth, the representation of Signed Motion was only locally stable but lasted well into the delay period supporting the original author's interpretation of an abstract signal of accumulated visual evidence. The new knowledge about stability, dynamics and interdependence of these signals also serves as comparison point for our PMd and M1 results despite the differences in the behavioral tasks used.

While we obtained significant findings, we also faced a few limitations with our approach, given the data available. First, the number of neurons recorded during all three tasks was extremely low (56 neurons). The small sample size can be a limiting factor in characterizing multiple functional signals in a brain area with highly diverse neural responses (Meister et al., 2013). Our results could certainly be more incisive, and might even be qualitatively different, had the researchers recorded 10x that number of neurons. In retrospect, results for a similarly complex task (Mante et al., 2013) would have been extremely hard to interpret had it not been for the large number of neurons collected.

Second, we were limited by the number of trials per condition. In this study there were 3 tasks, 3 motion strengths, 2 directions of motion, 2 choices and 2 contexts for a total of 72 conditions! Given the range of trials per session ranged from ∼600-1000 we only had (on average) 8-13 trials per condition. This lack of power makes it harder to correctly estimate average population projections onto individual task axes, but more importantly it makes error trial analyses very noisy. Error trial analysis was the tool used by the authors to justify their interpretation of the signed motion signal as being choice related and not stimulus driven. Their argument was that the sign of the signed motion signal reversed for errors on low coherence trials, suggesting the integration process was accurate but yielded the wrong result as is expected occasionally for low magnitude, noisy sensory evidence. In contrast, the sign remained the same for (rare) high coherence trials, which would instead be caused by applying the wrong mapping between motion direction and choice. This effect was only significant for some combinations of task version and motion coherence but not for others, raising questions about the power of this analysis and thus the interpretation about the nature of the signed motion signal. Having more trials per condition could shed light on this discrepancy.

Third, the training history of the monkeys could have introduced some neural effects that would not be present otherwise. The most notable is the overwhelming preference for red over green targets in the LIP population. This huge neural bias combined with non-orthogonal representations of color and choice made us wonder if

the monkeys were actually pre-planning saccades to the red target in Task 1 before the dots were shown. This possibility could explain why the initial color signal is slightly different from the late choice signal (Figure 4.5 a). In the end, the monkeys were not behaviorally biased, meaning that even if pre-planning bias was present for either or both monkeys, the bias was usually resolved by the subsequent sensory evidence about the correct direction of motion.

The other surprising observation in Task 1 that could perhaps be a result of the specific training history concerned the latency of the Choice signal in the neural population response. This latency has been repeatedly estimated at around 200-250 ms for LIP (Shadlen and Newsome, 2001; de Lafuente et al., 2015), but in this study it was closer to 400 ms even in task 1 when the mapping between motion and choice was known before the stimulus presentation. We wondered if the monkeys were a bit complacent with the start of the decision since the timing of all the events of the task was constant and likely well known by the monkeys. Another possibility we considered was whether this increased latency was due to a possible intermediate transformation: the integration of motion supporting a choice into the RF vs opposite to the RF. We tested this idea by including the RF Motion regressor in our linear model but it turned out the representation of this potential signal was negligible. In contrast, when training a Recurrent Neural Network (RNN) with the help of David Sussillo (Sussillo and Abbott, 2009) to perform this task, the network seemed to have an analogue to the RFMotion signal along which integration continued until it lead to a categorical choice. Resolving these questions would require training another 2 monkeys in the same task, obtaining much higher trial counts and (preferably) recording simultaneously from many units. Nevertheless, we believe re-analysing the LIP data was a worthwhile project, that once again validated TDR and allowed us to learn new features about the LIP responses in this task.

4.3.2 PMd and M1 results

When applying TDR to our PMd and M1 datasets it was reassuring to confirm certain features of the data we had already observed with our logistic regression analysis, such

as the latency of the choice signal and its stronger dependence on coherence for PMd compared to M1. The purpose, of this exercise however was to discover new features of PMd and M1 responses that went beyond those already known from the logistic regression analysis. This goal was achieved and resulted in several new findings. First, we verified the choice signal is very stable in both PMd and M1 during the stimulus period, indicating the same units carry this information in a stable way without a hand-off from one ensemble of neurons to another. Second we discovered that while stimulus motion and choice are correlated, similarly to PFC (Mante et al., 2013), there is a remaining robust representation of the stimulus motion that is orthogonal to the choice in both areas. This representation is much more transient in M1 than PMd but, in both areas, its latency is similar to LIP's. Third, we discovered the presence of a stimulus difficulty representation in PMd but not in M1, providing an additional distinctive feature between the two areas. Finally, and similarly to LIP and PFC (Mante et al., 2013), despite the diversity of signals the population responses were fairly low-dimensional. We shy away from direct comparisons of dimensionality given the difference of units recorded in PMd and M1 ($\sim$ 150) and those used from the LIP dataset (56) and the difference in complexity between tasks and how it can affect the expected dimensionality of the data (Gao and Ganguli, 2015).

We decided to focus exclusively on the dots presentation period as to have the best chance of understanding how choice, signed motion and stimulus difficulty are represented while the visual evidence is being presented. However, it would be interesting to further analyse how signals change through the course of the whole trial. Preliminary analyses show that when adding the first 400 msec of the delay period to the analysed period, the choice signal magnitude increases very significantly and its direction rotates quite dramatically after the dots offset. This is another departure from the results obtained for LIP and could be either a result of a more diverse sampling of neurons for PMd and M1 or an actual difference in terms of how choice information is carried through time in LIP compared to PMd or M1. These observations will become important in Chapter 5.

The second approach we took to expand our understanding of signals present in

PMd and M1 was to perform a task manipulation that required the monkey to use two different motor effectors: arm reaches and saccadic eye movements. We used this manipulation to assess how the strength and dynamics of the choice signal in PMd and M1 would differ when alternative effector was used. To our surprise the latency of the choice signal during the evidence integration period was not dramatically changed though its magnitude was slightly attenuated. This attenuation was comparatively much stronger during the delay and response period due to the lack of strong peri-movement activity in saccade blocks. Our interpretation of these results is two-fold. First, we conclude there exist supra-modal signals in PMD and M1 during the evidence integration period. Second, the stronger attenuation of choice signals during the delay and response periods suggest there is a transformation of choice signals from decision signals to strong reach planning and execution signals in the reach blocks throughout the trial. This interpretation is compatible with the observation that the choice axis seems to rotate during the delay period, mentioned above.

Unfortunately, the literature on supra-modal signals in primates is scarce (de Lafuente et al., 2015), which complicates the analyses of the broader implications of our findings. An interesting possibility that we can't quite exclude is that the monkey could still be imagining performing an arm reach during the saccade trials. It has been shown that BMI decoders can successfully be trained on imagined movements due to the similarity of the neural responses between imagined and actual movements (Simeral et al., 2011). It would be worthwhile to record from PMd and M1 from a monkey that had only ever been trained on saccade tasks to determine if the results would be different. If not, we would be able to virtually rule out the possibility of imagined movements explaining our results.

Our analysis of PMd and M1 activity during this task was by no means exhaustive but it allowed a somewhat direct comparison with previous studies (Mante et al., 2013; Bennur and Gold, 2011; Meister et al., 2013; de Lafuente et al., 2015) and expanded the repertoire of signals known to be represented in these areas.

5

Real-Time decoding of decision states

In Chapter 3 we showed how single trial choice classification based on PMd and M1 neural activity was not only possible but highly accurate from early in the trial, and how the single trial choice signals had the expected features of a decision variable in a drift diffusion decision process. However, even though our estimates were done on single trials, most analyses were performed on conditioned average data for increased statistical power. In this chapter we move beyond average data and address the fleeting, unpredictable dynamics of decision formation that can only be understood at the level of single trials.

Estimating neural states on single trials and correlating them with behavior is an important goal in systems neuroscience that is often very challenging to implement, especially when studying covert processes like decision-making or attention. Several groups have used individual spike trains (Latimer et al., 2015), up to a dozen spike-trains (Bollimunta et al., 2012) and LFP and MEG single trial traces (Hunt et al., 2015). In our case having 192 channels and an even larger number of units, many with decision-related activity, could put us in a good position to obtain reliable and interpretable single-trial readouts. Similar techniques have been used to implement Brain Machine Interfaces with great success (Santhanam et al., 2006; Gilja et al., 2012, 2015) using online signals from Utah arrays. Despite their own technical challenges, BMIs get around the difficult problem of validation of single trial states:

the algorithm used to decode brain activity in order to control a device is dictated by the experimenter and its performance can be carefully quantified and optimized. Moreover, in some cases, these decoders don't even need to take into account the natural directional preference of neurons during arm movements to allow good performance (Ganguly and Carmena, 2009). In contrast, during a covert process like decision-making a plausible algorithm to decode neural activity has to be learned, which leaves us again with the difficult problem of validation. How can we demonstrate that on a particular trial a fluctuation in our estimate of neural state had an actual bearing on behavior? Our solution to this problem was to combine a BMI approach with our motion discrimination task: we decoded the activity in PMd and M1 in real-time while the monkey performed the task. Having a real time read-out gave us the ability to *act* based on the estimated instantaneous state of these circuits and validate it using the monkey's behavior.

Author contributions: Diogo Peixoto, Roozbeh Kiani, Krishna Shenoy and William Newsome designed the experiments. Diogo Peixoto, Julian Brown, Jonathan Kao and Paul Nuyujukian built the real-time setup. Diogo Peixoto and Chandramouli Chandrasekaran created the training protocol for the real-time decoder. Diogo Peixoto and Sania Fong ran the experiments to collect the data. Diogo Peixoto designed and implemented the analysis and generated the figures presented in this chapter.

5.1 Methods

5.1.1 Real Time Setup

For all data collection described in previous chapters we used a traditional setup in which both neural data and behavioral data are continuously collected with very high resolution (up to 1kHz for eye position; 75Hz for Hand position and 30kHz for neural activity) and stored onto disk. Analyses were then performed offline on previously recorded data. Converting our traditional high resolution setup into a real-time, closed-loop setup was challenging and only possible through a concerted team effort

with collaborators from the Shenoy laboratory, who lent their considerably expertise in real-time decoding of motor cortex signals. Additional computing capabilities were also required, which led us to add two computers to our existing setup: one xPC server and one xPC client for compiling the decoder and executing the real time calculations, respectively.

An essential requirement to compute a real-time read-out of neural activity is the ability to continuously and (nearly) instantaneously access and perform computations on the neural activity being recorded. This step is not at all trivial since it requires perfect parsing and decoding of the network packets being sent by the neural signal processor and extracting the data in a meaningful way. To accomplish this, the spikes from the most recent 50 ms for each effective recording channel were binned, summed and stored in a 192x1 (96x1 for Monkey F) vector of neural activity. To mitigate spurious Poisson fluctuations in the spike counts, this vector was temporally smoothed using a causal Gaussian kernel with 50 ms standard deviation. Then, the vector of smoothed spike counts was z-scored individually for each channel, using previously calculated μ (mean) and σ (standard deviation) vectors. Z-scoring neural activity was crucial to ensure a reliable and stable real-time readout: it both prevents the highest firing channels from dominating our readout, and also normalizes against strong Poisson fluctuations, preventing them from hindering our readout.

Finally, we projected the z-scored neural activity onto a previously calculated linear decoder (a set of β weights, one for each channel) to obtain our linear readout of choice commitment, a real time decision variable:

$$DV = -\beta_0(t) + \sum_{i=1}^{n} \beta_i(t) \times r_i(t) \tag{5.1}$$

The value of the decision variable was updated every 10 msec, reflecting the neural activity of the preceding 50 msec. Note that neural data for this closed loop experiment consisted simply of threshold-crossings for each channel, defined as voltages lower than -4.5 RMS noise for each channel. We considered online spike sorting but rejected it mostly because of concerns about neural signal stability and drift through-

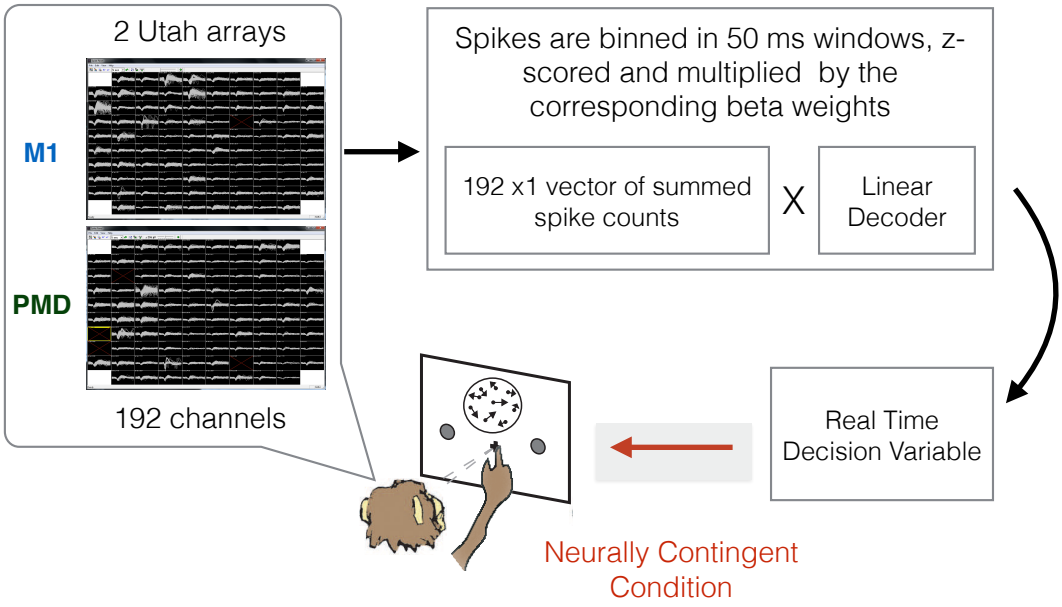

Figure 5.1: **Real Time Setup.** Neural Activity from 2 96-channel Utah Arrays was continuously recorded and processed while the Monkey performed the motion discrimination task. The activity was then binned, summed and z-scored and projected on a single dimension: a linear choice decoder. The result of this operation was our real time read out of decision state and could be used to stop the stimulus presentation in a neurally contingent manner (red arrow), closing the loop in our experiment.

out a session, but also due to the added complexity of determining the additional decoder weights. The decision variable (DV) value and its history on a single trial could then be used (if desired) to impose conditions for termination of the random dots stimulus, effectively closing the loop and allowing us to directly measure the predictive efficacy of real-time fluctuations in the DV value.

5.1.2 Real Time Task

In the previous section we described the broad implementation of a setup for decoding decision state in real time during a cognitive task. In this section we'll describe the practical details of the implementation and its scientific basis and implications.

In Chapter 3 we described the effects of introducing uncertainty about stimulus duration and removing the delay period on choice predictive signals: they are greatly increased across both areas while preserving decision-variable like features. Excellent prediction accuracy is required for a reliable moment by moment decision state read-out, especially with the added difficulties of a real time implementation: for offline analysis the decoder can be optimized for each specific session and even timestep, having access to hundreds of trials for training, something that is not a possibility for online experiments. With this in mind we wanted to take advantage of the choice predictive signals' boost while at the same time have long enough trials to observe rare and interesting phenomena such as changes of mind. A good compromise between these two aims was to increase the minimal stimulus duration to 0.5 s while keeping a similarly wide variability in the duration, meaning the maximum stimulus duration was also extended and could now reach 1.2 s.

Analogously, we prioritised no-delay trials so that the monkey would be required to report its decision immediately after the stimulus offset at which point the momentary decision variable could be more tightly related to the integration of evidence. Nevertheless, we were still interested in how the decision variable would evolve in the absence of additional evidence (besides the visual signals in the pipeline). Again, we struck a compromise by having on average 70% no-delay trials and 30% delay trials. Every trial was randomly assigned as delay or no-delay according to those probabilities.

Having implemented the real time setup and trained the monkeys on the new task structure, the final challenge was to design a decoder that could work reliably with little adjustment on a day-to-day basis while still yielding excellent prediction accuracy. Minimizing the number of trials for adjusting / retraining the decoder was also essential to collect as many trials as possible with a reliable real-time feedback control for every condition. We opted for a logistic regression classifier based on our excellent offline prediction accuracy results (Chapter 3) and ease of interpretation. One of the main departures from the offline procedures was that for Monkey H, instead of comparing and contrasting PMd and M1, we combined signals from both

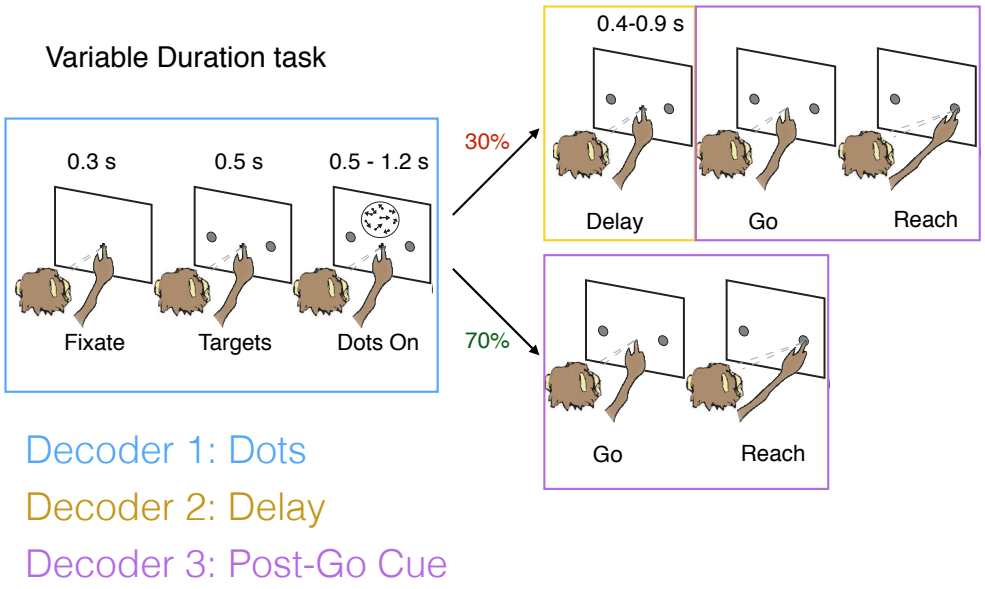

Figure 5.2: **Real Time Task.** The motion discrimination task used was a variant of the variable duration timing with longer stimulus presentation periods. On 70% of the trials there was no delay period, while on the remaining 30% the usual delay duration (400-900) ms was used. Three different decoders were used throughout the trial shown by the different colored boxes.

areas to obtain the best possible prediction accuracy. For Monkey F, the M1 array was not usable by the time these experiments took place, so the analyses for this animal were based on PMd only. In addition, and for simplicity, we decided to use only 3 different decoders for an entire trial, instead of a different one for each time window as implemented in chapters 2 and 3. As shown in Figure 5.2, we used one decoder from fixation up to and including the dots period, another one for the delay period and the third for the post go cue period.

While using only three decoders could seem to hurt our performance it was far more efficient to implement than using a different decoder for each time point: as previously mentioned firing rate z-scoring was key for accurate decoding, and the μ and σ vectors had to be learned anew every session. Having a single decoder for the

entire dots period meant that every 50 msec sample during this same epoch was used to update the same μ and σ vectors. This would mean, for instance, that for a 1 second stimulus presentation we would obtain 20 independent samples for calculating the values of μ and σ: had we used different decoders (and thus different and vectors) for each window we would only obtain one sample per trial, resulting in much slower convergence. The slower convergence would in turn result in using many more trials in a session for adjusting the decoder instead of addressing the scientific questions. As a bonus, using a single decoder in a given epoch prevents an important confound: putative changes of mind (CoMs), identified as decision variable zero-crossings could be spuriously caused by a moving classification boundary, which could have happened had we used different decoders for different time points within an epoch. In summary, while we might sacrifice prediction accuracy, having a single decoder per epoch made the implementation much more feasible, allowing the parameters to converge faster on any given session and preventing confounds in interpreting putative CoMs. A single decoder for an entire trial was also considered, but the firing rate modulations change too dramatically between the dots, delay and post go periods, which would mean the best decoder across all epochs would perform fairly poor on any given epoch.

After extensive offline tests on a few sessions the precise epochs for classifier training were defined as the following:

- Dots epoch: [150 , 1000] ms aligned to dots onset;
- Delay epoch: [250 , 350] ms aligned to dots offset;
- Post-go cue epoch: [200,400] ms aligned to go cue;

Figure 5.3 shows beta weights for an example decoder for Monkey H ranked by magnitude. Positive weights correspond to rightward preferring channels while negative weights correspond to leftward preferring channels.

LASSO regularization sets betas of channels with little or no predictive activity to zero to prevent over-fitting. The weights are smaller and more distributed for the dots period (Figure 5.3 a) than for the delay period (Figure 5.3 b) or the post-go

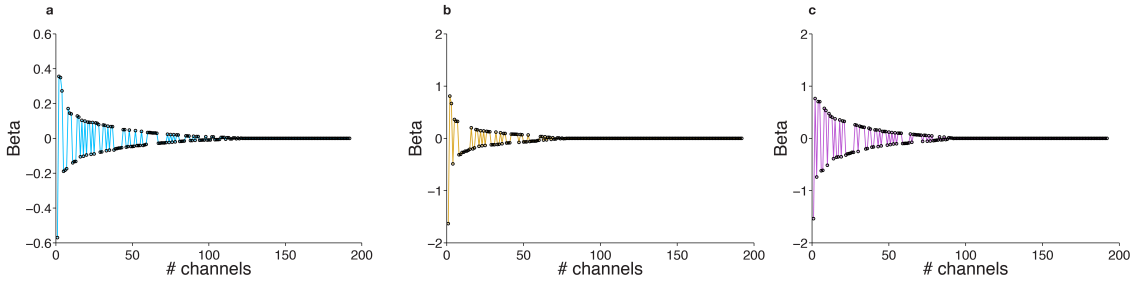

Figure 5.3: **Real time decoder beta weights. a)** Beta weights during the dots period ranked by magnitude for an example decoder used in real time experiments. Channels with no or little choice predictive activity during this period had their weights set to zero by using LASSO regularization to prevent over fitting. **b)** Delay period and **c)** Post go cue Beta weights. Choice predictive signals are stronger in these epochs as shown by the larger magnitude of highest beta weights.

period (Figure 5.3 c) . This result is expected since choice predictive signals become stronger the closer in the trial we get to the go cue.

The linear classifier was determined offline using recently collected data (from real time experiments). All valid 50 ms samples of neural data during the selected period (above) for each epoch were used to train the classifier. The classifier was trained on 90% of the trials and tested on 10% of the trials using 10 fold cross-validation. The weights for one of the folds were then used in the upcoming real-time experiments. New classifiers were typically used every 5 sessions but some proved to be stable over up to 14 sessions.

While the beta weights were not updated online (during the course of one experiment), the μ and σ vectors for each epoch were updated during the course of the experiment, due to changing recording conditions and signals from day to day. The μ and σ vectors were initialized at the beginning of the session using average values calculated offline when also training the most recent decoder. Once the session started, the initial μ and σ vectors were blended with online calculated values for the first 25 trials, using a blending factor α:

$$\alpha(j) = max((25 - j)/25, 0) \tag{5.2}$$

where j is the trial number.

For trial j, sample number t and for a given *epoch* in trial, the μ and σ vectors were defined as a weighted mixture between the initial values $\mu_{initial}(epoch)$ and $\sigma_{initial}(epoch)$ and the estimate of the current session's values $\mu_{current}(t, epoch)$ and $\sigma_{current}(t, epoch)$:

$$\mu_{blended}(t, epoch) = \alpha(j) * \mu_{initial}(epoch) + (1 - \alpha(j)) * \mu_{current}(t, epoch) \tag{5.3}$$

$$\sigma_{blended}(t, epoch) = \alpha(j) * \sigma_{initial}(epoch) + (1 - \alpha(j)) * \sigma_{current}(t, epoch) \tag{5.4}$$

After the first 25 trials α goes to zero which implies the μ and σ vectors kept being continuously updated throughout the session but were no longer blended with values from the previous days.

The update rule for $\mu_{current}(t, epoch)$ was:

$$\mu_{current}(t, epoch) = (\mu_{current}(t - 1, epoch) * K + r)/(K + 1) \tag{5.5}$$

$$K = N_{Samples}(t, epoch) \tag{5.6}$$

where r is the most recently sampled vector of spike counts and K is the current number of samples of spike count vectors obtained so far for this particular *epoch*.

The update rule for $\sigma_{current}(t, epoch)$ was:

$$\sigma_{current}(t, epoch) = \sqrt{\frac{K - 1}{K} * \sigma_{current}(t - 1, epoch)^2 + \frac{1}{K} * (r - \mu_{current}(t, epoch))^2} \tag{5.7}$$

After updating the $\mu_{current}(t, epoch)$ and $\sigma_{current}(t, epoch)$ vectors, the number of

samples for the corresponding *epoch* was also updated:

$$N_{Samples}(t, epoch) = N_{Samples}(t-1, epoch) + 1 \tag{5.8}$$

Importantly even though we had only 3 different decoders (Figure 5.3) we effectively used 5 different epochs: Fixation, Targets, Dots, Delay and Post Go-Cue. The Dots decoder was also used in the Fixation and Targets epochs but because firing rates are so different between these and Dots, different μ and σ vectors had to be used. Every valid 50 ms sample of neural data for a given epoch was used to update the corresponding μ and σ vectors as described above.

We typically let the μ and σ vectors converge for ∼200-300 trials, in the beginning of each experimental session, before starting any closed loop experiments. One way to check for this convergence was to monitor the DV offset: the average DV value for the first 150 ms of the Dots epoch. Since, on average, there is no predictive activity in PMd or M1 during this time window (as verified by offline analyses) we expect the DV to be on average ∼0.

5.1.3 Closed Loop Experiments

The main scientific motivation to implement a real-time system to readout a decision state was the ability to intervene in the task and probe the subject's behavior in a neurally contingent way. More specifically this means closing the loop in our setup as shown in Figure 5.1 (red arrow) and using the current value and/or the history of the DV on the current trial to stop the stimulus presentation and query the monkey about its decision. While the neuro-engineering required to obtain a reliable readout is fascinating to us and its results serve as proof of concept for the feasibility of our experiments they are only a tool to answer specific scientific questions:

1. Can we predict the likelihood of a given choice based on instantaneous DV?

2. Can we detect and validate rare covert events such as changes of mind (CoM) in real time?

3. How do detected CoMs relate to the behavioral CoMs observed in other studies?

To answer the first question we designed our first closed loop experiment (Figure 5.4), which we named Threshold Experiment. In this experiment on a given trial we set a virtual threshold, or bound (B) for the magnitude of the DV during the dots epoch. If the DV on the current trial approaches B or $-B \pm$ tolerance, after a minimum stimulus duration, the dots presentation is terminated and the monkey asked to report its decision. In this manner we can obtain a mapping between the nearly instantaneous readout of commitment state and the likelihood of a given behavioral choice. Besides confirming the validity of our readout this mapping will give us a quantitative measure of how likely the subject is to stick with a given choice given its DV magnitude as the stimulus is terminated. Importantly, the threshold values can and will be reached at different stimulus durations for different trials but if our readout is reliable our mapping should be robust to a wide range of conditions. Typically, 5 values for thresholds spanning 0.5 to 5 were used every session. Closed loop trials were randomly interleaved with open loop trials in which no termination condition was imposed. The motivation for interleaving closed loop and open loop trials was to make it extremely hard for the monkey to learn that boosting its predictive signals (and thus hitting bounds sooner) could increase its reward rate. Not accounting for this possibility could lead do an undesirable change in the monkey's strategy during the course of the closed loop experiments, which could become problematic when combining data across days. For closed loops trials, the specific threshold value for each trial was randomly assigned as one of 5 possible values (0.5 - 5 in 0.5 increments). We imposed a minimum stimulus duration, during which the threshold conditions were never imposed, i.e. the stimulus would always run for this duration and only then the termination conditions (based on the threshold value for the current trial) were assessed. The minimum duration used in most sessions was 250 msec, a conservative estimate of how long choice related signals driven by the visual stimulus take to appear in PMd and M1. A few sessions using a shorter minimum duration (100 msec) yielded similar results.

Once the dots had been presented for the minimum duration, at every 10 ms we

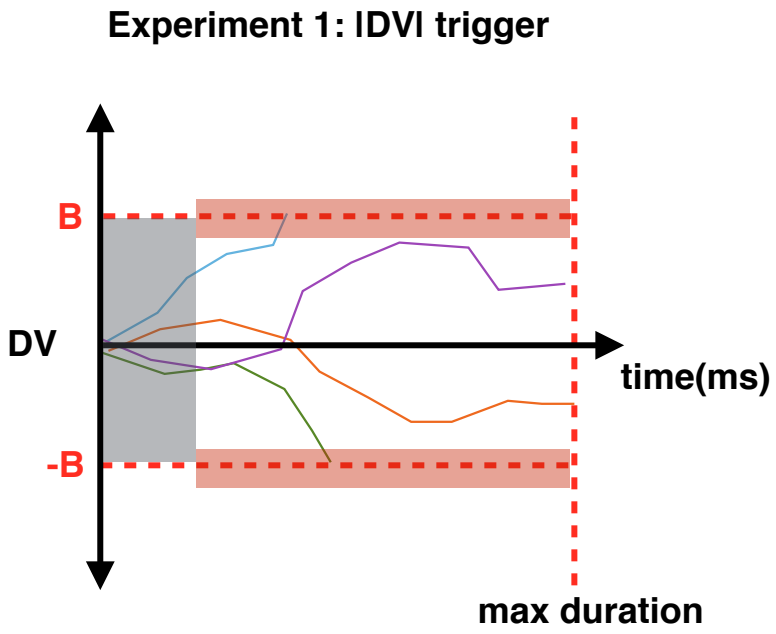

Figure 5.4: **Closed Loop experiment 1 - Thresholding.** Schematic of the first closed loop experiment implemented in real time. Virtual thresholds for DV magnitude (shaded red regions) were imposed and if reached, triggered the termination of the stimulus presentation. The subject was then immediately asked to report its decision. A minimum stimulus duration was imposed such that random fluctuations in the beginning of the trial did not trigger stimulus termination. If the threhsold wasn't reached, the stimulus would be presented for a preselected random duration (500-1200 msec). Colored traces show different trials. 5 different threshold values were used on each experiment

assessed whether the current dv was within $\pm$ 0.25 dv units of the threshold chosen for the current trial (B or $-B$). If so, the stimulus was terminated immediately, if not the presentation would continue. At the beginning of each trial, a maximum stimulus duration was randomly assigned from an exponential distribution ranging from 500-1200 msec. If the threshold was not reached before this time point, the dots presentation would stop regardless of the current dv value. Closed loop trials for which the threshold was not reached were effectively indistinguishable from open loop trials.

To answer questions 2 and 3 we designed another closed loop experiment that could capture the elusive and unpredictable putative changes of mind (Figure 5.5). Under our logistic regression framework the signature of a putative CoM is a sign change of the decision variable. Since these sign changes can happen at any point during the trial, capturing them required not only monitoring the most recent state of the DV, but its history throughout the trial. Because there is noise in our DV estimation and DVs usually start close to 0 at the beginning of the trial we imposed selection criteria to establish likely CoMs based on the neural data. A necessary feature for all potential CoMs was a zero crossing in the sign of the DV: change of DV sign from negative to positive reflected a change in the likelihood of a rightward decision from less than 50% to greater than 50% (equation 5.1), and vice versa for the opposite change in sign. To eliminate zero crossings resulting solely from measurement noise, we imposed four additional criteria:

- Minimum DV value after zero crossing;
- Minimum DV value with opposite sign before zero crossing;
- Minimum duration of DV sign stability after zero crossing;
- Minimum duration of DV sign stability before zero crossing;

The minimum DV values before and after zero crossing were identical, except for the sign (e.g. -3 and +3). Similarly, the minimum duration of DV sign stability (negative or positive values for all time points) was identical before and after the sign change (e.g. 150 ms). If a zero crossing was detected and *all* four minimums were met, the stimulus presentation was interrupted and the animal was immediately prompted to report a decision.

By sweeping the parameter space we could test zero crossings that differed in magnitude and stability. Analogously to the threshold experiment, if the minimums were not met and a CoM thus not detected, the stimulus presentation continued uninterrupted for a random duration ranging from 500-1200 msec, selected prior to the start of the trial. A minimum stimulus duration of 250 msec was also in place.

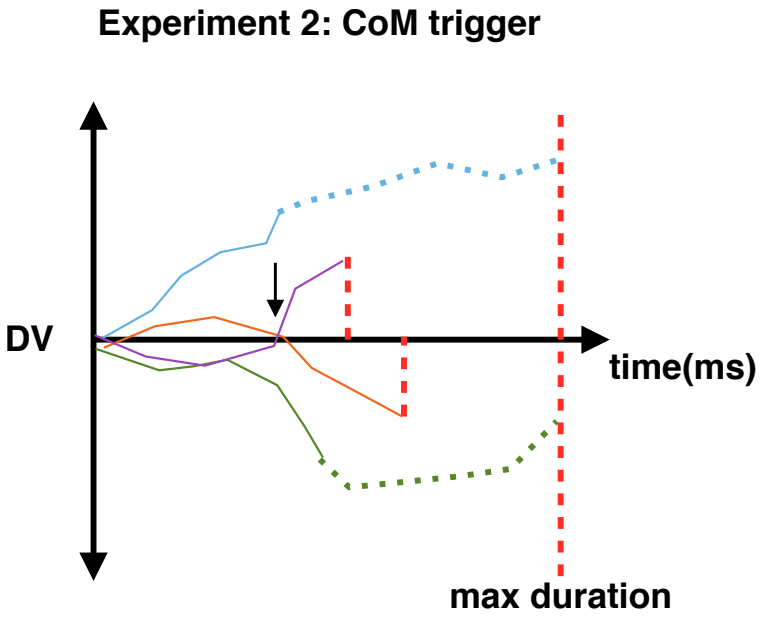

Figure 5.5: **Closed Loop experiment 2 - CoM detection.** Schematic of the second closed loop experiment implemented in real time. DV values on the current trial were tracked to detect sign changes in DV. Sign changes would need to meet all criteria set for that particular trial to be considered putative CoMs and trigger stimulus termination. Trials in which qualifying CoMs were not detected the stimulus was presented for a random duration ranging from 500-1200 msec. Colored traces show different trials.

5.2 Results

5.2.1 Decoding performance: open loop results

The feasibility of the closed loop experiments depended entirely on the quality of the real-time read out. If our read out was too noisy, inaccurate or unstable the data from the closed loop experiments would not be interpretable. As a gold standard we had our offline results: the accuracy that is possible to reach on individual sessions when the classifier has access to 90% of the data and after spike sorting has been performed. While we knew reaching the same level of performance online would be

tremendously challenging, we could now take advantage of combining the information from both brain areas (at least in Monkey H) instead of just comparing them.

After introducing Z-scoring and experimenting with different decoder training methods and online implementations we obtained the results shown in Figure 5.6 and Figure 5.7 for Monkey H and F respectively.

Prediction accuracy is calculated for each timepoint as the fraction of trials for which the most likely outcome as predicted by the model, using only neural activity, matched the eventual choice of the monkey at the end of the trial.

Similarly to the offline results and reassuringly, prediction accuracy starts at chance levels during the targets epoch but quickly departs from chance $\sim$ 220 msec after dots presentation. Strikingly, the rise in prediction accuracy is still very sharp with values reaching 99% and 98% for the longest stimulus presentations for Monkey H and F, respectively. These results were extremely encouraging and confirmed the quality of our real-time choice prediction. Since all our closed loop conditions were going to be imposed during this epoch, they also reassured our DV could be trusted and the results interpretable. Interestingly, a difference between the two monkeys remains: while baseline prediction accuracy during the first 200 msec for Monkey H is right at chance, for Monkey F it is slightly elevated and mostly driven by low coherence trials, for which this monkey occasionally sticks with a pre-planned choice regardless of motion direction. Finally, despite only using neural activity one Utah array in PMd (96 channels) for decoding upcoming choices, Monkey F's maximum prediction accuracy was only very slightly decreased across all the epochs compared to Monkey H's (192 channels).

Despite not using DV values during the delay or post go period to perform closed loops experiments the single trial dynamics during these periods were still of interest to us and it was important to establish good prediction accuracy. We had observed in Chapter 3 that the closest we get to the go cue the stronger the choice signals become and similarly, in real time, we are able to predict choice at above 90% accuracy throughout. The sharp decline at the very end of the post go cue period is a consequence of the very fast changing choice preferences and weights of many neu-

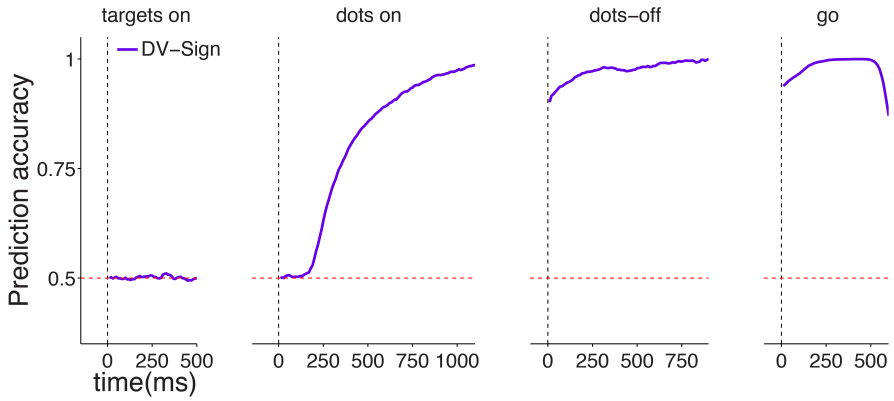

Figure 5.6: **Real time choice prediction accuracy - Monkey H.** Accuracy is calculated for each time point using the real time DV and quantified as the fraction of trials in which the classifier correctly predicted the Monkey's upcoming choice. For logistic regression this is equivalent to comparing the DV sign to the choice sign. Data for Monkey H using 192 channels and 16468 trials.

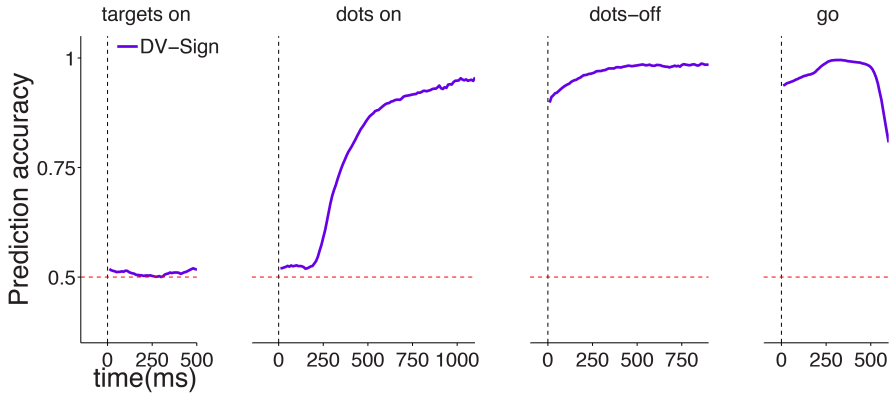

Figure 5.7: **Real time choice prediction accuracy - Monkey F.** Same as Figure 5.6 but for Monkey F. For this monkey real-time DV was calculated using only 96 channels. Data from 15826 trials.

rons (and thus channels) in these brain areas around the time of reach. These rapid changes make it impossible for a single linear classifier to perform equally well for a long period of time.

Besides high prediction accuracy on individual sessions, stability over multiple days was also crucial to perform closed loop experiments: having to retrain our classifier every single session would cost us too many precious trials we would rather

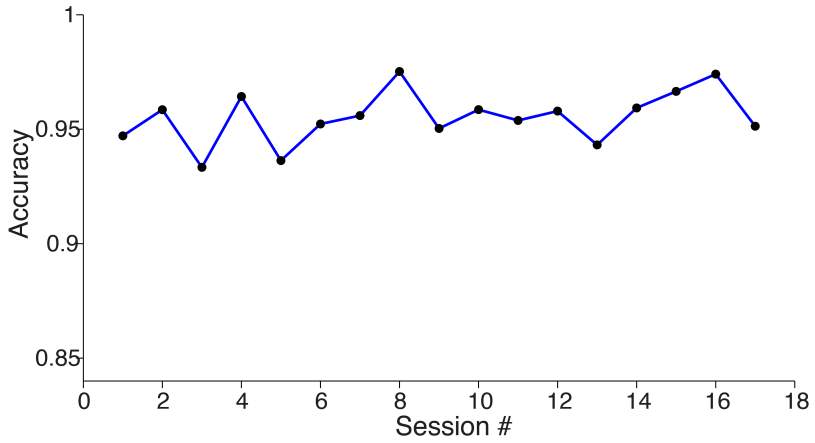

Figure 5.8: **Real time decoding performance reliability.**. Average prediction accuracy during the second half of the stimulus presentation (600-1200) msec across 17 sessions. The same decoder was used for the first 14 sessions.

use for testing our closed loop conditions. Fortunately however, and due to good recording stability and robust decoder choice, our decoders were usable for at least 5 consecutive sessions without significant performance decline. In fact in some cases we used the same exact decoder for up to 14 consecutive sessions spanning 4 weeks, with a maximum accuracy difference of only 2.5% (Figure 5.8). It is important to highlight that while the decoder, and hence the Beta weights were left unchanged, the μ and σ matrices were retrained every session. This difference tells us that while the relative preferences of each channel were very consistent over time its average spike counts changed significantly from day to day, requiring adjustments every session.

Having demonstrated high accuracy in binary classification and stability in our readout quality over weeks, the last validation test on our real time DV concerned its temporal dynamics and coherence effects. Based on our offline results described in chapter 3 we expected the DV to: (i) start around 0 at the time of dots onset, (ii) separate by choice after $\sim$ 200-220 msec (iii) rise faster for easier trials. All these predictions were verified in our online DV (Figure 5.9). Unsurprisingly the DV values were slightly larger for Monkey H than Monkey F, which is explained by the additional information provided by an M1 array.

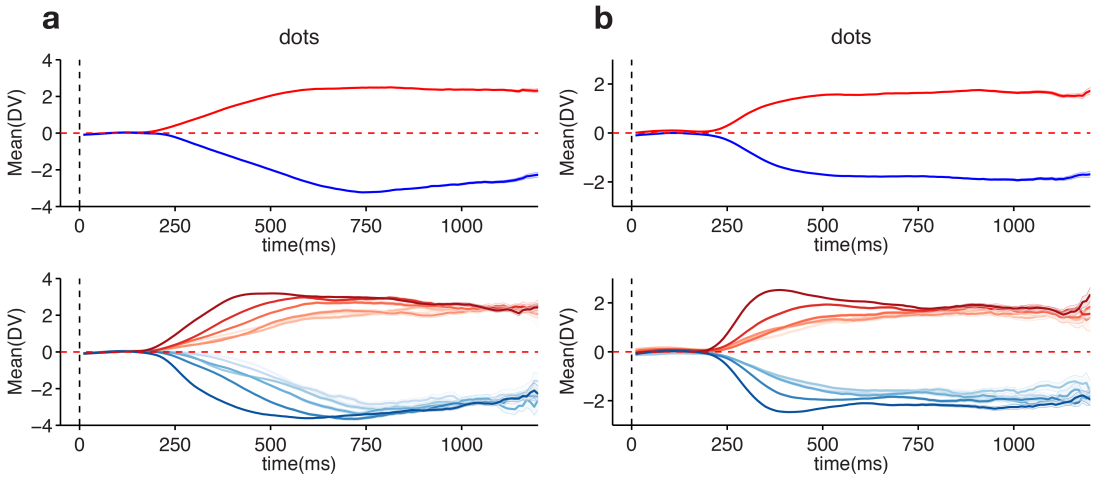

Figure 5.9: **Decision Variable during dots. a)** Top panel: Average DV during the dots epoch for right (red) and left (blue) choices. Bottom panel: same data as the top panel but sorted by stimulus cohence. Darker shades correspond to higher stimulus coherence. **b)** Same as **a)** for Monkey F.

5.2.2 Closed loop results - Thresholding

So far we demonstrated many impressive and desirable features of our real time decision readout: (i) prediction accuracy comparable to offline results, (ii) differential DV rise that is proportional to stimulus coherence and (iii) consistent performance across many days. As impressive these results might be in of themselves they mostly serve as a proof of concept for real-time readouts of decision activity in premotor/motor cortex using threshold crossings from ∼100-200 units. The real payoff of the implementation of the real-time readout comes with the possibility of performing closed loop experiments: the use of neurally contingent conditions to probe both the circuit and the subject with enormous precision and negligible latency.

Inspired by drift diffusion models, the first test we wanted to perform in closed loop was to impose virtual decision boundaries that if reached would immediately lead to stimulus termination prompting the subject to report its decision right away. In Figure 5.6 and Figure 5.7 when calculating prediction accuracy we are simply using a binary mapping from DV values: if DV is positive we predict a right choice and if DV is negative we predict a left choice and then we compare our prediction with the animal's response. The magnitude of the DV itself has no influence on our

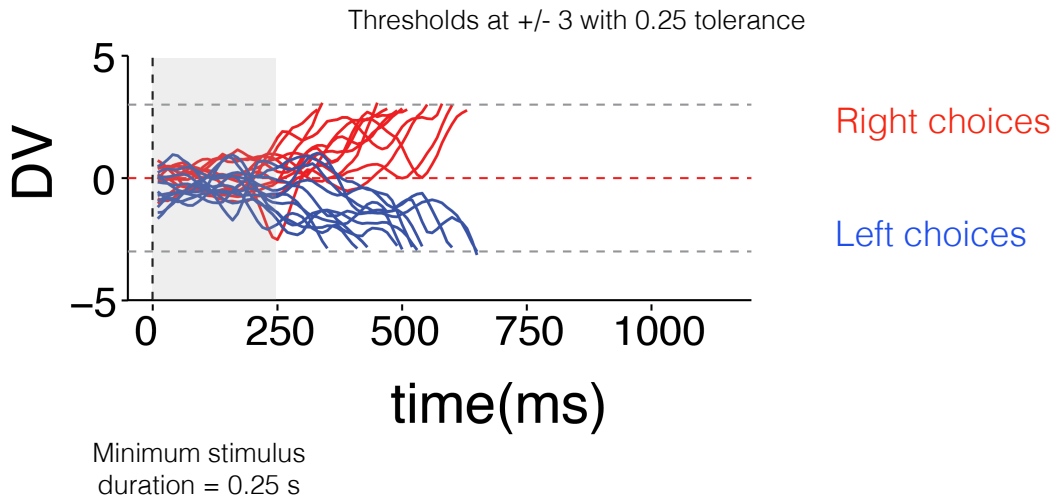

Figure 5.10: **Example threshold trials.** Real Time DV time courses for example trials with thresholds set at +3 and −3. Traces are colored according to behavioral choice at the end of the trial: right choices in red and left choices in blue.

prediction. However, and by definition, we expect larger values of DV to be associated with stronger commitment to a choice and hence higher prediction accuracy. By imposing virtual thresholds in closed loop we can directly test this hypothesis: by using thresholds of different magnitude we can verify if indeed our prediction accuracy is higher for higher values of instantaneous DV.

To illustrate what the experiment looks like with actual data and build intuition for further analyses, we first focus on example DV traces from trials that lead to stimulus termination by reaching a fixed threshold (Figure 5.10). In this case we were using a threshold of 3 and a tolerance of ± 0.25 DV units. It is remarkable how precise our termination method is with all traces ending within a very close range to the chosen threshold. Keep in mind the DV values are being evaluated every 10 ms and the latency for terminating the stimulus was only ∼26 ms, the equivalent

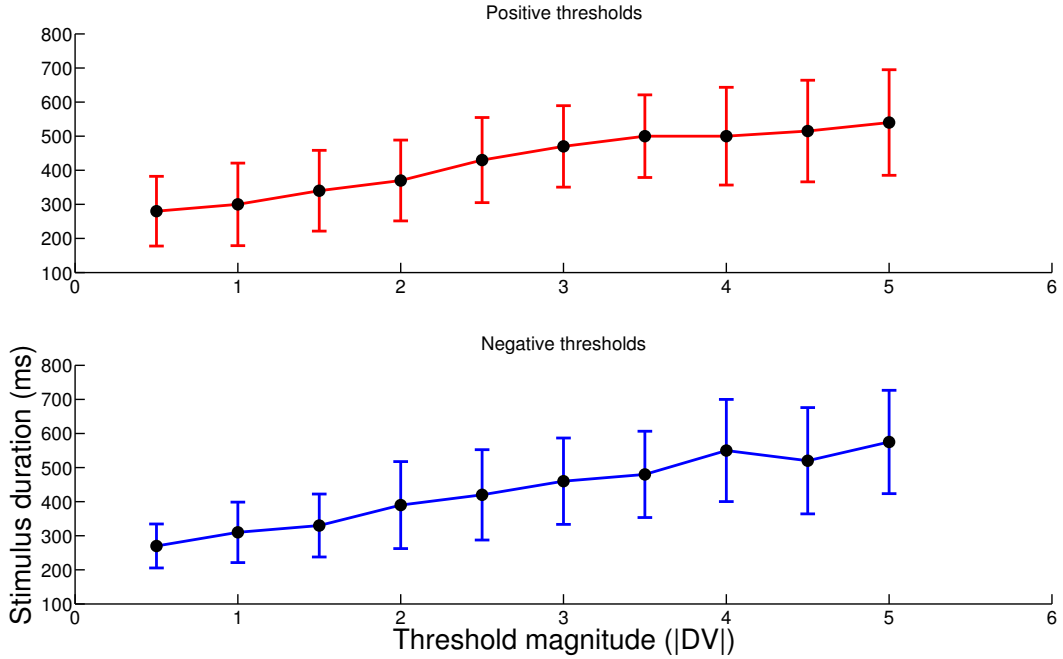

Figure 5.11: **Median stimulus duration as a function of threshold magnitude** Median stimulus duration required to trigger termination is plotted as a function of threshold magnitude in DV units. Top panel shows data for positive thresholds and bottom panel for negative thresholds. Error bars show standard deviation.

to two screen frames at 75Hz. Another feature of the data worth highlighting is the diversity of paths the Decision Variable takes to reach ±3. Trials span a wide range of durations (and coherences) but all were stopped at the threshold vicinity. This diversity enriches our dataset and will allow us to ask questions about the effect of stimulus features (duration and coherence) on the prediction accuracy. Finally, for all trials depicted the final decision of the subject was correctly predicted: all red traces (right choices) ended around +3 and all blue traces (left choices) ended around -3. This was naturally not the case every time. To characterise the relationship between DV at termination and prediction accuracy we systematically swept the parameter space for the threshold height using values spanning 0.5-5 DV units (in 0.5 increments). As expected from drift diffusion models, the higher the boundary magnitude the longer, on average, it will take to reach it (Figure 5.11). For the lowest boundary used (0.5 DV units) the median stimulus duration required to reach the threshold was ∼280 ms, whereas for the highest (5 DV units) the median duration

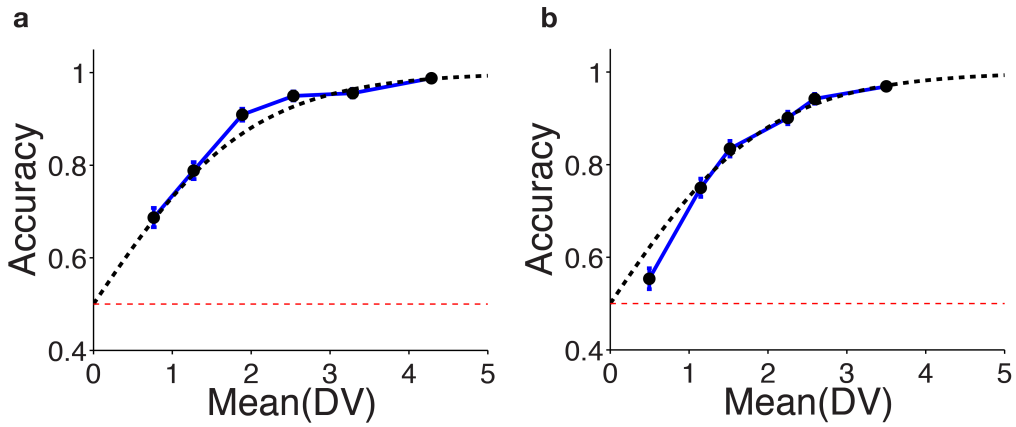

Figure 5.12: **Prediction accuracy as a function of DV. a)** Choice prediction accuracy for all trials collected during thresholding experiment. Trials were split in 6 quantiles sorted by DV magnitude at termination. Prediction accuracy and median DV magnitude was calculated and plotted separately for each quantile (blue line with black markers). Blue error bars show standard error of the mean for a binomial distribution. Dashed black line shows predicted accuracy from log-odds equation and red dashed line shows chance level. Data from 2973 threshold trials from Monkey H. **b)** Same as **a)** for Monkey F using 2518 trials.

was ∼540 ms. The relationship between boundary height and stimulus duration is approximately linear and very consistent for both positive (Figure 5.11 top) and negative (Figure 5.11 bottom) DV values.

In (Figure 5.12) we show that indeed prediction accuracy increases monotonically with DV magnitude at termination as expected. Strikingly, using only 50 ms of data to estimate the DV that triggered termination, the difference between the observed likelihood of a given choice and that predicted by the logistic function was only, on average, 1.5%/1.8% for Monkey H/F. This is all the more impressive taking into consideration the classifier has never been trained on the current day's data causing the results to be inherently cross-validated. Moreover, for each quantile there is a wide range of stimulus durations, coherences and data aggregated across different days, and yet we still recover the expected relationship between DV and prediction accuracy with a very small error.

With this data, collected through carefully parametrized experiments, we can now ask questions about the influence of experimental factors on the observed relationship between DV at termination and prediction accuracy. We started by re-sorting the

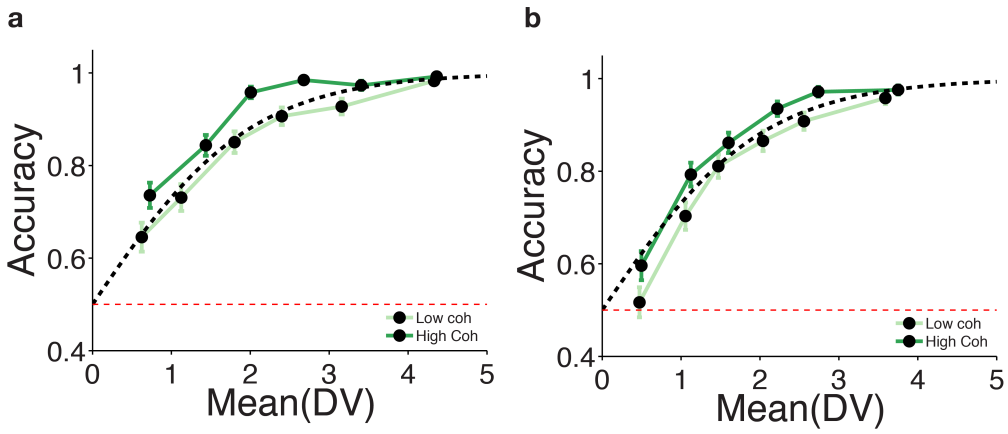

Figure 5.13: **Prediction accuracy as a function of DV- stimulus coherence effects.** **a)** Same data shown in Figure 5.12 a) but having pre-sorted the trials by coherence. Dark green trace shows high coherence results and light green, low coherence results **b)** Same as **a)** for Monkey F.

same trials that went into (Figure 5.12) by stimulus coherence. The results show that there is a small separation between the curves for high and low coherence trials (Figure 5.13). The shift is small but reliable across monkeys. It is tempting to speculate this difference is due to stronger motion energy in the visual system's pipeline leading us to slightly underestimate the DV values at termination or before movement initiation for high coherence stimulus. Whether or not this is the exact cause, this relationship seems lawful with high coherence traces being just slightly vertically shifted above the predicted curve for a wide range of DV values.

Doing the same analysis on the same data but now pre-sorting trials by duration (Figure 5.14), reveals a different effect: the center of the quantiles are strongly shifted to the right (higher magnitudes) for longer stimuli compared to shorter stimuli. This result is a consequence of a lower likelihood of terminating a long trial at a low decision threshold and matches a prediction from drift diffusion models (Kiani and Shadlen, 2009). For Monkey F there is also a slight vertical shift that is not present for Monkey H.

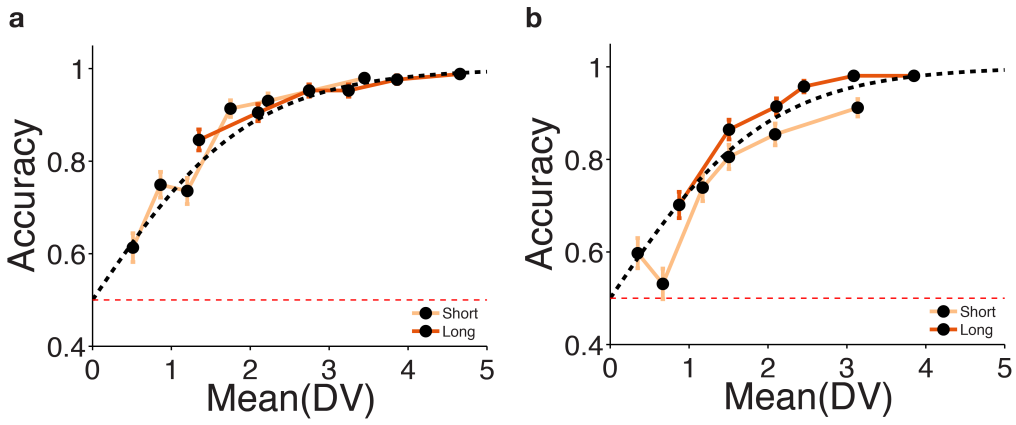

Figure 5.14: **Prediction accuracy as a function of DV - stimulus duration effects. a)** Same data shown in Figure 5.12 a) but having pre-sorted the trials by stimulus duration. Orange trace shows results for long trials and yellow trace results for short trials **b)** Same as **a)** for Monkey F.

5.2.3 Closed loop results - CoM

In the previous section we demonstrated that there is a lawful mapping between instantaneous DV value and choice likelihood over a wide range of stimulus parameters. In the current section we want to take advantage of this predictable mapping to study vacillations in commitment which we call Changes of Mind (CoM). We conceptually divide a CoM trial in two parts: the initial preference or commitment and the final (opposite) commitment that leads to the decision. While we have a direct way to validate the final commitment, the behavioral choice itself, we only have an indirect way to validate the initial commitment. This is where the mapping result is crucial: we know, across a wide range of stimulus parameters, the likelihood of the monkey sticking with the initially predicted choice as a function of instantaneous DV, had the stimulus been stopped there. Moreover, the threshold experiment was performed on the same session as the CoM detection experiments in a randomly interleaved manner. This means the threshold results were obtained for the exact same datasets, decoders and neural states as the ones for the CoM experiment and provide the most faithful indirect validation of initial commitment we could possibly get. CoMs are quite rare so we devoted 70% of the closed loop trials to detect them leaving the remaining 30% as threshold trials. The exact fraction of trials with CoM depends dramatically on

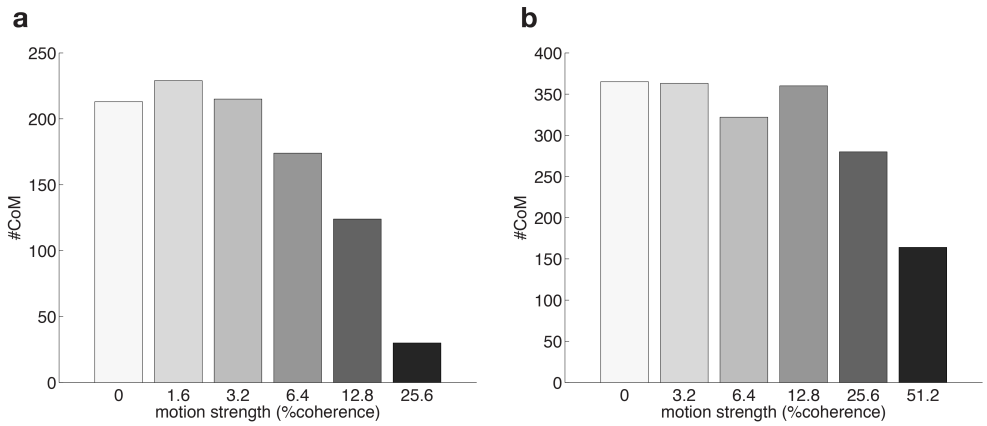

Figure 5.15: **CoM frequency as a function of coherence. a)** Total number of CoMs detected for each coherence for Monkey H **b)** Same as **a)** for Monkey F.

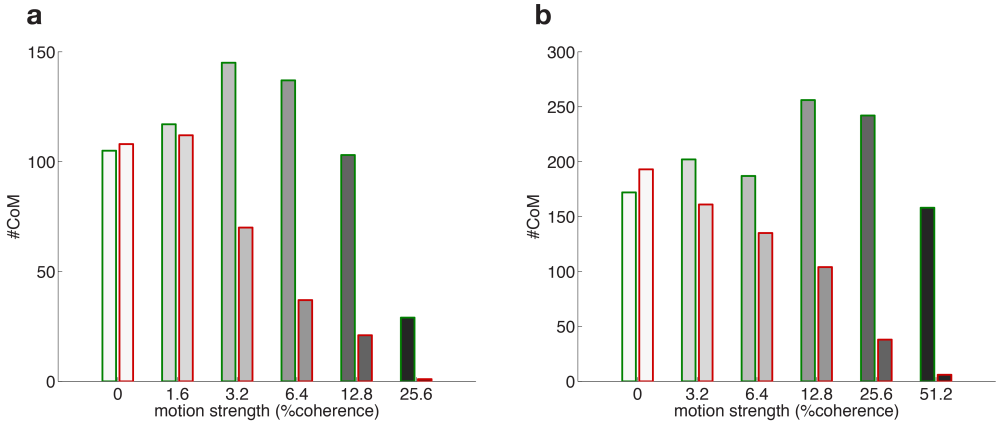

Figure 5.16: **CoM frequency as a function of coherence and direction. a)** Total number of CoMs detected for each coherence and direction for Monkey H. Red bars correpond to erroneous CoMs and green bars to corrective CoMs. **b)** Same as **a)** for Monkey F.

how we parametrise them. The longer the minimum periods of consistent sign and the higher the minimum DV value in the initial commitment stage, the rarer they become. In our first analysis we collapse across all our detected CoMs that span a large range of parameters. Our first pass analysis was to describe the statistical regularities (if any) of these events and compare them to those of overt changes of mind (Resulaj et al., 2009).

The first observation made in that study was that CoMs were more frequent for low and intermediate coherence trials as opposed to high coherence trials. This is hardly surprising: easy trials are more likely to lead to an easy and direct integration

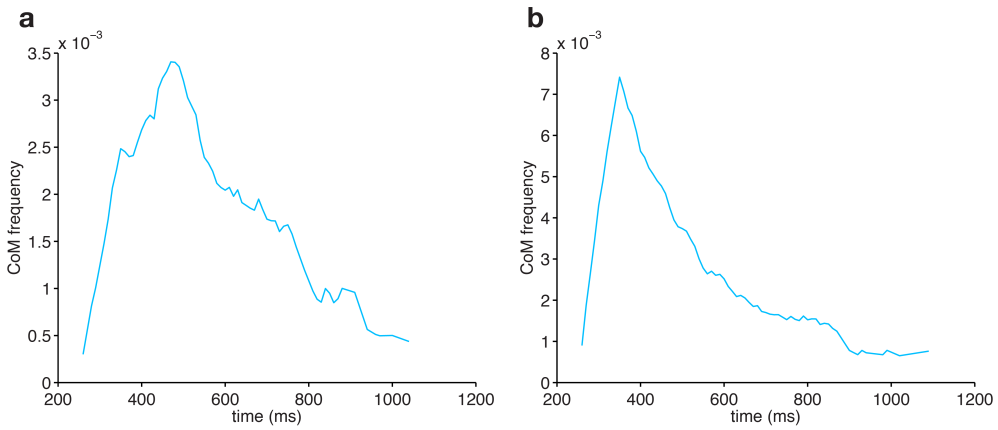

Figure 5.17: **CoM frequency as a function of time in the trial. a)** Frequency of CoMs detected as a function of time during stimulus presentation for Monkey H **b)** Same as **a)** for Monkey F.

of evidence to the correct choice unlike intermediate or hard trials. We verified the same trend in our detected CoMs (Figure 5.15) for both Monkeys. For Monkey H because its behavioral performance was so good, we chose to drop 51.2% coherence stimuli and introduce 1.6% instead to keep the task challenging. And yet, when comparing the proportion of CoMs for the highest coherence used for each monkey we see it is still lower for Monkey H, suggesting better integration of evidence in this subject.

The second observation was that CoMs are more likely to be corrective than erroneous. This prediction is far more interesting and results from the corrective role of additional visual evidence on the initial commitment of the subjects. Indeed, this trend was also verified in the CoMs we detected (Figure 5.16). In fact, for every non-zero coherence and for both monkeys there were more corrective CoMs than erroneous ones. The relative difference within each coherence also increases as a function of coherence with erroneous CoMs being virtually non-existent for the highest coherence. Importantly, the results for 0% coherence trials serve as an important sanity check and help us get a measure of the ground noise of our estimate: for these trials *correct* and *incorrect* choices are arbitrarily assigned on every trial so we shouldn't see any significant difference between the two types of CoMs. That is indeed the case in our results (Figure 5.16) and if anything the small difference goes in opposite way as the

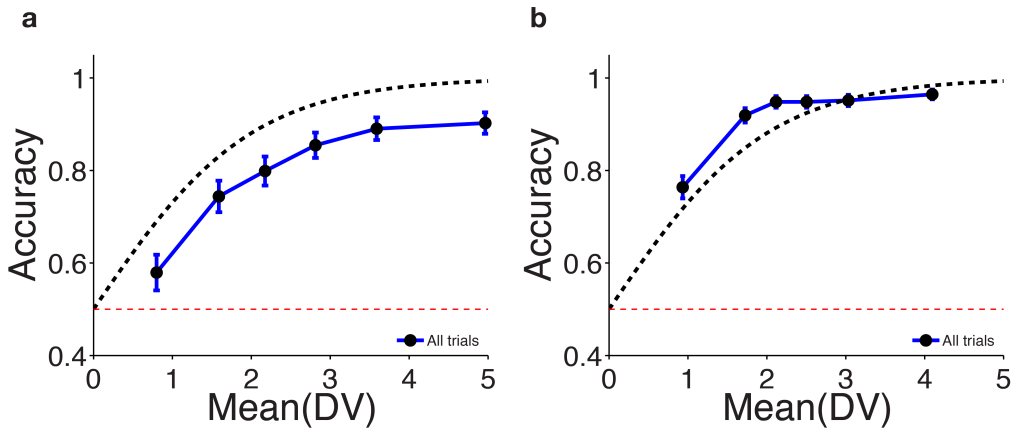

Figure 5.18: **Prediction accuracy as a function of DV for CoM trials. a)** Choice prediction accuracy for all trials collected during the CoM detection experiment. Trials were split in 6 quantiles sorted by DV magnitude at termination. Prediction accuracy and median DV magnitude was calculated and plotted separately for each quantile (blue line with black markers). Blue error bars show standard error of the mean for a binomial distribution. Dashed black line shows predicted accuracy from log-odds equation and red dashed line shows chance level. Data from 985 CoM trials from Monkey H. **b)** Same as **a)** for Monkey F using 1727 CoM trials.

rest of trials increasing our confidence about this effect.

Finally, the third observation made in this previous study was that CoMs were more frequent early in the trial than later in the trial. According to drift diffusion models the longer in the trial we get more likely we are to hit a decision bound or at least the least likely we are to be around the classifying boundary (0). This is also what we found in our detected CoMs (Figure 5.17). Notice that we are only considering CoMs that would have resolved by 250 msec after stimulus presentation. This was because we don't take the DV values too seriously before that period, as choice predictive activity has not emerged yet in PMd in M1. This creates an edge effect with CoM briefly increasing between ∼250-450 msec after which, it steadily and steeply declines as expected from the model predictions.

As a sanity check we verified that even after a CoM, when the trial was terminated the DV predicted the likelihood of choice in a monotonic way (Figure 5.18). The values were slightly lower than expected for Monkey H and thus slightly different across subjects but nevertheless, a lawful relationship was observed.

5.3 Discussion

In this chapter we set out to decode neural activity in real time and summarize the neural state in a single variable that represented the commitment of the monkey to either choice. This framework could provide a unique opportunity to probe the subject based on the instantaneous state of the recorded neural circuit, a manipulation that, to our knowledge, has never been accomplished before.

We transformed this concept into a reality by building a real time system that accurately predicts choice throughout the trial at a performance level that rivals our previous offline results. We did so with remarkably high stability across days and even weeks, performing at most minimal decoder re-training in the process. Moreover, all the features expected for the real time decision variable were present: (i) chance levels for the first ∼200 msec, followed by (ii) a faster rise for easier trials and (iii) an overall increase throughout the trial.

Having such a faithful readout of decision activity enabled us to answer a fundamental question about the signals we had previously characterised: how meaningful are fluctuations in the DV and how do they influence choice? The answer is nearly instantaneous DV values are to be taken seriously and translate very tightly into choice probability in a manner that closely follows the log odds equation. This observation held across all stimulus coherences and durations and was key to indirectly validate the initial commitment state in trials in which a Change of Mind is observed. For clarification by "commitment" we solely mean a preference towards a given choice whose strength correlates with magnitude of DV, as there is no direct way of proving the monkey reached a consolidated commitment to that same choice. Still, trials in which the initial commitment is reversed and that indeed lead to the opposite choice follow all the statistical regularities we would expect from drift diffusion models and behavioral observations (Resulaj et al., 2009). The ability to capture and parametrise these rare events was only made possible by using a real-time system.

6

Final remarks

To best address our questions about decision formation in the somatomotor system we modified a classical motion discrimination task replacing the eye movement responses with arm movement responses. In parallel, we implemented multi-electrode recordings widely used to study motor preparation and execution and combined them with the rich perceptual decision-making framework to allow for novel analysis. These analyses can now be performed across the population and at the single-trial level, an important leap from the single-neuron averaged response approach. This leap is especially relevant for covert phenomena such as decision-making which can unfold very differently on different trials without any behavioral signature.

One of the main results derived from this novel combination of techniques was the close involvement of dorsal premotor cortex and to a lesser extent primary motor context in the decision formation process. This involvement was displayed in the form of short latency and high accuracy choice predictive activity across the population that carried the key features expected from a decision variable. Even more surprising was how flexibly both areas respond when temporal uncertainty is introduced by boosting their predictive activity even further. The ability to adapt and cope with temporal constraints was previously unknown for these areas and only briefly documented for LIP (Shadlen and Newsome, 2001).

Though novel, these results are easily reconcilable with the classical view of (pre)motor areas and suggest additional roles to their well established repertoire.

Motor preparation and execution signals are indeed not just present but very strong in both brain areas but they coexist with high accuracy and low latency decision formation signals. Observations of mixed selectivity (Mante et al., 2013) and multiplexing (Meister et al., 2013) have become more and more frequent in frontal and parietal areas as unbiased and thorough electrophysiological recordings and analyses are performed. Despite going against the more easily interpretable view of perfect segregation of functions in an area or class of neurons, mixed selectivity could indeed be a desirable feature for areas implementing high dimensional representations of complex phenomena (Rigotti et al., 2013).

Beyond characterising decision activity on single trials, we wanted to have the possibility to intervene and query the subject based on the instantaneous neural state as a way to further validate our interpretation of our Decision Variable (DV). This possibility became a reality through our implementation of a real-time system that decodes neural activity and computes a DV value every 10 msec. The implementation itself constituted a tremendous engineering challenge that proved fruitful in the end by yielding an excellent real-time decision read out that rivalled in accuracy with our offline results. Having such a reliable readout enabled us to validate fluctuations in decision activity, stimulus driven or internal, and to capture rare but fascinating events events such as changes of mind. These changes of mind were indirectly and directly validated and followed the statistical regularities expected from previous studies (Resulaj et al., 2009; Kiani et al., 2014).

To our knowledge, we were the first to use of a real-time system to decode neural activity during a decision-making task and query the subject in a neurally contingent manner. We believe this framework is unique could be extended to many other decision-making tasks and modalities and even other fields such as attention. Finally, it provides tantalizing evidence that decoding cognitive activity in real-time is possible a key finding that strongly supports the feasibility of implementing cognitive prosthetics (Andersen et al., 2010).

References

Afshar, A., Santhanam, G., Yu, B. M., Ryu, S. I., Sahani, M., and Shenoy, K. V. Single-trial neural correlates of arm movement preparation. *Neuron*, 71(3):555–64, aug 2011. ISSN 1097-4199. doi: 10.1016/j.neuron.2011.05.047. URL http://www.ncbi.nlm.nih.gov/pubmed/21835350.

Albright, T. D., Desimone, R., and Gross, C. G. Columnar organization of directionally selective cells in visual area MT of the macaque. *Journal of neurophysiology*, 51(1):16–31, January 1984.

Andersen, R. a., Asanuma, C., Essick, G., and Siegel, R. M. Corticocortical connections of anatomically defined subdivisions within the inferior parietal lobe. *The Journal of comparative neurology*, 296:65–113, 1990.

Andersen, R. A., Hwang, E. J., and Mulliken, G. H. Cognitive Neural Prosthetics. *Annual Review of Psychology*, 61(1):169–190, 2010. ISSN 0066-4308. doi: 10.1146/annurev.psych.093008.100503. URL http://www.annualreviews.org/doi/abs/10.1146/annurev.psych.093008.100503.

Barash, S., Bracewell, R. M., Fogassi, L., Gnadt, J. W., and Andersen, R. A. Saccade-related activity in the lateral intraparietal area. I. *J Neurophysiol*, 66(3):1095–1107, 1991. ISSN 00223077.

Bennur, S. and Gold, J. I. Distinct representations of a perceptual decision and the associated oculomotor plan in the monkey lateral intraparietal area. *The Journal of neuroscience : the official journal of the Society for Neuroscience*, 31(3):913–

21, jan 2011. ISSN 1529-2401. doi: 10.1523/JNEUROSCI.4417-10.2011. URL http://www.ncbi.nlm.nih.gov/pubmed/21248116.

Bollimunta, A., Totten, D., and Ditterich, J. Neural dynamics of choice: single-trial analysis of decision-related activity in parietal cortex. *J Neurosci*, 32(37):12684–12701, 2012. ISSN 0270-6474, 1529-2401. doi: 10.1523/JNEUROSCI.5752-11.2012. URL http://www.ncbi.nlm.nih.gov/pubmed/22972993.

Boussaoud, D. and Wise, S. P. Primate frontal cortex: effects of stimulus and movement. *Experimental Brain Research*, 95(1):28–40, 1993. ISSN 00144819. doi: 10.1007/BF00229651.

Britten, K. H., Shadlen, M. N., Newsome, W. T., and Movshon, J. A. The analysis of visual motion: a comparison of neuronal and psychophysical performance. *The Journal of neuroscience*, 12(12):4745–4765, December 1992.

Britten, K. H., Newsome, W. T., Shadlen, M. N., Celebrini, S., and Movshon, J. A. A relationship between behavioral choice and the visual responses of neurons in macaque MT. *Visual neuroscience*, 13(1):87–100, January 1996.

Brunton, B. W., Botvinick, M. M., and Brody, C. D. Rats and humans can optimally accumulate evidence for decision-making. *Science (New York, N.Y.)*, 340:95–8, 2013. ISSN 1095-9203. doi: 10.1126/science.1233912. URL http://www.sciencemag.org/cgi/doi/10.1126/science.1233912$\delimiter"026E30F$nhttp://www.ncbi.nlm.nih.gov/pubmed/23559254.

Carandini, M. and Churchland, A. K. Probing perceptual decisions in rodents. *Nature neuroscience*, 16(7):824–31, 2013. ISSN 1546-1726. doi: 10.1038/nn.3410. URL http://dx.doi.org/10.1038/nn.3410.

Chandrasekaran, C., Lemus, L., and Ghazanfar, A. a. Dynamic faces speed up the onset of auditory cortical spiking responses during vocal detection. *Proceedings of the National Academy of Sciences of the United States of America*, 110(48):E4668–77, 2013. ISSN 1091-6490. doi: 10.1073/pnas.

1312518110. URL http://www.pubmedcentral.nih.gov/articlerender.fcgi?artid=3845123{&}tool=pmcentrez{&}rendertype=abstract.

Churchland, M. M. and Shenoy, K. V. Temporal complexity and heterogeneity of single-neuron activity in premotor and motor cortex. *J Neurophysiol*, 97(6):4235–4257, 2007a. ISSN 0022-3077. doi: 00095.2007[pii]\r10.1152/jn.00095.2007. URL http://www.ncbi.nlm.nih.gov/entrez/query.fcgi?cmd=Retrieve{&}db=PubMed{&}dopt=Citation{&}list{_}uids=17376854$\delimiter"026E30F$nhttp://jn.physiology.org/content/97/6/4235.full.pdf.

Churchland, M. M. and Shenoy, K. V. Delay of movement caused by disruption of cortical preparatory activity. *Journal of neurophysiology*, 97(1):348–359, 2007b. ISSN 0022-3077. doi: 10.1152/jn.00808.2006.

Churchland, M. M., Yu, B. M., Ryu, S. I., Santhanam, G., and Shenoy, K. V. Neural variability in premotor cortex provides a signature of motor preparation. *The Journal of neuroscience : the official journal of the Society for Neuroscience*, 26 (14):3697–712, apr 2006. ISSN 1529-2401. doi: 10.1523/JNEUROSCI.3762-05.2006. URL http://www.ncbi.nlm.nih.gov/pubmed/16597724.

Churchland, M. M., Cunningham, J. P., Kaufman, M. T., Ryu, S. I., and Shenoy, K. V. Cortical Preparatory Activity: Representation of Movement or First Cog in a Dynamical Machine? *Neuron*, 68(3):387–400, 2010. ISSN 08966273. doi: 10.1016/j.neuron.2010.09.015. URL http://dx.doi.org/10.1016/j.neuron.2010.09.015.

Cisek, P. Integrated neural processes for defining potential actions and deciding between them: a computational model. *The Journal of neuroscience : the official journal of the Society for Neuroscience*, 26(38):9761–70, September 2006. ISSN 1529-2401. doi: 10.1523/JNEUROSCI.5605-05.2006. URL http://www.ncbi.nlm.nih.gov/pubmed/16988047.

Cisek, P. and Kalaska, J. F. Neural correlates of reaching decisions in dorsal premotor cortex: specification of multiple direction choices and final selection of action. *Neu-*

ron, 45(5):801–14, mar 2005. ISSN 0896-6273. doi: 10.1016/j.neuron.2005.01.027. URL http://www.ncbi.nlm.nih.gov/pubmed/15748854.

Coallier, É., Michelet, T., and Kalaska, J. F. Dorsal premotor cortex: neural correlates of reach target decisions based on a color-location matching rule and conflicting sensory evidence. *Journal of neurophysiology*, page jn.00166.2014, 2015. ISSN 0022-3077. doi: 10.1152/jn.00166.2014. URL http://eutils.ncbi.nlm.nih.gov/entrez/eutils/elink.fcgi?dbfrom=pubmed{&}id=25787952{&}retmode=ref{&}cmd=prlinks.

de Lafuente, V., Jazayeri, M., and Shadlen, M. N. Representation of Accumulating Evidence for a Decision in Two Parietal Areas. *Journal of Neuroscience*, 35(10): 4306–4318, 2015. ISSN 0270-6474. doi: 10.1523/JNEUROSCI.2451-14.2015. URL http://www.jneurosci.org/cgi/doi/10.1523/JNEUROSCI.2451-14.2015.

Diester, I., Kaufman, M. T., Mogri, M., Pashaie, R., Goo, W., Yizhar, O., Ramakrishnan, C., Deisseroth, K., and Shenoy, K. V. An optogenetic toolbox designed for primates. *Nature neuroscience*, 14(3):387–97, mar 2011. ISSN 1546-1726. doi: 10.1038/nn.2749. URL http://www.ncbi.nlm.nih.gov/pubmed/21278729.

Dmochowski, J. P. and Norcia, A. M. Cortical Components of Reaction-Time during Perceptual Decisions in Humans. *PloS one*, 10:e0143339, 2015. ISSN 1932-6203. doi: 10.1371/journal.pone.0143339. URL http://www.pubmedcentral.nih.gov/articlerender.fcgi?artid=4658144{&}tool=pmcentrez{&}rendertype=abstract.

Donner, T. H., Siegel, M., Fries, P., and Engel, A. K. Buildup of Choice-Predictive Activity in Human Motor Cortex during Perceptual Decision Making. *Current Biology*, 19(18):1581–1585, 2009. ISSN 09609822. doi: 10.1016/j.cub.2009.07.066. URL http://dx.doi.org/10.1016/j.cub.2009.07.066.

Dum, R. P. and Strick, P. L. The origin of corticospinal projections from the premotor areas in the frontal lobe. *The Journal of neuroscience : the official journal*

of the Society for Neuroscience, 11(March):667–689, 1991. ISSN 0270-6474. doi: S0022510X0200268X[pii].

Dum, R. P. and Strick, P. L. Motor areas in the frontal lobe of the primate. *Physiology and Behavior*, 77(4-5):677–682, 2002. ISSN 00319384. doi: 10.1016/S0031-9384(02)00929-0.

Erlich, J. C., Brunton, B. W., Duan, C. A., Hanks, T. D., and Brody, C. D. Distinct effects of prefrontal and parietal cortex inactivations on an accumulation of evidence task in the rat. *eLife*, 2015(4):1–28, 2015. ISSN 2050084X. doi: 10.7554/eLife.05457.001.

Ganguly, K. and Carmena, J. M. Emergence of a stable cortical map for neuroprosthetic control. *PLoS biology*, 7(7):e1000153, jul 2009. ISSN 1545-7885. doi: 10.1371/journal.pbio.1000153. URL http://www.pubmedcentral.nih.gov/articlerender.fcgi?artid=2702684{&}tool=pmcentrez{&}rendertype=abstract.

Gao, P. and Ganguli, S. On simplicity and complexity in the brave new world of large-scale neuroscience. *Current Opinion in Neurobiology*, 32:148–155, 2015. ISSN 18736882. doi: 10.1016/j.conb.2015.04.003. URL http://dx.doi.org/10.1016/j.conb.2015.04.003.

Georgopoulos, A. P., Kalaska, J. F., Caminiti, R., and Massey, J. T. On the relations between the direction of two-dimensional arm movements and cell discharge in primate motor cortex. *The Journal of neuroscience*, 2(11):1527–1537, November 1982.

Georgopoulos, A. P., Crutcher, M. D., and Schwartz, A. B. Cognitive spatial-motor processes - 3. Motor cortical prediction of movement direction during an instructed delay period. *Experimental Brain Research*, 75(1):183–194, 1989. ISSN 00144819. doi: 10.1007/BF00248541.

Gilja, V., Nuyujukian, P., Chestek, C. A., Cunningham, J. P., Yu, B. M., Fan, J. M., Churchland, M. M., Kaufman, M. T., Kao, J. C., Ryu, S. I., and Shenoy, K. V. A high-performance neural prosthesis enabled by control algorithm design. *Nature neuroscience*, 15(12):1752–7, 2012. ISSN 1546-1726. doi: 10.1038/nn.3265. URL http://www.pubmedcentral.nih.gov/articlerender.fcgi?artid=3638087{&}tool=pmcentrez{&}rendertype=abstract.

Gilja, V., Pandarinath, C., Blabe, C. H., Nuyujukian, P., Simeral, J. D., Sarma, A. a., Sorice, B. L., Perge, J. a., Jarosiewicz, B., Hochberg, L. R., Shenoy, K. V., and Henderson, J. M. Clinical translation of a high-performance neural prosthesis. *Nature medicine*, 21(10):6–8, 2015. ISSN 1546-170X. doi: 10.1038/nm.3953. URL http://www.ncbi.nlm.nih.gov/pubmed/26413781.

Gnadt, J. W. and Andersen, R. A. Memory related motor planning activity in posterior parietal cortex of macaque. *Experimental Brain Research*, 70:216–220, 1988.

Graham, N. V. S. *Visual pattern analysers*. Oxford University Press, Oxford, 1989.

Graziano, M. S. A., Taylor, C. S. R., and Moore, T. Complex movements evoked by microstimulation of precentral cortex. *Neuron*, 34(5):841–851, 2002. ISSN 08966273. doi: 10.1016/S0896-6273(02)00698-0.

Hanks, T. D., Ditterich, J., and Shadlen, M. N. Microstimulation of macaque area LIP affects decision-making in a motion discrimination task. *Nature neuroscience*, 9(5):682–689, May 2006.

Hanks, T. D., Kopec, C. D., Brunton, B. W., Duan, C. A., Erlich, J. C., and Brody, C. D. Distinct relationships of parietal and prefrontal cortices to evidence accumulation. *Nature*, 520(7546):220–3, 2015. ISSN 0028-0836. doi: 10.1038/nature14066. URL http://www.ncbi.nlm.nih.gov/pubmed/25600270.

He, S.-Q., Dum, P., and Strick, P. L. Topographic organization of corticospinal projections from the frontal lobe: motor areas on the medial surface of the hemisphere. *The Journal of Neuroscience*, 5(May):3284–3306, 1995.

Hoshi, E. Cortico-basal ganglia networks subserving goal-directed behavior mediated by conditional visuo-goal association. *Frontiers in neural circuits*, 7(October):158, 2013. ISSN 1662-5110. doi: 10.3389/fncir.2013.00158. URL http://www.pubmedcentral.nih.gov/articlerender.fcgi?artid=3800817{&}tool=pmcentrez{&}rendertype=abstract.

Huk, A. C. and Shadlen, M. N. Neural activity in macaque parietal cortex reflects temporal integration of visual motion signals during perceptual decision making. *The Journal of neuroscience : the official journal of the Society for Neuroscience*, 25(45):10420–36, dec 2005. ISSN 1529-2401. doi: 10.1523/JNEUROSCI.4684-04.2005. URL http://www.ncbi.nlm.nih.gov/pubmed/16280581.

Hunt, L. T., Behrens, T. E., Hosokawa, T., Wallis, J. D., and Kennerley, S. W. Capturing the temporal evolution of choice across prefrontal cortex. *eLife*, 4:1689–1699, 2015. ISSN 2050-084X. doi: 10.7554/eLife.11945. URL http://elifesciences.org/lookup/doi/10.7554/eLife.11945.

Kaufman, M. T., Churchland, M. M., Ryu, S. I., and Shenoy, K. V. Cortical activity in the null space: permitting preparation without movement. *Nature neuroscience*, 17(3):440–8, 2014. ISSN 1546-1726. doi: 10.1038/nn.3643. URL http://www.ncbi.nlm.nih.gov/pubmed/24487233.

Kaufman, M. T., Churchland, M. M., Ryu, S. I., and Shenoy, K. V. Vacillation, indecision and hesitation in moment-by-moment decoding of monkey motor cortex. *eLife*, 4:e04677, 2015. ISSN 2050-084X. doi: 10.7554/eLife.04677. URL http://elifesciences.org/content/4/e04677.abstract.

Kiani, R. and Shadlen, M. N. Representation of confidence associated with a decision by neurons in the parietal cortex. *Science (New York, N.Y.)*, 324(May):759–764, 2009. ISSN 0036-8075. doi: 10.1126/science.1169405.

Kiani, R., Hanks, T. D., and Shadlen, M. N. Bounded integration in parietal cortex underlies decisions even when viewing duration is dictated by the environment. *The Journal of neuroscience*, 28(12):3017–3029, March 2008.

Kiani, R., Cueva, C. J., Reppas, J. B., and Newsome, W. T. Dynamics of Neural Population Responses in Prefrontal Cortex IndicateChanges of Mind on Single Trials. *Current Biology*, 24:1–6, 2014. doi: 10.1016/j.cub.2014.05.049. URL http://dx.doi.org/10.1016/j.cub.2014.05.049.

Kiani, R., Cueva, C., Reppas, J., Peixoto, D., Ryu, S., and Newsome, W. Natural Grouping of Neural Responses Reveals Spatially Segregated Clusters in Prearcuate Cortex. *Neuron*, 2015. ISSN 08966273. doi: 10.1016/j.neuron.2015.02.014. URL http://linkinghub.elsevier.com/retrieve/pii/S0896627315001282.

Kubanek, J., Snyder, L. H., Brunton, B. W., Brody, C. D., and Schalk, G. A low-frequency oscillatory neural signal in humans encodes a developing decision variable. *NeuroImage*, 83:795–808, 2013. ISSN 10538119. doi: 10.1016/j.neuroimage.2013.06.085. URL http://dx.doi.org/10.1016/j.neuroimage.2013.06.085.

Latimer, K. W., Yates, J. L., Meister, M. L. R., Huk, A. C., and Pillow, J. W. Single-trial spike trains in parietal cortex reveal discrete steps during decision-making. *Science*, 349(6244):184–187, 2015. ISSN 0036-8075. doi: 10.1126/science.aaa4056. URL http://science.sciencemag.org/content/349/6244/184.

Mante, V., Sussillo, D., Shenoy, K. V., and Newsome, W. T. Context-dependent computation by recurrent dynamics in prefrontal cortex. *Nature*, 503(7474):78–84, November 2013.

Mazurek, M. E., Roitman, J. D., Ditterich, J., and Shadlen, M. N. A role for neural integrators in perceptual decision making. *Cerebral cortex (New York, N.Y.: 1991)*, 13(11):1257–1269, November 2003.

Meister, M. L. R., Hennig, J. A., and Huk, A. C. Signal multiplexing and single-neuron computations in lateral intraparietal area during decision-making. *The Journal of neuroscience*, 33(6):2254–2267, February 2013.

Murakami, M. and Mainen, Z. F. Preparing and selecting actions with neural populations: toward cortical circuit mechanisms. *Current Opinion in Neurobi-*

ology, 33:40–46, 2015. ISSN 09594388. doi: 10.1016/j.conb.2015.01.005. URL http://linkinghub.elsevier.com/retrieve/pii/S0959438815000148.

Murakami, M., Vicente, M. I., Costa, G. M., and Mainen, Z. F. Neural antecedents of self-initiated actions in secondary motor cortex. *Nature neuroscience*, 17(11): 1574–82, 2014. ISSN 1546-1726. doi: 10.1038/nn.3826. URL http://www.ncbi.nlm.nih.gov/pubmed/25262496.

Newsome, W. T. and Paré, E. B. A selective impairment of motion perception following lesions of the middle temporal visual area (MT). *The Journal of neuroscience*, 8(6):2201–2211, June 1988.

O'Connell, R. G., Dockree, P. M., and Kelly, S. P. A supramodal accumulation-to-bound signal that determines perceptual decisions in humans. *Nature neuroscience*, 15(12):1729–35, 2012. ISSN 1546-1726. doi: 10.1038/nn.3248. URL http://www.ncbi.nlm.nih.gov/pubmed/23103963.

Pastor-Bernier, A. and Cisek, P. Neural correlates of biased competition in premotor cortex. *The Journal of neuroscience : the official journal of the Society for Neuroscience*, 31(19):7083–8, may 2011. ISSN 1529-2401. doi: 10.1523/JNEUROSCI.5681-10.2011. URL http://www.ncbi.nlm.nih.gov/pubmed/21562270.

Pesaran, B., Nelson, M. J., and Andersen, R. a. Dorsal premotor neurons encode the relative position of the hand, eye, and goal during reach planning. *Neuron*, 51(1):125–34, jul 2006. ISSN 0896-6273. doi: 10.1016/j.neuron.2006.05.025. URL http://www.pubmedcentral.nih.gov/articlerender.fcgi?artid=3066049{&}tool=pmcentrez{&}rendertype=abstract.

Purcell, B. and Kiani, R. Neural Mechanisms of Post-error Adjustments of Decision Policy in Parietal Cortex. *Neuron*, 2016. ISSN 08966273. doi: 10.1016/j.neuron.2015.12.027. URL http://linkinghub.elsevier.com/retrieve/pii/S0896627315011290.

Raposo, D., Sheppard, J. P., Schrater, P. R., and Churchland, a. K. Multisensory Decision-Making in Rats and Humans. *Journal of Neuroscience*, 32(11):3726–3735, 2012. ISSN 0270-6474. doi: 10.1523/JNEUROSCI.4998-11.2012.

Raposo, D., Kaufman, M. T., and Churchland, A. K. A category-free neural population supports evolving demands during decision-making. *Nature Neuroscience*, 17(12):1784–1792, 2014. ISSN 1097-6256. doi: 10.1038/nn.3865. URL http://www.pubmedcentral.nih.gov/articlerender.fcgi?artid=4294797{&}tool=pmcentrez{&}rendertype=abstract.

Ratcliff, R. A theory of memory retrieval. *Psychological Review*, 85(2):59–108, March 1978.

Resulaj, A., Kiani, R., Wolpert, D. M., and Shadlen, M. N. Changes of mind in decision-making. *Nature*, 461(7261):263–6, sep 2009. ISSN 1476-4687. doi: 10.1038/nature08275. URL http://www.pubmedcentral.nih.gov/articlerender.fcgi?artid=2875179{&}tool=pmcentrez{&}rendertype=abstract.

Rigotti, M., Barak, O., Warden, M. R., Wang, X.-J., Daw, N. D., Miller, E. K., and Fusi, S. The importance of mixed selectivity in complex cognitive tasks. *Nature*, 497(7451):1–6, 2013. ISSN 1476-4687. doi: 10.1038/nature12160. URL http://dx.doi.org/10.1038/nature12160$\delimiter"026E30F$npapers3://publication/doi/10.1038/nature12160.

Roitman, J. D. and Shadlen, M. N. Response of neurons in the lateral intraparietal area during a combined visual discrimination reaction time task. *The Journal of neuroscience*, 22(21):9475–9489, November 2002.

Romo, R., Hernández, A., Zainos, A., and Salinas, E. somatossensory discrimination based on cortical microstimulation. *Nature*, 392(March):387–390, 1998. ISSN 1476-4687. doi: 10.1038/nature02376.1.

Salzman, C. D., Britten, K. H., and Newsome, W. T. Cortical microstimulation

influences perceptual judgements of motion direction. *Nature*, 346(6280):174–177, July 1990.

Santhanam, G., Ryu, S. I., Yu, B. M., Afshar, A., and Shenoy, K. V. A high-performance braincomputer interface. *Nature*, 442(7099):195–198, 2006. ISSN 0028-0836. doi: 10.1038/nature04968. URL http://www.nature.com/doifinder/10.1038/nature04968.

Shadlen, M. N. and Newsome, W. T. Neural basis of a perceptual decision in the parietal cortex (area LIP) of the rhesus monkey. *Journal of neurophysiology*, 86(4): 1916–36, October 2001. ISSN 0022-3077. URL http://www.ncbi.nlm.nih.gov/pubmed/11600651.

Shadlen, M. N. and Gold, J. I. The Neurophysiology of Decision Making as a Window on Cognition. *The Cognitive Neurosciences*, pages 1229–1242, 2004.

Shadlen, M. N. and Kiani, R. Decision making as a window on cognition. *Neuron*, 80(3):791–806, October 2013.

Shadlen, M. N. and Newsome, W. T. Motion perception: seeing and deciding. *Proceedings of the National Academy of Sciences of the United States of America*, 93 (January):628–633, 1996. ISSN 00278424. doi: 10.1073/pnas.93.2.628.

Simeral, J. D., Kim, S.-P., Black, M. J., Donoghue, J. P., and Hochberg, L. R. Neural control of cursor trajectory and click by a human with tetraplegia 1000 days after implant of an intracortical microelectrode array. *Journal of Neural Engineering*, 8 (2):025027, 2011. URL http://stacks.iop.org/1741-2552/8/i=2/a=025027.

Song, J.-H. and McPeek, R. M. Roles of narrow- and broad-spiking dorsal premotor area neurons in reach target selection and movement production. *Journal of neurophysiology*, 103(February 2010):2124–2138, 2010. ISSN 0022-3077. doi: 10.1152/jn.00238.2009.

Strick, P. L. and Preston, J. B. Multiple representation in the primate motor cortex.

Brain Research, 154(2):366–370, 1978. ISSN 00068993. doi: 10.1016/0006-8993(78)90707-2.

Sussillo, D. and Abbott, L. F. Generating coherent patterns of activity from chaotic neural networks. *Neuron*, 63(4):544–57, aug 2009. ISSN 1097-4199. doi: 10.1016/j.neuron.2009.07.018. URL http://www.pubmedcentral.nih.gov/articlerender.fcgi?artid=2756108{&}tool=pmcentrez{&}rendertype=abstract.

Tanji, J. and Evarts, E. Anticipatory activity of motor cortex neurons in relation to direction of an intended movement. *Journal of neurophysiology*, 39(5):1062–1068, 1976. ISSN 0022-3077.

Thura, D. and Cisek, P. Deliberation and commitment in the premotor and primary motor cortex during dynamic decision making. *Neuron*, 81(6):1401–1416, 2014. ISSN 10974199. doi: 10.1016/j.neuron.2014.01.031. URL http://dx.doi.org/10.1016/j.neuron.2014.01.031.

Uchida, N. and Mainen, Z. F. Speed and accuracy of olfactory discrimination in the rat. *Nature neuroscience*, 6(11):1224–1229, 2003. ISSN 1097-6256. doi: 10.1038/nn1142.

Weinrich, M. and Wise, S. P. The premotor cortex of the monkey. *The Journal of neuroscience : the official journal of the Society for Neuroscience*, 2(9):1329–1345, 1982. ISSN 0270-6474.

Weinrich, W., Wise, S. P., and Mauritz, K. H. A neurophysiological study of the premotor cortex in the rhesus monkey. *Brain*, 107:385–414, 1984.

Zalocusky, K. A., Ramakrishnan, C., Lerner, T. N., Davidson, T. J., Knutson, B., and Deisseroth, K. Nucleus accumbens D2R cells signal prior outcomes and control risky decision-making. *Nature*, 531(7596):642–6, 2016. ISSN 1476-4687. doi: 10.1038/nature17400. URL http://www.

nature.com/doifinder/10.1038/nature17400$\delimiter"026E30F$nhttp://www.ncbi.nlm.nih.gov/pubmed/27007845.

ITQB-UNL | Av. da República, 2780-157 Oeiras, Portugal
Tel (+351) 214 469 100 | Fax (+351) 214 411 277

www.itqb.unl.pt